RADIO SOURCE MAPPING

FOR PRECISION GEODESY

by

GAETAN JEAN FRANCOIS JOSEPH CUVELIER

Ingenieur civil de
l'Ecole Nationale de l'Aeronautique et
de l'Espace, Toulouse, France
(1981)

SUBMITTED TO THE DEPARTMENT OF EARTH
AND PLANETARY SCIENCES IN PARTIAL
FULFILLMENT OF THE REQUIREMENTS FOR
THE DEGREE OF

MASTER OF SCIENCE

at the
MASSACHUSETTS INSTITUTE OF TECHNOLOGY
September 1982

Signature of Author _____
Department of Earth and Planetary
Sciences, September 7, 1982

Certified by _____
Irwin I. Shapiro
Thesis Supervisor

Accepted by _____
Chairman, Departmental Committee on
Graduate Students

RADIO SOURCE MAPPING

FOR PRECISION GEODESY

by

Gaëtan Jean Francois Joseph Cuvelier

Submitted to the department of Earth and Planetary Sciences on September 7, 1982 in partial fulfillment of the requirements for the degree of Master of Science

ABSTRACT

In precision geodesy, an accuracy of one centimeter in the measurements of intercontinental distances requires that the brightness distributions of the extragalactic radio sources which are used in the VLBI technique be very well known. Because there is resolution at the milliarcsecond level, a point source model which has been used so far has become a coarse approximation. The purpose of the following study is to show how these brightness distributions can be determined from a VLBI "geodetic" schedule. On June 15, 1981 a large amount of data was collected for the radio source 1641+399 (3C345); during the two following days of the geodetic schedule regular observations were also made. Thus, 3C345 is first studied in order to determine a more systematic method of mapping other quasars. Subsequently, other sources such as the double quasar 0923+392 (4C39.25) and the extended quasar 1226+023 (3C273B) which have more complex distributions were mapped from a smaller amount of data. To perform this work, a "hybrid" mapping program was used with the data collected at X-band ($\sim$ 8 GHz) at four antennas located at Haystack and Westford, Massachusetts; Fort Davis, Texas; and Owens Valley, California, on 15, 16 and 17 June 1981. The two maps of 3C345, one obtained from the observations made only during the geodetic schedule and the other obtained from all the observations show little difference in the brightness distribution and indicate that at least for some sources brightness distributions can be determined adequately solely from observations made during a geodetic VLBI experiment.

Thesis Supervisor : Irwin I. Shapiro
Title : Professor of Geophysics and Physics

ACKNOWLEDGEMENTS

I would like to thank my thesis supervisor I.I. Shapiro who gave me the opportunity to study the VLBI technique and broaden my knowledge in Radio-Astronomy. I am especially grateful to Tom Herring whose help and advice throughout the preparation of this thesis made its realization possible. I wish to express a special thanks to Jim Davis and Yves Bernabe for helpful discussions and remarks.

Table of contents

1. The hybrid mapping program

1.1 Introduction

Since the achievement of a few centimeters precision in the measurement of intercontinental distances using the VLBI technique, the determination of the structure of extragalactic radio sources on a scale of one milliarcsecond, or even less, has become crucial for further improvements in geodetic precision. The determination of source structure is complicated by the loss of phase information at each element of an array of very long baseline interferometers, which is one of the problems inherent to such VLBI measurements. This phase information is masked by the instability of atomic clocks, whose behaviour is at present not fully understood, and by fluctuations of the atmosphere over each site. The other important problem is the poor coverage of the (u-v) plane now obtained in VLBI observations.

The purpose of this work is to demonstrate the effectiveness of a method of constructing the brightness distribution of a source from data obtained with a small number of interferometers. These data consist of fringe-amplitude and closure-phase information with checks being made of closure amplitude consistency.

D.B. Shaffer's hybrid mapping program [1] uses this fringe-amplitude and phase-closure information in addition to an initial model. This program has been used to perform the following work.

1.2 Description of the phase closure test

NOTE Mathematical expressions, indices and notations are defined in Appendix 1.

For each baseline, we deduce the fringe phase, Ψ_{ij} , of the incoming wave from data collected at the two sites i and j. These data contain information about the local oscillator frequency, the clock readings, epoch and rate errors of the clocks, and the phase shift caused by the propagation medium. The phase Ψ_{ij} is the sum of the phase Φ_{ij} of the complex visibility (a function of the source structure) and the sum of all perturbations θ_{ij} added to Φ_{ij} (Equation 1). These perturbations have different origins: propagation effects in the medium between the source and each antenna, clock drifts and any other experimental errors inherent to only one site [2].

$$\Psi_{ij} = \Phi_{ij} + \theta_{ij} \qquad (1)$$

If we sum the fringe phases, Ψ_{ij} , for three baselines,

so as to form the so-called phase closure, C_{ijk} , the θ_{ij} terms almost cancel. The derivation is given by Rogers et al. [2].

$$C_{ijk} = \Psi_{ij} + \Psi_{jk} - \Psi_{ik} = \Phi_{ij} + \Phi_{jk} - \Phi_{ik} \qquad (2)$$

Thus, we are left with information only about the structure of the source. This new observable can now be used along with the fringe amplitudes in trying to reconstruct the brightness distribution. To produce a map we need to know Φ_{ij}. One step of the mapping process consists of finding the least squares estimate for the phase Φ_{ij} of the complex visibility function for every baseline. A simple method of estimating this phase without altering the phase closure is to estimate the station phases. To each Station i is assigned a θ_i such that for the i-j^{th} baseline

$$\theta_{ij} = \theta_i - \theta_j \qquad (3)$$

These station phases contain no intrinsic information because an arbitrary constant θ_o can be added to all of them and will not affect the fringe phases nor the closure phases. If an iterative scheme is utilized, then the adjustment in the phase of the complex visibility of the i-j^{th} baseline for the n^{th} iteration is:

$$\Delta\Phi_{ij}^{n} = -\Delta\theta_{ij}^{n} = \Delta\theta_{j}^{n} - \Delta\theta_{i}^{n} \qquad (4)$$

where $\Delta\theta_i^n$ is the adjustment in the i^{th} station phase. Since by construction $\Sigma\ \Delta\ \theta_{ij}^n = 0$ for any set of three stations, then

$$C_{ijk}^{n+1} = C_{ijk}^n \tag{5}$$

i.e. the phase closure is always preserved. For each iteration, the problem is to find the least squares station phase correction $\Delta\theta_i^n$ for each station using the phase closure information. For every baseline two phases are calculated: a "model" phase Φ_{ij}^m is derived from a model updated after each iteration and a phase called the "observed" phase Φ_{ij}^o is calculated from the fringe phase and each station phase estimated during the previous iteration. The fringe phase is obtained from cross correlation of the signals received at the two antennas of an interferometer [3]. Thus we have

$$\Phi_{ij}^o = \Psi_{ij} + \theta_j - \theta_i \tag{6}$$

We use superscripts "o" and "m" to stand for "observed" and "model", respectively. The "model" phase is then subtracted from the "observed" phase and their difference is stored in the vector $(\underline{Y}^o-\underline{Y}^m)$ (see App.2). If the vector $\delta\underline{X}$ is composed of the corrections to the station phases, then we have the following relationship between $(\underline{Y}^o-\underline{Y}^m)$ and $\delta\hat{\underline{X}}$, the

estimate of $\delta\underline{X}$ obtained by weighted least squares:

$$\hat{\delta\underline{X}} = (A^t P^{-1} A + \Lambda_X^{-1})^{-1} A^t P^{-1} (\underline{Y}^o - \underline{Y}^m) \qquad (7)$$

The number of elements in the vector $\delta\underline{X}$ is the number of stations N whereas the number of elements in vector $\underline{Y}$ is the number of interferometers N(N-1)/2. This problem is over-determined and can be solved as per Equation (7). The matrix Λ_X contains the a priori variance-covariance of $\delta\underline{X}$. The matrix P^{-1} is a weighting matrix. It is composed of the squares of the signal to noise ratios of each observation. The matrix A relates the vector of the station phases $\underline{X}$ and $\underline{Y}$ through the relationship $A = \partial\underline{Y}/\partial\underline{X}$ (see App.2).

1.3 Description of the amplitude closure test

For the baseline (i-j) the normalized correlation coefficient ρ_{ij} is related to the fringe visibility γ_{ij} by [3]:

$$\rho_{ij} \simeq \gamma_{ij} \sqrt{\frac{T_{ai}T_{aj}}{T_{si}T_{sj}}} \quad , \qquad (8)$$

where T_{ai} is the antenna temperature (K) and T_{si} is the system temperature (K). For a given source and telescope, the antenna gain G_i and the antenna temperature T_{ai} are defined as [4]:

$$G_i = 4\pi A_{gi} \eta_i/\lambda^2 \qquad (9)$$

and

$$T_{ai} = \frac{S\ A_{gi}\ \eta_i}{2\ k} \quad , \tag{10}$$

where k is the Boltzmann constant ($1.38\ 10^{-23}\ JK^{-1}$), S is the flux density of the radio source ($Wm^{-2}Hz^{-1}$), η_i is the efficiency of the antenna, λ is the wavelength (m) and A_{gi} is the geometric area of the antenna (m^2). Combining Equations (8), (9) and (10) we have for any baseline

$$\rho_{ij} = \gamma_{ij}\ S\ K \sqrt{\frac{G_i}{T_{si}}} \sqrt{\frac{G_j}{T_{sj}}} \quad , \tag{11}$$

where

$$K = \frac{\lambda^2}{8k\pi} \tag{12}$$

$S\ \gamma_{ij}$ is called the correlated flux density for the baseline i-j. Unfortunately, because antenna gains and system temperatures are time dependent it is difficult to infer an accurate value of the fringe visibility γ when no precise and regular radiometry measurements have been made. These time variations in gains and temperatures are expressed in a correction factor h_i according to

$$\frac{G_i}{T_{si}} = \frac{G_i^n}{T_{si}^n}\ \frac{1}{h_i} \quad , \tag{13}$$

where G_i^n is the constant nominal value of the gain and T_{si}^n the constant nominal system temperature. It allows us to rewrite Equation (11) as

$$\rho_{ij} = K\ S\ \gamma_{ij} \sqrt{\frac{G_i^n}{T_{si}^n\ h_i}} \sqrt{\frac{G_j^n}{T_{sj}^n\ h_j}} \qquad (14)$$

However, for four stations an interesting relationship between the correlation coefficients can be written so that the gains and the system temperatures for each member of an interferometer pair cancel out [5]. This gain-independent relationship, called the amplitude closure, provides a new piece of information about the source.

Let 1, 2, 3 and 4 be the stations and, for simplicity, let us write $y_k = \rho_{ij}$ and $\gamma_k = \gamma_{ij}$. The index k is determined from the station labels as follows: Index 1 represents stations 1 and 2 , 2 represents stations 1 and 3 , 3 represents stations 2 and 3, 4 represents stations 1 and 4, 5 represents stations 2 and 4, 6 represents stations 3 and 4. We define the amplitude closure variable R_{ijkl} to be

$$R_{ijkl} = \frac{y_i\ y_j}{y_k\ y_l} \qquad (15)$$

For example, for i=1, j=6, k=2 and l=5 we have

$$R_{1625} = \frac{y_1\ y_6}{y_2\ y_5}$$

Replacing the y_i by their expression given in Equation (14) yields:

$$\frac{y_1\ y_6}{y_2\ y_5} = \frac{KS\sqrt{\frac{G_1^n}{h_1 T_{s1}^n}\ \frac{G_2^n}{h_2 T_{s2}^n}}\ \gamma_1\ \ KS\sqrt{\frac{G_3^n}{h_3 T_{s3}^n}\ \frac{G_4^n}{h_4 T_{s4}^n}}\ \gamma_6}{KS\sqrt{\frac{G_1^n}{h_1 T_{s1}^n}\ \frac{G_3^n}{h_3 T_{s3}^n}}\ \gamma_2\ \ KS\sqrt{\frac{G_2^n}{h_2 T_{s2}^n}\ \frac{G_4^n}{h_4 T_{s4}^n}}\ \gamma_5} \qquad (16)$$

After cancellation of the terms relative to the gains and temperatures, we obtain

$$R_{1625} = \frac{y_1\ y_6}{y_2\ y_5} = \frac{\gamma_1\ \gamma_6}{\gamma_2\ \gamma_5} \qquad (17)$$

A model for the correlation coefficient y_k can be derived from Equation (14): let

$$y_k = y_k^n\ x_i\ x_j \quad , \qquad (18)$$

where

$$x_i = 1/\sqrt{h_i}$$

and

$$y_k^n = KS\ \gamma_{ij}\sqrt{G_i^n/T_{si}^n}\ \sqrt{G_j^n/T_{sj}^n} \qquad (19)$$

The coefficient y_k^n corresponds to the theoretical value for the correlation coefficient if gains and system temperatures are at their nominal values. We want to find the least squares estimate of the x_i given the observed correlation coefficient y_k^o and the model (Equation 18). Expanding Equation (18) to the first order about the a priori values of x_i and x_j, x_{io} and x_{jo} respectively, we obtain:

$$y_k^o \simeq y_k(x_{io},x_{jo}) + (\partial y_k/\partial x_i)|_o \, \Delta x_i + (\partial y_k/\partial x_j)|_o \, \Delta x_j \ , \quad (20)$$

where $\Delta x_i = (x_i - x_{io})$. The partial derivatives with respect to x_i and x_j evaluated at the a priori values are calculated from Equation (18). If we let $y_k^m = y_k(x_{io},x_{jo})$, then Equation (20) can be rewritten as:

$$y_k^o - y_k^m \simeq (y_k^n \, x_{jo}) \, \Delta x_i + (y_k^n \, x_{io}) \, \Delta x_j \quad (21)$$

We now have a linear relation of the form $(\underline{Y}^o - \underline{Y}^m) = A \, \delta\underline{X}$. The least squares formulation gives the same mathematical formulation as seen in §1.2 for the phases. This time the matrix A contains the different theoretical values for the correlation coefficients (see App.3). The matrix P^{-1} is a weighting matrix. Λ_x is the a priori variance-covariance matrix for the gains. The estimate of $\delta\underline{X}$ is given by:

$$\hat{\delta\underline{X}} = (A^t \, P^{-1} \, A + \Lambda_x^{-1})^{-1} \ A^t \, P^{-1} \, (\underline{Y}^o - \underline{Y}^m) \quad (22)$$

Another possible formulation of the problem is the logarithmic linearization. Taking the logarithm of both terms in Equation (18) yields:

$$\log y_k = \log y_k^n + \log x_i + \log x_j \quad (23)$$

which is the model for the logarithm of the correlation coefficient. Expanding to the first order about the a priori values of log x_i and log x_j we obtain similarly:

$$\log y_k^o - \log y_k^m \simeq \Delta\log x_i + \Delta\log x_j \qquad (24)$$

where $\log y_k^m = \log y_k(x_{io}, x_{jo})$. The matrix formulation is still of the form $(\underline{Y}^o - \underline{Y}^m) = A\ \delta\underline{X}$, but the elements of the matrix A and the vectors $\underline{Y}$ and $\underline{X}$ are not the same as for the linear approximation (see App.3).

1.4 Mapping procedure

The purpose of the mapping procedure is to find the brightness distribution of a radio source given a set of correlation data obtained at irregular values on the u-v plane. The main reason for this incomplete and irregular u-v coverage is the limited number of baselines which determine the number of ellipsoidal tracks. Moreover, the points along each track for which data were obtained are often separated by several tens of minutes in an irregular manner. This separation can be due to several reasons. The principal reason is that the radio sources are scattered all over the sky, and unless some of them happen to be in the beam at the same time, they cannot be observed simultaneously. Moreover, if many sources are widely scattered over the sky, one tends to randomize the order of observation to avoid a

possibility of a systematic error. Another reason is that each observation requires an integration time between 100 seconds and 15 minutes depending on the type of experiment. Yet another reason is that if one observes several compact extragalactic radio sources, one must allow time for the antennas to slew. Other reasons can be low declination of the source that shortens the period of common visibility, technical failures, weather and problems during correlation procedures.

The irregular u-v coverage is responsible for undesirable sidelobes in the synthesized beam which can add features to the synthesis map, making it difficult or sometimes impossible to interpret. The synthesis map (or dirty map) M which is obtained by taking the Fourier transform of the weighted measurements (§2.4.4) is by definition the convolution product of the synthesized beam (or dirty beam) D with the brightness distribution of the source seen by the antennas [6]:

$$M(x,y) \backsim \int\int V(u,v)\, g(u,v)\, \exp(2\pi i(ux+vy))\, du\, dv \qquad (25)$$

$$M(x,y) = B(x,y) \ast D(x,y) \qquad (26)$$

where x,y are sky coordinates (directional cosines with respect to the u and v axes, respectively). The components of the baseline vector are u along the east-west direction and v along the north-south direction. V is the complex visibility function and g is the u-v plane weighting function.

The dirty beam D(x,y) is proportional to the transform of the weighting function. In other words D(x,y) is the dirty map of a point source as seen by the synthesized beam (interferometer array):

$$D(x,y) \propto \iint g(u,v)\ \exp(2\pi i(ux+vy))\ du\ dv \qquad (27)$$

The Fourier integral (Equation 25) can be calculated only if we know the product of V by g for all u and v. But, as already stated, V(u,v) is only available for a limited set of points. At points for which no data are available the weighting function is taken to be zero, then the continuous sum can be replaced by a discrete sum.

$$M(x,y) = \sum \sum g(u,v)\ V(u,v)\ \exp(2\pi i(ux+vy)) \qquad (28)$$

This approximation has been discussed by J.A Högbom (1974) from the standpoint of Information Theory [6] and J.G Ables (1974) from the standpoint of Maximum Entropy [7].

So far we have determined the dirty map M(x,y). In order to clean it we use an iterative procedure which uses the shape of the dirty beam to recover the brightness B(x,y). The purpose of this cleaning is to separate the real structure of the source from sidelobe disturbances. The center of the dirty beam is set on the peak value of the dirty map and some fraction of its value is subtracted. The process is iterated until the peak remaining value is

thought to be purely noise. When finished, we are left with a set of clean components that are presumed to be representative of the source brightness distribution. The final map is produced by convolution of these clean components with a clean beam taken to be similar to the main lobe of the dirty beam. The shape and the size of this restoring beam depend on the interferometers, the length of the experiment, and the frequency.

1.5.1 Description of the program MAPA

The method used in D.B. Shaffer's program to produce maps of radio sources has features common with the two mapping procedures described by Cotton [8] and Readhead & Wilkinson [9]. The three important characteristics of this program are:

i) the use of an initial model to determine the fringe phases,

ii) the interpolation of the data to a grid in the (u,v) plane, and

iii) the use of a two-dimensional fast Fourier transform (see App. 4)

The brightness distribution is calculated as follows. Inspecting the maxima and the minima of the visibility in the (u,v) plane, one guesses at an initial model from which

one derives the model phases for every baseline. The subroutine MAP uses these phases and the correlated flux densities to calculate the complex visibility function at the u-v points where observations exist:

$$V(u,v) = Amp(u,v)\ \exp(i\Phi(u,v)) \qquad (29)$$

where Amp is the correlated flux density and Φ a model phase. The following step consists in gridding the u-v plane because the fast Fourier transform used in MAP to compute the dirty map requires that the observations are gridded: to each (u,v) point for which data exist there will correspond a grid point (u_o,v_o). These grid points are equally spaced in the u-v plane. The first step of the gridding is to define the visibility function at the grid points. Let V(u,v) be the visibility at points where data were collected and $V'(u_o,v_o)$ the interpolated visibility. The relationship between V and V' is:

$$V'(u_o,v_o) = \frac{\sum_{j=1}^{N} V(u_j,v_j)\ c(u_o-u_j,v_o-v_j)}{\sum_{j=1}^{N} c(u_o-u_j,v_o-v_j)} \qquad (30)$$

where N is the number of observations and (u_j,v_j) are the coordinates of the point where an observation was taken. In the subroutine MAP, the average of the visibility data is taken for each grid cell, each of which has the dimensions

$\Delta u, \Delta v$. This is equivalent to taking $c(u,v)$ as follows:

$$c(u,v)=1 \quad \text{if } |u|<\Delta u/2 \text{ and } |v|<\Delta v/2$$
$$=0 \quad \text{otherwise}$$

Then, the two-dimensional complex fast Fourier transform inverts the "interpolated" visibility function.

Note that the choice of $\Delta u, \Delta v$ is important because, since the visibility function is sampled at intervals $\Delta u, \Delta v$, there will be aliasing if the brightness distribution is nonzero for $|x|>1/\Delta u$ and $|y|>1/\Delta v$. There will be emission outside the field of mapping which will be reflected within the field of view (sampling theorem [10]). The influence of the spacing $\Delta u, \Delta v$ will be studied in §2.4.8.

The second part of the subroutine MAP computes the dirty beam. The weighting function is nonzero only at the grid points. At these points,

$$g(u_o,v_o) = 1 \text{ if there is an observation}$$
$$= 0 \text{ if there is no observation}$$

This type of weighting is called "uniform" weighting. The second type of weighting which is available is defined by

$$g(u_o,v_o) = n$$

where n is the number of observations in the cell.

The subroutine CLEAN, called right after MAP, deconvolves the dirty beam from the dirty map. Firstly, it locates the maximum value of the brightness in the (x,y) plane, centers the beam at that location, and removes a fraction of the peak value. This fraction is called the loop gain and its influence on the final map is studied in

§2.4.3. This iterative procedure is repeated until the peak remaining value is greater than some fraction of the original peak value (see §2.4.4). In its present configuration the program can only restore the map using a circular beam roughly 2 times smaller than the main lobe of the dirty beam. This clean beam is defined by:

$$D(x,y) = \exp(-k(x^2+y^2)) \qquad (31)$$

In the subroutine PCLOS, the corrections to the station phases are computed from the model phases and the "observed" phases as defined in §1.2. The model phases are deduced from the clean components of the previous iteration. A least squares estimation method is used to derive these corrections. Moreover, the method assumes equally likely errors in the fringe-phase for any baseline.

In the subroutine ACLOS, the gains at each station are assumed to be known with an equal accuracy. The least squares technique is either of the two different methods already discussed to determine the estimates for the gains : logarithmic or linear methods. Once the corrections for station phases and gains are computed, they are used to adjust the initial values of the "observed" phases and the correlated flux densities. During the following iterations these new values are used to produce a new map and are tested in PCLOS and ACLOS to find a new estimate of phases and gains. Phase residuals, gain residuals, adjustments to

1.5.2 Flow chart of the hybrid mapping program

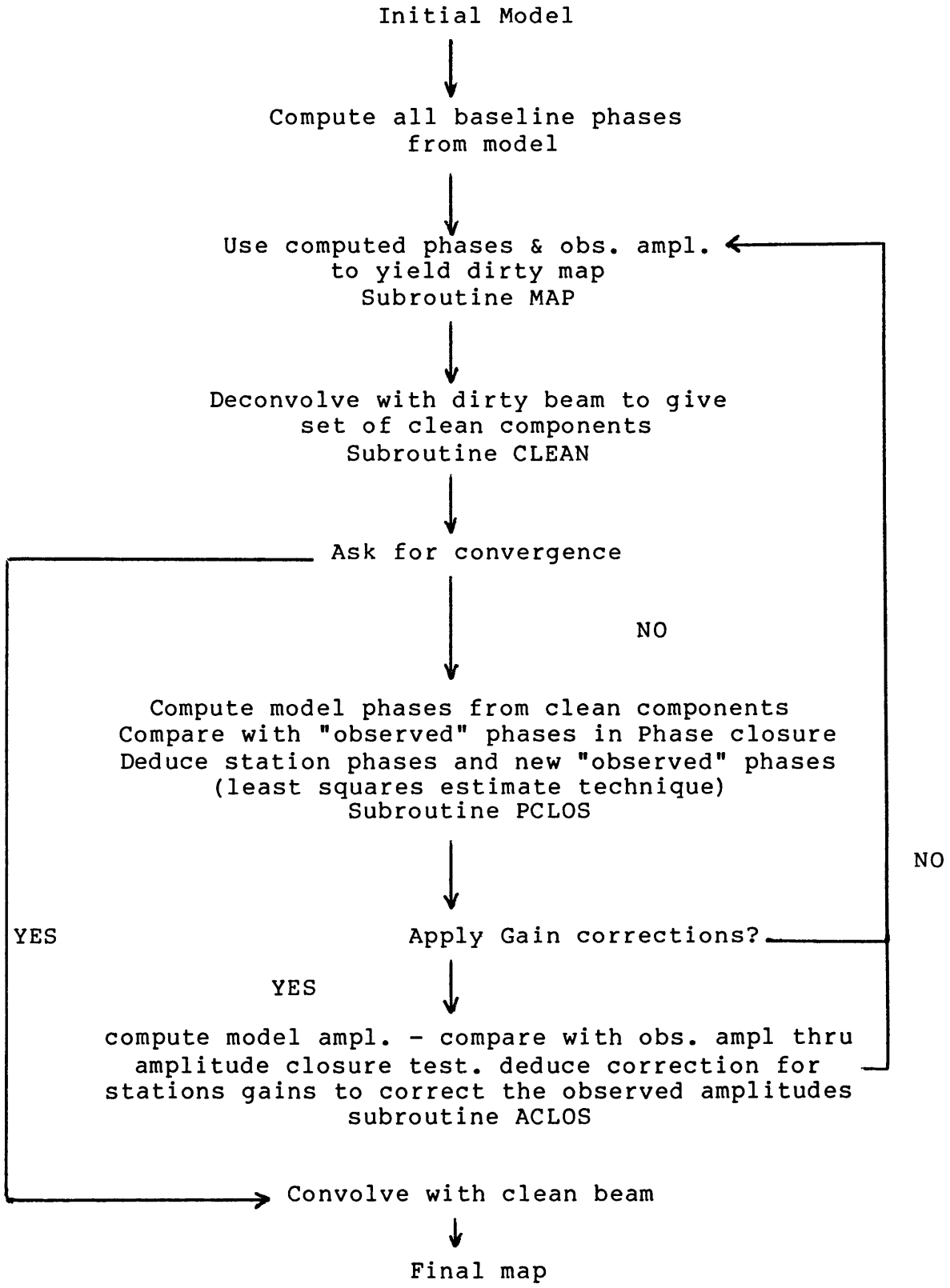

phases and adjustments to gains are calculated each time the program goes into the loop. The flow chart of the hybrid mapping program (Figure 1.5.2) shows how the different subroutines are connected to each other.

1.6 Description of the programs CLNFL and PLOT

The program CLNFL treats the output of the program MAPA. Its purpose is to plot the clean maps and display graphically the clean components which have been determined in the subroutine CLEAN of MAPA. In the cleaning process it often happens that several clean components are removed from the same grid point. The clean components for each grid point are therefore summed and displayed as a matrix: the largest value is normalized to 100% and the others are expressed as some fractions of it. Then to get a clean map, the clean components are convolved with a clean beam defined by its two full widths at half maximum (FWHM) along the major and minor axes. The orientation of the X-axis (the first listed) is given with respect to the north. The clean map can be convolved with different sizes of beam and can also be shown on different scales: an X-band map can be shown at S-band scale or an X-band set of components convolved with an S-band beam. However, because of a storage limitation the contours may appear coarse if the plotting cell size is of the same dimension as the FWHMs of the clean

beam.

The program PLOT is used to show how well a map agrees with the phase and amplitude closures and the individual correlated flux densities from each baseline. The RMS fits are computed for the two types of closures constraints. The user can also edit (downweight or upweight some points) a data file. All the plots can be shown on different scales.

1.7 Importance of the cleaning procedure, or influence of a small component on the group delay correction.

One of the purposes of this study is to estimate the effect of source structure on the measurement of the group delay, since this is the quantity which usually determines the accuracy with which baseline vectors can be estimated. At X-band ($\sim$8 GHz) 0.1 ns accuracy on the group delay corresponds to 3cm accuracy on the length of the baseline. For instance, when the radio source is almost a point source, one can show that neglecting a component equal to 1% of the peak value whose position is 4 mas north of the main component and 4 mas east may change the group delay by 3 ps and thus may cause an error of the order of 0.1 cm in the measurement of baseline length. In this case the error is negligible, but it can be shown that the contribution of the source structure on the group delay can be significant (see App.5).

2. X- and S-band maps of 1641+399 (3C345) for June 1981

2.1 Introduction

The second part of this thesis will try to justify the different assumptions used by the hybrid mapping program. Usually the initial model consists of circularly symmetric Gaussian components. This initial guess is indeed subjective and may be a critical step in the computation of the brightness distribution. It is advisable to check whether different models converge to the same hybrid map. Gain corrections may or may not be evaluated through the subroutine ACLOS. It is useful to study the manner in which gain corrections influence and modify the map. A comparison between the logarithmic and the linear procedure appears interesting because they use two different types of linearization. Gridding the u-v plane before convolution introduces modifications in the determination of the brightness distribution. These modifications can be studied by examining the influence of the number of cells and their sizes. The purpose of these studies is the elaboration of a method and the formulation of a set of criteria to produce well-defined radio source maps which are reliable enough to allow the possibility of a study of their evolution as a function of time and their utilization in performing precise geodetic measurements. Because 3C345 was observed quite intensively during 15, 16 and 17 June 1981, it was chosen to determine a

systematic method of mapping.

2.1.1 Notation

In June 1981 the data were collected at X-band (∿8.3 GHz) and at S-band (∿2.3 GHz) at four different stations during three days. The observations on the first day, June 15, 1981, is referred to as the "special" experiment and those of the two following days are called the geodetic experiment. The stations are located at Haystack and Westford in Massachusetts, Fort Davis in Texas and Owens Valley in California. For reason of simplicity, a certain number of abbreviations are used in the following paragraphs: PC stands for phase closure, AC stands for amplitude closure, HA for Haystack, WE for Westford, HR for Fort Davis, OV for Owens Valley. The phase and amplitude closures are numbered and the correspondance is given below:

PC1	Phase closure 1	Haystack-Westford-Fort Davis
PC2	Phase closure 2	Haystack-Westford-Owens Valley
PC3	Phase closure 3	Haystack-Fort Davis-Owens Valley
PC4	Phase closure 4	Westford-Fort Davis-Owens Valley
AC1	Amplitude closure 1	HA-WE,WE-OV,OV-HR,HR-HA
AC2	Amplitude closure 2	HA-WE,WE-HR,HR-OV,OV-HA
AC3	Amplitude closure 3	HA-OV,OV-WE,WE-HR,HR-HA

2.2 Theoretical uncertainties of the closures

a) Phase closure

For the usual case where $\rho << 1$, the uncertainty of the fringe-phase estimate is $\sigma(\hat{\Psi}) \simeq 1/\mathrm{SNR}$, where the SNR is the signal-to-noise ratio, defined as $\rho\sqrt{2BT}$ [3]. The B refers to the bandwidth and T to the duration of the observation. The correlation coefficient ρ can be approximated by $F\sqrt{A_{c1}\ A_{c2}}$ where the A_{ci} are the antenna sensitivity constants. For some sources the flux density F of the source taking into account it is resolved on the baseline is expressed reasonably well by [11]:

$$F = S_o \exp(-\alpha b_p) \tag{32}$$

where b_p is the length of the baseline as projected on a plane perpendicular to the direction to the source, $b_p=\sqrt{u^2+v^2}$, S_o $(\mathrm{WHz^{-1}m^{-2}})$ is the estimated flux density for zero baseline length and α is a constant derived from previous observations. Recalling Equation (2), we define the theoretical uncertainty in the phase closure to be the standard deviation in the phase closure which is given by:

$$\sigma(C_{ijk}) = \sqrt{\Sigma\sigma^2(\Psi_{ij})} \tag{33}$$

From Equation (32) one can estimate the correlation coeffi-

cient and compute the standard deviations. For 3C345, these standard deviations $\sigma(C_{ijk})$ are of the order of a few tenths of a degree compared to the experimental RMS scatter of a few degrees. At S-band for instance, the phase closure HA-WE-HR is inconsistent: it should be flat and of zero value (see Figure 2.1). The structure contribution is the same on WE-HR and HA-HR since the HA-WE interferometer cannot resolve the source. This situation is certainly the result of a systematic error that cannot be explained by random noise.

b) Amplitude closure

Recalling the amplitude closure (Equation 15) and assuming that the standard errors of the y_i are zero mean and independent, the variance of the error in the amplitude closures can be defined as

$$\frac{\sigma_R^2}{R^2} = \sum_i \frac{\sigma_{yi}^2}{y_i^2} \qquad (34)$$

where σ_R^2 is the variance of the error in R and σ_{yi}^2 is the variance of the error in y_i. The theoretical uncertainty in the amplitude closure can be taken as σ_R^2. Note that the σ_{yi}/y_i are by definition the inverse of the signal-to-noise ratios. For 3C345 they are above 200, and consequently the theoretical standard error is 0.01.

2.3 The point source approximation and the so-called "bad" points

If we consider the quasar as an unresolved source then the phase closure should be exactly zero and the amplitude closure should be unity. It is interesting to see how incorrect this assumption is. For this purpose, "equivalent" phase closure and amplitude closure RMS residuals have been defined (see §2.4.1).

When we first display the closure phases and the observed amplitudes, some of them have large deviations from their neighboring points for no apparent reason: the kinds of deviations that were encountered were rapid variations in amplitudes and jumps in phases. Since no realistic model will match such observations, it appears reasonable to delete them and see how this deletation changes the maps. For the point-source model, equivalent RMS on the different phase closures and amplitude closures have been computed in both cases (see Table 1). At X-band for 3C345, 20 points out of 513 were deleted to produce the final map.

Table 1

	all data	20 "bad" points deleted
PC1	2.1^{o}	2.1^{o}
PC2	2.6^{o}	2.6^{o}
PC3	8.37^{o}	8.30^{o}
PC4	8.70^{o}	8.24^{o}
AC1	0.501	0.505
AC2	0.484	0.487
AC3	0.028	0.028

In this case, the "bad" points have very little influence on the different RMS fits because of the number of data. However, one will see that significant changes may occur in the RMS fits and in the brightness distribution of the small components if the amount of data is smaller (see §3.1 for instance). The deletion of a point implies the deletion of its amplitude and its phase at the same time.

2.4 Determination of a map at X-band

2.4.1 Elaboration of a set of criteria for convergence

Since the hybrid mapping is an iterative process, one needs to know when to stop iterating. For our purpose, we decide to terminate iteration when two statistics, defined below, remain constant within the precision of the computer from iteration to iteration. The first statistic is given by [1]

$$R1 = \sqrt{(1/N) \sum_{ij} (\Phi^{o}_{ij} - \Phi^{m}_{ij})^{2}} , \qquad (35)$$

where i-j is the label of a baseline where we have a measure of correlation coefficient, N is the number of measurements, Φ^m_{ij} is the phase predicted by the model and Φ^o_{ij} is defined in Equation (6). It can be seen that Equation (35) is a measure of the quality of the fit in the phase. The second statistic is given by [1]

$$R2 = \sqrt{\frac{1}{N} \sum_{ij} \frac{(y^o_k - y^m_k)^2}{(y^m_k)^2}} \qquad (36)$$

where the y_k are the correlated flux densities. Equation (36) is a measure of the quality of the fit in the amplitude. Because of the quality of the data, the simultaneous minimization of R1 and R2 may not always be possible and the adjustments in phase and in gain which are applied in the subroutine PCLOS and ACLOS between each iteration never become zero (i.e. these adjustments add and subtract small components of flux density). Thus, a measure of the convergence and reliability of the map is based on the magnitude of the amplitude and phase fit residuals and the magnitude of the gain and phase adjustments. The smaller these adjustments and residuals are, the more certain the convergence is because one cannot expect any improvement from further iterations.

After several iterations (usually around 10), the quality of the fits are similar for maps obtained from different initial models. Moreover, the adjustments between

iterations are of comparable magnitudes. At this stage it appears necessary to define other criteria to determine if a given map can be considered as the final map which will be used to correct geodetic measurements for source structure. To do so, we have two tests at our disposal. The first one tells how well the model satisfies the phase closure test, and the other one concerns the amplitude closure test. For the phase closure test we compute the observed phase closures. Each phase closure involves three stations which were observing a given source at the same GST (Greenwich Sidereal Time). This phase closure is compared with the one predicted by the model by means of the following formula:

$$\sqrt{(1/N) \sum_{GST} (C^{o}_{ijk}(GST) - C^{m}_{ijk}(GST))^2} \quad , \quad (37)$$

where N is still the number of closures for a given set of three stations. Thus, for four stations Equation (37) gives four similar quantities. There are four different ways of choosing 3 stations out of 4. A given map will be said "good" when the RMS residuals on the phase closure are the same as the theoretical uncertainty (see §2.2). In reality the RMS is always greater than the theoretical uncertainty and thus, a map which minimizes the RMS is called the "best" map. A map is all the more reliable if the RMS residuals are close to the theoretical uncertainty. The second statistic gives a measure of the residual amplitude closure. For four stations we have six ways of combining four ampli-

tudes out of six, to form a closure. Recalling Equation (15), it is easy to see that $R_{ijkl} = R^{-1}_{klij}$. Thus, we have only three independent closures (6 divided by 2). Every conjugate pair of amplitude closures R_{ijkl} and R_{klij} is calculated with the same observed amplitudes and gives the same intrinsic information. For every independent configuration of closure we compute

$$\sqrt{\sum_{GST} \frac{1}{N} \frac{(R^o_{ijkl} - R^m_{ijkl})^2}{(R^m_{ijkl})^2}} = f(R_{ijkl}), \qquad (38)$$

where N is the number of closures obtained for the configuration (ij-jk-kl-li). The summation is done over the GST's of common observations. As for the phase closures, the "best" map is a map which gives RMS residuals on the amplitude closures closest to the theoretical uncertainty (see §2.2 b). However, for reasons stated earlier, it may happen that the RMS residuals on the phase closures and the amplitude closures are not at their minimum values simultaneously.

If one takes the point-source approximation, $C^m_{ijk} = 0$ and $R^m_{ijkl} = 1$, Equations (37) and (38) become respectively:

$$\sqrt{(1/N) \sum_{GST} (C^o_{ijk})^2} \qquad (39)$$

and

$$\sqrt{(1/N) \sum_{GST} (R^o_{ijkl} - 1)^2} \qquad (40)$$

It is important to keep in mind that the following maps have been made using these four criteria. The ones which are presented minimize the 4 statistics, when possible. When it was not possible to satisfy the 4 minimizations simultaneously, the minimization of the statistics relative to the phase were the criteria. A good phase closure is more important than a good amplitude closure because, as discussed in §1.2, the phase closure is the only existing phase information, whereas there is other amplitude information available which are contained in the correlated flux densities from every baseline. For the correlated flux densities, agreements between the model and the observations are easily obtained when gain corrections are calculated in the subroutine ACLOS (see Table 10).

2.4.2 Remarks about the mapping of 3C345 from June 1981 data

a) Relative location of the antennas

The relative locations of the four radio-telescopes have a remarkable characteristic: two stations are very close to each other. Haystack and Westford are separated by only 1.2 kilometers. As a consequence the minimum fringe spacing is $\sim$ 6 arcseconds at X-band and thus, the Haystack-Westford interferometer is sensitive only to large scale

structures which cannot appear on our map. However, if there is a large scale structure which appears on the closures, no model made at the milliarcsecond level will be able to fit the closures. The hybrid mapping program cannot distinguish between the two baselines Westford - Owens Valley and Haystack - Owens Valley. Also the two baselines Haystack - Fort Davis and Westford - Fort Davis cannot be distinguished from each other (see geometry of the stations). Thus, we cannot expect any milliarcsecond scale source structure contribution to the closure phase for the two triplets WE-HA-HR and WE-HA-OV : the phase closures #1 and #2 will exhibit only noise. For the same reason the amplitude closure #3 will always be close to unity and will exhibit only noise. Source structure will be seen only on the two remaining phase closures and two remaining amplitude closures. Moreover, because Haystack and Westford are very close to each other, the two PC and AC should differ only in the contribution of noise from Haystack and Westford. Tables 1 to 12 show that the phase closure fits on HA-HR-OV are constantly better than the phase closure fits on WE-HR-OV. This can be an indication that Haystack has a more sensitive system at X-band than does Westford.

Geometry of the amplitude closures

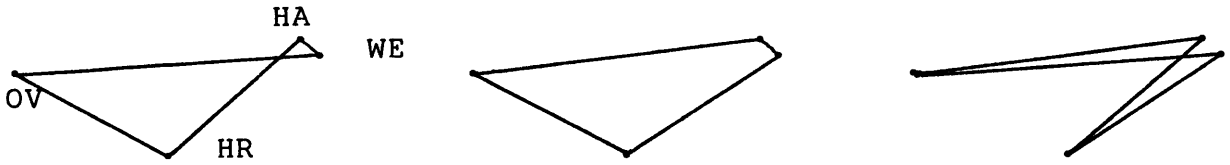

Not to scale

AC 1 AC 2 AC 3

b) Characteristics of the data

The flux densities (Jy) are given as an approximation: calibration of the data requires that the measurements of the antenna and system temperatures are taken regularly (once each hour at each of the antennas for instance) and accurately. For the June experiment only approximations of the system temperatures and the gains were taken to compute the correlated flux density of each baseline. However, the amplitudes can be made self-consistent by adjusting each antenna gain at each station (see §1.3). This procedure has been used to produce the following maps.

2.4.3 Influence of the loop gain on the maps

As seen in §1.5.1 the fraction of flux density which is subtracted from the peak value for each iteration of the subroutine CLEAN is called the loop gain. This gain can be chosen to be any value between 0 and 1, but a value near 0.5

gives better results (i.e. better phase and amplitude agreement).

If the gain is greater than 0.5, then the cleaning procedure seems to pick up more flux components located on the edges of the map. Moreover, because more flux density is subtracted at each iteration, the list of the clean components contains a greater number of strong components, but the total number of components is less for the same cleaning limit (see §2.4.4). The result is that the oscillations are larger in amplitude and in frequency for the phase closure.

If the loop gain is smaller than 0.5, the cleaning process is less sensitive to the sidelobes of the dirty beam and small clean components are smoothly distributed around strong ones. Thus, it would seem much better to have an infinitesimal loop gain. However, the total number of clean components is limited by the size of the computer, and if the number of iterations necessary to reach the cleaning level (see §2.4.4) is greater than 100 (this number is fixed by storage limitation) we lose information about components and flux density. In these conditions, it seems optimal to take the loop gain as small as possible to obtain a number of clean components as close to 100 as possible. However, the PC is not improved by taking a loop gain much smaller than 0.5 (see Table 2). It is also interesting to note that the absolute values of the adjustments in phases after each iteration are much greater for a loop gain of 1 (0.4^{o}) than

for a loop gain of 0.50 (0.1^{o}). In other words, for a loop gain of 1, the program does not seem to be able to make the map converge uniformly to the solution according to the criteria which have been set in §2.4.1. This instability may be a consequence of subtracting the whole dirty beam from the dirty map, since the sidelobes have an adverse effect on the convergence.

In the following Tables, all quantities relative to the phases (PC) are in degrees, and the quantities relative to the amplitudes (AC) or gains are in fractions of unity.

Table 2

Results for loop gains of 0.25, 0.5 and 1

loop gain	0.25	0.50	1.00
# of cells	64x64	64x64	64x64
cell size	0.25 mas	0.25 mas	0.25 mas
# of iterations	10	10	10
flux density(Jy)	17.	18.	19.
# of components	100	65	30
phase fit	1.6	1.6	1.8
phase adjustments	0.1	0.1	0.4
PC 3 fit	3.3	3.2	3.9
4	4.2	4.2	4.5
AC 1 fit	0.208	0.142	0.110
2	0.196	0.133	0.110
3	0.028	0.028	0.028

The phase fit is the statistic given by Equation (35), and the phase adjustments indicate the absolute value of the adjustments for the station phases after the 10^{th} iteration.

The fraction of flux density subtracted from the dirty beam and located at a grid point is called clean component. The number of clean components refers to number of times the dirty map was cleaned by the dirty beam. The effective number of clean components is smaller for a reason already discussed in §1.6.

2.4.4 Influence of the cleaning process

a) The cleaning limit

When one deconvolves the dirty map with the dirty beam, one progressively cleans the map as previously discussed until the peak value reaches a certain fraction of the original peak value, called the cleaning limit. The consequences of this limit on the closure fits are the following: the 0.3% limit gives a better AC fit ($f(R_{ijkl})$ in Equation (38) is reduced by 1.5) than 1% . The 1% limit gives half the number of clean components obtained for the 0.3% limit, the stronger of which retain the same relative position. The consequences on the PC are negligible (Table 3): in both cases it remains just as well satisfied but the AC, as already stated, is remarkably changed. This points out the importance of small components on the amplitude closure. Following this remark, it seems interesting to see what happens to the different closures when we intentionally

neglect the smaller components (§2.4.4 b)). Table 3 shows how well the model agrees with the data for two cleaning limits: 1% and 0.3% .

Table 3

Results obtained with a cleaning limit of 1% and 0.3%

# of cells	64x64	64x64
cell size	0.25 mas	0.25 mas
# of iterations	10	10
loop gain	0.50	0.50
cleaning limit	0.3%	1%
# of components	65	36
RMS phase fit	1.6	1.6
PC 3 fit	3.2	3.3
4	4.2	4.2
AC 1 fit	0.142	0.220
2	0.133	0.208

b) Influence of small components on the closures

The strongest components are responsible for the overall shape of the PC. On the other hand, Table 4 shows that the smaller components have a significant effect on the AC. This difference can be related to the fact that the convergence occurs faster for the phases than for the amplitudes. It was noticed that the RMS residuals of the PC decreased rapidly during the first few iterations, which recover the strongest components, and that thereafter the PC improved very little whereas the AC residuals were still decreasing. The following table shows the different fits when some of the clean components are neglected.

Table 4

Variation of the AC and PC fits
with the number of clean components

# of iterations	10	10	10
# of cells	64x64	64x64	64x64
cell size	0.25 mas	0.25 mas	0.25 mas
# of components	65(all)	first 30	first 15
flux density(Jy)	18.	16.	15.
PC 3 fit	3.2	3.4	4.2
4	4.2	4.3	4.8
AC 1 fit	0.142	0.231	0.322
2	0.133	0.218	0.308

c) The weighting function and the dirty beam

The dirty beam can be defined many different ways depending on the choice of the weighting function. The program allows two choices. The first one utilizes the uniform weighting: the weighting function $g(u_o,v_o)$ is either equal to unity if there is at least one observation at (u_o,v_o) or zero if none. In this case downweighting some points will change the dirty map and may not change the dirty beam at all. The second way proposed is a non-uniform weighting: the weighting function $g(u_o,v_o)$ is equal to the number of observations at (u_o,v_o). As shown in Figure 2.2, the dirty beam obtained from non-uniform weighting has more irregular contours than the uniformly weighted one.

For a given value of the cell size, field of view, loop gain and cleaning limit, the two weighting functions have been tested. The results are displayed in Table 5.

Table 5

Influence of the uniform and the non-uniform weighting on the different fits

uniform weighting		non-uniform weighting
more components	65	less components 31
less flux	18.0 Jy	more flux 18.5 Jy
fits phases and phase closures	better	fits amplitude closures better
P.C 1	2.1	2.1
2	2.6	2.6
3	3.2	4.0
4	4.2	4.8
A.C 1	0.142	0.113
2	0.133	0.107
3	0.028	0.028

It can be concluded that, since the uniform weighting gives better agreement in phase closures, it will be used henceforth.

2.4.5 Number of iterations

The hybrid mapping program is a fast convergent process in the sense that after about 10 iterations the RMS fits on the phase and on the amplitude closures do not change significantly. They seem to reach a state of equilibrium wherein the adjusted model oscillates around a mean model: adjustments are less than 0.1 degree in absolute value for the phases and less than 0.01 in absolute value for the gain at each iteration. Table 6 shows the difference in fits

after 10 and 25 iterations.

Table 6

Influence of the number of iterations on the quality of the fits

# of cells	64x64	64x64
cell size	0.25 mas	0.25 mas
# of iterations	10	25
flux density(Jy)	18.	18.
# of components	65	70
phase adjustment	0.1	0.1
gain adjustment	0.008	0.008
phase fit	1.6	1.6
PC 3 fit	3.2	3.3
4	4.2	4.2
AC 1 fit	0.142	0.138
2	0.133	0.130

2.4.6 Initial model

One of the checks which were performed on the convergence ability of the program was to test the sensitivity of the final model to changes in the initial model in the hope that the answer would be as independent as possible of the initial model. Different brightnesses, shapes and positions of the components have been tried successively.

From these tests, it can be concluded that the absolute brightness of the various components does not affect the phase closures and the amplitude closures. What matters only is the relative flux density between the components.

The phases predicted by the initial model are calcu-

lated in the program MODX. They are used only during the first iteration in addition to the observed amplitudes to compute the complex visibility. Any symmetric model (point source, circular, elliptical) at the center of the map will give zero phase for any (u,v) point. Consequently, the program does not make any distinction between these different models. The shapes of the components affect the solution when they are not at the center of the map since the visibility is expressed as [1]:

$$V(u,v) = \sum_j F(j)\ \exp\{-kS_j^2\ [(u\sin\phi_j+v\cos\phi_j)^2+R^2(u\cos\phi_j-v\sin\phi_j)^2]\}$$
$$\exp(2\pi i\ d_j(u\sin\alpha_j+v\cos\alpha_j)) \qquad (41)$$

where d_j is the distance of the j^{th} component from the center of the map, S_j is the FWHM of the component along the major axis and R is the ratio of the length of minor axis to that of the major axis. The angles ϕ_j and α_j are defined in the figure below:

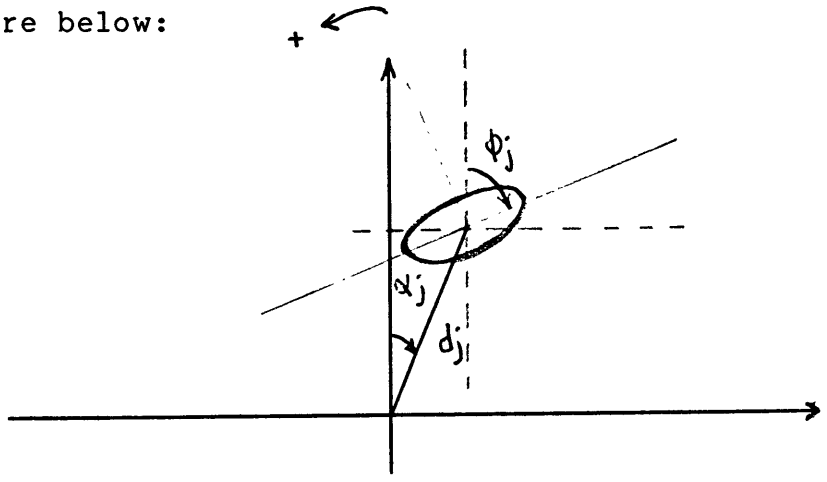

During the mapping of 3C345, a small component of brightness appears 2 mas west of the main component even

using several different initial models. It seems interesting to see how well an initial model which is close to the final result would converge towards the presumed solution. The result is disappointing in the case of 3C345: no major improvements are noticed in the different RMS fits. However, the results tend to be much better for 4C39.25 when a double point model is given instead of the point source model at the first iteration (see §3.1).

In the a priori model if the main component is not put at the center of the map but no more than a few cells away (thus displacing artificially the center of brightness from the physical center of the map) the final map has many other "noisy" components which do not appear in other maps (see Figure 2.3). This situation gets worse when the component is displaced from the center by more than two or three cells.

Having mapped 3C345, a model (see Figure 2.4) which does not correspond to the model for the final map which was previously obtained was given as initial guess: the process did not converge. One cannot distinguish the true features from the other imaginary features which have been picked up. The ACs and PCs do not agree any more. The phases are badly predicted (Equation 35): they agree to 7.6^{o} after 10 iterations compared to the 1.4^{o} obtained for the "final" map, 7.5^{o} after 20 iterations and 10.9^{o} after 30 iterations. The fits do not improve beyond the 30^{th} iteration (see Figures 2.4).

It can be concluded that it seems critical to choose a good model since the program has trouble translating components when they are not at the correct location with respect to each other and when the center of brightness does not correspond to the physical center of the map. Choosing the simple point-source model has the advantage of highlighting the basic overall structure of the source, and then, one can redo the solution with a more precise initial model whose center of brightness is at the center of the map.

Table 7

Differences in the maps obtained from different initial models

initial model	any symmetrical model	2pt-model	July 80 model	main comp. offset by 0.5 mas
# of cells	64x64	64x64	64x64	64x64
cell size	0.25 mas	0.25 mas	0.25 mas	0.25 mas
# of iterations	10	10	10	10
flux density(Jy)	18.	18.	17.	18.
# of components	65	71	55	53
RMS phase fit	1.6	1.7	1.7	1.7
PC3 fit	3.2	3.5	3.9	3.6
PC4	4.2	4.4	4.5*	4.4*
AC1	0.142	0.133	0.067*	0.073*
AC2	0.133	0.125	0.061	0.075

* linear gain corrections were applied from the first iteration in the subroutine ACLOS.

2.4.7 Gain correction

a) Linear gain correction

As stated earlier, the antenna gains are not constant during a single experiment because they are functions of the antenna efficiency, η, which depends on the source elevation. At X-band for the HA-WE interferometer, although the correlated flux density should be constant, we notice an obvious decreasing trend with time (see Figure 2.5) which will affect the dirty map. One way to solve this problem is to introduce gain adjustments to the initial antenna gain. These adjustments can be calculated by two similar but different methods: linear and logarithmic (see § 1.3 and App.3).

If we apply these corrections the RMS residuals on the AC are improved by a factor of two and the fit on the correlated flux density between the model and the observations given in Equation (36) improves (see Table 8 first and second column). Roughly ten iterations after application of gain correction, the PC and AC residuals converge because these corrections are done independently of the convergence on the phases (see Table 8 columns 3 and 4). Still, better RMS residuals are not obtained by further iterations (see Table 8 columns 2 and 3). When one applies gain corrections, the corrections are done for each GST of observation. When no AC is available for a given time, it is possible to

make the observed amplitudes match the model amplitudes by arbitrarily increasing or decreasing the gains because there is no constraint on the gain adjustments. Thus, the adjustments can introduce unrealistic wiggles in the correlated flux density.

Table 8

Results obtained from a point source initial model with a cellsize of 0.25 mas and 64x64 cells

	10 it No gain cor	10 it Gain cor from 1 it	25 it Gain cor from 1 it	25 it Gain cor after 10 it
RMS phase fit	1.6	1.6	1.7	1.7
amplitude fit	0.075	0.022	0.021	0.022
PC 3 fit	3.2	3.7	4.2	4.2
PC 4	4.2	4.5	4.8	4.9
AC 1	0.142	0.082	0.064	0.064
AC 2	0.133	0.075	0.063	0.062

b) Logarithmic and linear correction

The two methods of logarithmic and linear correction give nearly the same results (see below Table 9). They give comparable phase and amplitude agreements and consequently one map can not be considered better than the other one.

Table 9

Results obtained from a point source initial model with a cellsize of 0.25 mas and 64x64 cells

	linear	logarithmic	logarithmic
# iterations	10	10	20
flux density	16.6	16.6	16.7
RMS phase fit	1.6	1.6	1.6
PC 1 fit	3.7	3.7	4.1
PC 2	4.5	4.5	4.8
AC 1	0.082	0.086	0.064
AC 2	0.075	0.079	0.062

2.4.8 Over- and Underresolution

a) Problems caused by the dimensions of the mapping field

In the model file one must give twice the dimensions of the largest source structure to be mapped. These dimensions determine the size of the cells used to grid the u-v plane. All maps were done with square cells. A Δu of 483 km corresponds to a field of view of 8 mas but Δu's of 967 km, 1208 km, 1611 km and 2417 km have been tried to study the influence of the field of mapping on the phase closures and the amplitude closures. For Δu=967 km there is evidence of flux density coming from a region 2 mas west of the main component. The following results have been derived when we restrict our field of view to 4 mas, 3.2 mas, 2.24 mas and 1.6 mas.

For a width of 4 mas the map shows a component just on the border of the map (Figure 2.6b). When the width is 3.2 mas the component cannot theoretically appear on the map since it is too small to contain both the main and the small component. One still gets a map which looks like the previous ones done at 8 and 4 mas (see Figure 2.6c). The small component appears on the edge and its flux density relative to the main component has increased from 0.09 to 0.12. The more one reduces the width of the mapping field, the worse the closures become (see Figures 2.7a, b, c, d and e and Table 10). However the divergence is not monotonic, as we can see in the second column of Table 10. For the extreme case where the width is 1.6 mas we are looking at the source through a window which is smaller than the geometric resolution of the longest baseline interferometer ($\simeq$ 2 mas). After 10 iterations the map still looks like it contains only one strong component. From this study it appears that one should be suspicious when contours are systematically found greater than 5% along the border. This appearance can be an indication of components outside the field of mapping.

Table 10

Influence of the field of mapping
on the quality of the fits

width(mas)	8.00	4.00	3.20	2.24	1.60
# of cells	64x64	64x64	64x64	64x64	64x64
flux density	18.0	16.2	16.2	15.0	14.6
# of iterations	10	10	10	10	10
# of components	65	46	44	30	25
RMS phase fit	1.6	1.8	2.2	2.4	2.5
PC 3 fit	3.2	4.4	6.2	7.1	8.0
PC 4	4.2	5.0	6.7	7.6	8.3
AC 1	0.142	0.280	0.147	0.169	0.322
AC 2	0.133	0.267	0.139	0.156	0.304

b) determination of the optimum field of view

Because the array dimensions are at most 64 by 64, when one increases the resolution by taking a smaller cell size, the mapping area is reduced. This reduction causes a deterioration of the results of the closure tests. When one enlarges the field of the map, one tends to reduce the different RMS residuals of the closures. However, there seems to be an optimum size of the cells for a given number of cells (see Table 11). This size is between 0.3 and 0.4 mas for the present case. One of the reasons for this possible optimization is that, as we have seen in the previous paragraph, taking too small a cell size makes the RMS fits on phase and amplitude closures increase. A good way to avoid this problem, if we do not know beforehand what the positions of the components are, is to map a larger field. However, if we increase the map size by too large an amount, we tend to lose our resolution ability by putting in the

middle of one cell two components that would be separated otherwise. Moreover, one cannot increase indefinitely the cell size because the corresponding gridding interval decreases in the u-v plane and may force some data to be left out: this limitation is called underresolution. The optimum cell size in our case seems to be about 0.35 mas (see Table 11).

At X-band for June 1981 the two principal axes of the elliptical beam are 1.6 mas and 1.1 mas. The major axis is oriented at a position angle of -25^{o}. The Figures 2.8a, b and c show the different phase closures and amplitude closures as well as the correlated flux density on the 6 baselines for the "final" map obtained with a cell size of 0.35 mas.

Table 11

Determination of the optimal cell size

# of cells	64x64	64x64	64x64	64x64	64x64
cell size	0.25	0.30	0.35	0.40	1.00
flux density	16.6	16.8	16.7	16.6	16.8
# of iterations	10	10	10	10	10
# of components	44	52	42	49	54
RMS phase fit	1.6	1.7	1.5	1.5	1.7
RMS amplitude fit	0.022	0.019	0.015	0.015	0.020
PC 3	3.7	3.8	2.9	3.8	3.9
PC 4	4.5	4.6	2.8	3.7	4.5
AC 1	0.082	0.072	0.067	0.063	0.072
AC 2	0.075	0.066	0.060	0.058	0.071

2.4.9 Map obtained from two days of geodetic data

A map of 3C345 can be deduced from the two days of geodetic observations obtained in June 1981: the time coverage is the same as for the previous maps but the data are more widely spaced. The purpose of making such a map is to compare the map with that obtained from the previous observations. The comparison is of interest for several reasons. Firstly, one would like to know if it is posible to recover the brightness distribution from fewer data obtained during a VLBI geodetic experiment. Secondly, one would see how different from each other the brightness distributions are. Indeed, one can expect some differences in the calculated brightness distribution since we are now using 23 phase closures instead of 98 and 117 correlated flux densities in the u-v plane instead of 493.

Table 12

Differences in the results between the 3-day experiment data and the geodetic experiment data

	98 phase closures	23 phase closures
# of iterations	20	20
# of cells	64x64	64x64
cell size	0.35 mas	0.35 mas
flux density(Jy)	16.8	16.8
# of components	39	45
RMS phase fit	1.4	1.0
amplitude fit	0.012	0.012
PC 1 fit	2.1	2.4
PC 2	2.0	1.3
PC 3	2.5	1.9
PC 4	2.7	2.7
AC 1	0.048	0.040
AC 2	0.044	0.037
AC 3	0.024	0.024

Figures 2.9a and b show the respective brightness distributions. The clean maps are shown in Figures 2.9c and 2.9d. The restoring beam is overresolved by 1.8 to enhance the differences between the two maps. The phase and amplitude closures for the geodetic experiment are shown in Figures 2.10a and b. The results show that the fits are of the same quality in both cases. The map obtained from 98 closures cannot be considered better than the other one. This study proves that for a duration close to 10 hours one can recover a reliable brightness distribution of a radio source with less data, provided that the u-v samples are taken at regular intervals. This kind of geodetic experiment allows a good brightness reconstruction.

2.4.10 Diffences between the July 1980 and the June 1981 maps

The map obtained from 3.6 cm MARK III VLBI observations [12] in July of 1980 is different from the one obtained in June 1981 in several respects. It seems certain that the flux density of the source increased because the standard errors for the phases and group delays obtained with the same interferometers were reduced severalfold from July 1980 to June 1981. If the June experiment had been done with same interferometers, the small component which appeared above the 10% contour in July 1980 (see Figure 2.11) would now, if unchanged, appear as a 5% contour. The resolution of the map was much better in July 1980 than in June 1981 because of the use in the earlier experiment of intercontinental baselines of 8000 km length. The longest baseline used in June 1981 was 4000 km. The FWHMs of the major and minor axes of the clean beam were respectively 1.6 mas and 1.1 mas for the June 1981 experiment compared to the corresponding FWHMs of 1.10 mas and 0.48 mas for the July 1980 experiment. The smaller baselines used in June 1981 and the change in flux density of the core tends to make the source appear more like a point-source.

2.5 S-band Map: Comparison with the X-band map

In July 1980 and in June 1981 the total flux density at S-band (ν2.3 GHz) was nearly the same - about 6 Jy - while at the same time there was an increase at X-band. The data at S-band are less numerous than at X-band: 386 correlated flux densities in the u-v plane instead of 493 and 75 phase closures compared to 98. Moreover, the data are not so good as at X-band: the closure test (HA-WE-HR) is not flat as expected (see Figure 2.1): we can conclude that a systematic error must have been introduced. Because of the quality of the data (inconsistency in the phases) it is much more difficult for any model to fit such data and as a consequence we obtain RMS fits less satisfying.

After taking out the "bad" points, approximately ten in number, we obtained the following results after 10 iterations. we found fast convergence as at X-band: the phase and amplitude RMS fits remain practically constant after 10 iterations and the phase and gain adjustments stay under a certain absolute value 0.1° and 0.006 respectively (see Table 13). Gain corrections were needed to fit the correlated flux densities on the individual baselines. The dirty beam and dirty map are shown in Figures 2.12a and b. The two FWHM's of the principal axes of the main lobe of the dirty beam are 5.4 mas and 3.6 mas. The major axis is oriented at a position angle of -25°. The matrix of the clean components and the clean map are shown in Figures

2.13a and 2.13b. The phase closures and amplitude closures are displayed in Figures 2.14a and 2.14b.

Table 13

Final results at S-band

# of cells	64x64	point source
cell size	1.15 mas	
loop gain	0.5	
cleaning limit	0.3%	
# of iterations	10	
flux density(Jy)	6.	
RMS phase fit	11.6	
amplitude fit	0.047	
PC 1	8.0	8.0
PC 2	4.1	4.1
PC 3	4.7	15.3
PC 4	4.5	15.4
AC 1	0.157	1.368
AC 2	0.093	1.339
AC 3	0.151	0.151

The map produced for the June experiment at X-band shows a very strong central component which contains more than 90% of the total flux density and thus, tends to wash out the other features. The X-band map appears more compact than the S-band. At S-band, the map is more extended and the main component contains only 50% of the total flux density. Figure 2.15 shows two maps made from the components determined at S-band and at X-band respectively. They are convolved with the same beam 1.60 mas by 1.10 mas oriented at a position angle of -25°. This beam corresponds to the X-band beam. For the S-band map it corresponds to a beam overresolved by 3.5 .

3. X-band maps of other radio sources for the June 1981 experiment

3.1 The double source 0923+392 (4C39.25)

As seen in Chapter 2, it was possible to determine adequately the brightness distribution of 3C345 from data obtained only during a geodetic VLBI experiment. For 4C39.25 the data obtained during the geodetic experiment in 16, 17 June 1981 are spread over 10 hours. They consist of 115 correlation flux density data and 30 phase closures. Unfortunately there are some gaps in the data, one as long as two hours. The correlated flux density varies greatly for the baselines HA-HR, HA-OV, WE-HR and WE-OV : the ratio of the largest value to the smallest is of the order of six. Moreover, at different times, the amplitudes come close to zero. A model consisting of two components of comparable brightness can explain this behaviour.

The procedure used to map 4C39.25 was to start from a point source model. The dirty map obtained after 10 iterations confirms this double structure, but it does not give a satisfying answer according to the criteria defined in §2.4.1: the map shows two components among many other noisy components. The term noisy components refers to components which do not retain the same location and the same strength from iteration to iteration. These noisy components tend to disappear and the RMS fits improve when the initial model is

changed to a double component model defined as follows:

	distance from the center	position angle	relative brightness
1^{st} component	1 mas	90^{o}	1.0
2^{nd} component	1 mas	-90^{o}	0.8

The same kind of problem had been encountered during the mapping of 3C345 when trying to offset the center of the brightness from the physical center of the map (see §2.4.6). When one starts with a point source model at the center, the program makes it coincide with the stronger component of 4C39.25; since there is another component of comparable brightness, the center of brightness is not at the center of the map and it was noticed that convergence does not occur. Based on the fits between the observed phase closures and the phase closures predicted by the model and between the observed correlation coefficients and the correlation coefficients predicted by the model, the optimal cell size was determined after several tries as 0.35 mas. As for 3C345, taking a bigger cell size introduces higher frequency oscillations in the phase and amplitude closures which do not exist in the data. On the other hand, if the cell size is too small the higher frequencies of the observed closures cannot be recovered. The map shown in Figure 3.1.1 has many components: its cleanness is limited by the gaps in the u-v coverage.

For comparison some simulated data were computed, then

several points were deleted to better match the conditions of the experiment. The fake data were obtained from a of a double point-source model and no noise was added. The mapping of this source was made from an initial model which was the the same double point-source model. The two maps are shown together in Figure 3.1.1 and one can notice their similarities. However, the simulated map predicts the phase closure better than the map made from the real data. The poor quality of the closures can partly explained this bad phase prediction: on the triplet HA-WE-HR, the PC predicted by the model gives an RMS scatter of 7.25^{o} about the predicted phase whereas one would expect, based on the SNR's of the different measurements, an RMS on the phases of 1^{o}. On the other hand the phase closure for the triplet HA-WE-OV gives an RMS of 2.0^{o}. From this test, it appears that reliability of the determination of the brightness distribution is limited by the amount of data. It was also noticed that even when no data are available the oscillations that appear in the amplitude closures and phase closures can be recovered.

The results are shown in Figure 3.1.2. The matrix of the clean components (Figure 3.1.3) shows that 4C39.25 is mainly composed of two components whose brightness ratio is 4:3 . From the brightness contours of the clean map one can also estimate the separation of the two components to be 1.8 $\pm$ 0.2 mas along a position angle of $-85^{o} \pm 10^{o}$.

3.2 0851+202 (OJ287)

OJ287 was observed during 3 days in June 1981. The corresponding time coverage spanned 10 hours. For each baseline, the correlated flux density varies only between 0.85 and 1.15 of its mean value. The final map shows that OJ287 is composed of one strong component whose flux density contains 80% of the total flux density. The data consist of 37 phase closures and 152 correlated flux density data. A cell size of 0.40 mas was taken to make the final map. The field of the map is a square box of width 12.8 mas. Besides the main component, the matrix of clean components (see Figure 3.2.1) shows small components which make the source appear elongated along the southwest direction. The dimension of the beam is 2.2 mas by 1.1 mas with a position angle of -15^{o}. The reliability of the map is still limited by the amount and the quality of the data: the RMS fits on the phase closures involving HA and WE are around 4^{o} whereas one would expect a random scatter of less than 2^{o} . The contours below 5% of the peak brightness are unreliable since their positions did not remain constant when other cell sizes were tried*. Figure 3.2.2 shows how the amplitude and phase closures are satisfied. The following table summarizes the different fits concerning OJ287 at X-band.

	final map	point source model
# of cells	64x64	
cell size	0.40 mas	
# of iterations	20	
# of clean components	28	
flux density	4	
PC1 fit	4.4	4.4
PC2	4.3	4.3
PC3	4.2	7.6
PC4	4.4	7.1
AC1 fit	0.131	0.553
AC2	0.096	0.479
AC3	0.081	0.081

Here and in the following tables, the quantities relative to the phases are given in degrees and the quantities relative to the gains or the amplitudes are given in fractions of unity. As for 3C345, the flux densities (Jy) are given as an approximation.

---

* The contours above 10% remain at the same location independently of the cell size whereas the contours below 5% depend on it. Since the shape of the dirty beam is a function of the grid spacing, the location of the contours below 5% is a artifact of the dirty beam and thus, the contours below 5% of the peak brightness are likely unreliable.

3.3 0355+508 (NRAO 150)

On June 16, 1981 during the geodetic experiment, NRAO 150 was observed for 10 hours with a 3-hour interruption. Seventy three correlated flux densities and 15 phase closures were used to produce a map. A point source was taken as the initial model. As for 4C39.25 the reliability of the map can be questioned because of the very small amount of data: only 9 amplitude closures are available for a period of 10 hours (Figure 3.3.1) The radio source appears almost as a square: the components are confined in a box 2.5 mas wide along the north south direction and 3.0 mas wide along the east-west direction (Figure 3.3.2). Wittels et al. described NRAO 150 as a source composed of two components. For the June 1981 experiment the matrix of the clean components still indicates the presence of two internal sources of flux density: the main component which contains 70% of the total flux density and a component whose brightness ratio is approximately 7:2 . One can estimate its separation from the main one as 0.8 mas along a position angle of approximately 65^{o}. This graphical determination does not give a more precise determination because the source is barely resolved. The following table summarizes the RMS fits for the phase closures and the amplitudes closures.

	final map	point source model
# of cells	64x64	
cell size	0.30 mas	
# of iterations	10	
# of clean components	39	
flux density	10	
PC1 fit	2.2	2.2
PC2	2.5	2.5
PC3	3.5	12.7
PC4	3.6	15.0
AC1	0.126	1.440
AC2	0.117	1.414
AC3	0.028	0.028

3.4 The extended radio source 1226+023 (3C273B)

The structure of the radio source 3C273 as determined by Hazard, Mackey and Shimmins in 1963 consists of two components separated by 20 seconds of arc [4]. The component A is much more extended than the component B and is resolved on baselines as short as a few kilometers for frequencies above 2 GHz. The scale of the component B is of the order of several milliarcseconds and is often used for geodetic measurements.

It was observed quite regularly during the 3 days of the experiment in June 1981. The following map was produced from 255 correlated flux densities and 49 phase closures (see Figure 3.4.1). After 10 iterations, the structure of 3C273B appears to be extended linearly and the components are distributed along a position angle of approximately 60^{o}. Compared to the radio sources mapped so far, this one is

much more elongated and consequently the field of mapping had to be extended to 16 mas. Because of the array dimensions a cell size of 0.50 mas had to be used. The total flux density of 3C273B is about 26 Jy.

The restoring beam is very elliptical: the axis ratio is 4. The reason for that is the very low declination of the quasar which makes the u-v elliptical track very elongated along the east west direction. Moreover, a low declination reduces a lot the period of common visibility between the antennas used in this experiment. The UT coverage is 7 hours long but quite regularly sampled.

However, the prediction of the phases (Equation 35) is no better than 6.6^{o}. Short baseline interferometers like HA-WE are sensitive to large scale structures: in the present case, the baseline HA-WE is sensitive to both components A and B. The phase closures involving HA-WE no longer have zero values because the phases of the visibility is no longer zero on HA-WE. Figures 3.4.2 show how well the model can predict the phase and amplitude closures. The following table summarizes the results obtained for the mapping of 3C273B.

	final map	point source model
# of cells	64x64	
cell size	0.5 mas	
# of iterations	10	
# of clean components	51	
flux density	26	
PC1 fit	17.18	17.18
PC2	17.61	17.61
PC3	4.86	28.11
PC4	7.85	30.25
AC1 fit	0.051	2.65
AC2	0.078	2.58
AC3	0.047	0.047

3.5 0552+398

The source 0552+398 was observed on two consecutive days during the geodetic experiment of June 1981: 108 correlated flux densities and 23 phase closures spread over 9 hours were taken. The map shown in Figure 3.5.1 was made from an initial point source model. A cell size of 0.30 mas and a window width of 9.60 mas were chosen to map this radio source because they produce a map which minimizes the RMS fits. This radio source is composed of one strong component which contains almost 70% of the total flux density of about 5 Jy (see Figure 3.5.1). There were some apparent inconsistencies in the amplitude data: jumps of 50% in less than 1 hour. As for other radio sources, it was noticed that changing the cell size made the contours below 5% of the peak brightness move: they are likely unreliable. The following table shows the different RMS fits. Figure 3.5.2

shows how well the model can predict the phase and amplitude closures.

	final map	point source model
# of cells	64x64	
cell size	0.30 mas	
# of iterations	10	
# of clean components	22	
flux density	5	
PC1 fit	3.6	3.6
PC2	4.8	4.8
PC3	3.7	6.8
PC4	4.7	7.9
AC1 fit	0.097	0.695
AC2	0.030	0.557
AC3	0.071	0.072

3.6 2200+420 (VRO 42.22.01)

This source was observed very irregularly on June 16, 1981. The data contain 71 correlated flux density data and 16 phase closures spread over 10 hours with one of the gaps being longer than two hours. The initial model is a point source and the cell size is 0.35 mas. The main component contains almost 50% of the total flux density of about 6 Jy. The components are distributed along an axis oriented at a position angle of 0^{o}. This distribution gives to the source its north south elongation (see Figure 3.6.1). This map confirms the assertion of Clark et al. [13] who suggested that although VRO 42.22.01 is highly variable, it maintains an elongation at a position angle of 0^{o}. Once again the u-v coverage is sparse and sometimes the data are of poor

quality: for the triplet HA-WE-HR the phase closure exists only for two hours out of ten and the RMS scatter is 5.2° although it should be less than 2° according to the signal-to-noise ratios of the observations. Changing the cell size also makes the contours below 5% move on the map: they are unreliable. The following table summarizes the RMS fits. Figure 3.6.2 shows how well the model can predict the phase and amplitude closures.

	final map	point source model
# of cells	64x64	
cell size	0.35 mas	
# of iterations	20	
# of clean components	31	
flux density	6	
PC1 fit	5.2	5.2*
PC2	2.2	2.2*
PC3	4.8	13.5
PC4	5.1	10.4
AC1 fit	0.055	1.985**
AC2	0.060	0.305**
AC3	0.050	0.075

* Theoretically one should get the same number on both phase closures, but since all stations did not always observe the same radio source at the same time, simultaneous measurements of the phase closure on both baselines are not always available; some phase closures which appear on one plot do not appear on the other and thus, give different statistics.

** Same reasoning as above but the statistics concern the amplitudes.

4. Conclusion

The maps which have been presented are the "best" according to previously discussed minimization criteria. The indications of a "good" map are the minimization of the phase closure and amplitude closure RMS fits. Unfortunately, the periods of time when closure data had been collected were as short as two or three hours for some radio sources. A method used to map other radio sources was derived from the mapping of 3C345 for which we had a large amount of data. The purpose of this study was to determine a systematic method to find these minimizations by changing cell size, the number of cells and the initial model.

For 3C345 the iterated map converged uniformly. The convergence is said to be uniform when gain and phase adjustments become monotonically smaller with iteration. Otherwise, when the absolute values of the phase adjustments did not tend to 0.5° or less and when the ratio of the absolute values of the gain adjustments over the gain did not tend to 1% or less, good agreement in phase closure and amplitude closure could never be obtained at the same time for a given iterated map.

Several other points should be stressed. The first one concerns the calibration of the data. Because system temperatures and gains at X-band are rarely constant during an experiment, estimates of their values need to be refined in order to calculate the correlated flux density accurately.

However, when one does not have precise amplitude calibration, one can still make these amplitudes self-consistent by adjusting the antenna gain at each station with checks provided by the amplitude closures.

As studied in §2.4.6 the initial model can be a critical step in the mapping procedure. The "best" approach is to start with a point source model: after several iterations the overall structure of the radio source can be inferred from the map and the initial model can be changed to improve and accelerate the convergence. The point source model is a good start for sources like OJ287 and 3C345 because they are composed of a very strong component which contains more than 80% of the total flux density. Troubles occur when the source has two or more components of almost equal brightness; it was noticed that the convergence is more difficult when the center of brightness is not situated at the center of the map. This problem was especially acute for the mapping of 4C39.25.

"Bad" points, as defined in §2.3, were deleted to produce different maps. Some components that appeared before deletion were no longer seen after. This "quick" mapping procedure does not take into account nor does it explain the reason for these points to be labelled "bad". The deletion of a point implies the deletion of both its amplitude and its phase although one or both of them might be correct: this causes the loss of useful information.

Finally, the most interesting results were

obtained for 3C345. The comparative study of this radio source made from data collected at X-band during the 3-day experiment and the geodetic experiment shows that a reliable determination of the brightness distribution of a radio source can be made solely from observations made during a geodetic VLBI experiment.

The cleaning procedure could be done in several steps to improve the convergence: initially, a small number of components could be determined. Then, when a convergence to a map using these components is obtained their number could be increased. This method would be interesting to test especially if it were noticed that the convergence was not obtained easily because the data were poor either in quality or in quantity. Better fits could be obtained if the sizes of the different arrays which store the position and the strength of the clean components were bigger. These sizes were, however, limited by the available memory. Also, there is no reason for the clean components to be located precisely at an integer number of cells from the center of the map. There are two methods with which one could alleviate this integerization. The first one is simply to reduce the cell size although there is a relationship between the smallest cell size and a given field of mapping. The second method is to use the values adjacent to the peak value located at a grid point to compute an interpolation of the new peak value of the map.

The next logical step is to correct the group delay for the effects of source structure and to study the resulting improvement, if any, in the accuracy on the estimates of the baseline vectors.

REFERENCES

[1] Shaffer D.B.,NASA GSFC, private communication

[2] Rogers A.E.E., H.F. Hinteregger, A.R Whitney, C.C. Counselman, I.I. Shapiro, J.J. Wittels, W.K. Klemperer, W.W. Warnock, T.A. Clark, L.K. Hutton, G.E. Marandino, B.O. Ronnang, O.E. Rydbeck, A.E. Niell, The Astrophysical Journal,193:293-301 (1974 October 15)

[3] Whitney A.R., Ph.D. Thesis, MIT (1974)

[4] Kraus J.D., Radio Astronomy, McGraw-Hill,Inc., (1966)

[5] Cornwell P.G. and Wilkinson P.N., MNRAS 196, 1067, (1981)

[6] Högbom J.A., Astron. Astrophys. Suppl.15, 417-426, (1974)

[7] Ables J.G., Astron. Astrophys. Suppl.15, 383-393, (1974)

[8] Cotton W.D., The Astronomical Journal, Volume 84, Number 8, (August 1979)

[9] Readhead A.C.S. and P.N. Wilkinson, The Astrophysical Journal, 223, 25-36, (July 1978)

[10] Bracewell R.N., The Fourier transform and its applications, McGraw-Hill, Inc., (1978)

[11] Herring T.A, MIT Department of Earth and Planetary Sciences, private communication

[12] Breidenthal J., Masters Thesis, MIT (1982)

[13] Clark B.G., K.I. Kellermann, M.H. Cohen, D.B. Shaffer, J.J. Broderick, D.L. Jauncey, L.I. Matveyenko, I.G.

Moiseev, Ap. J (Letters), 182, L57, (1973)

[14] Wittels J.J., C.A. Knight, I.I. Shapiro, H.F. Hinteregger, A.E.E. Rogers, A.R. Whitney, T.A.Clark, L.K.Hutton, G.E. Marandino, A.E. Niell, B.O. Rönnäng, O.E.H. Rydbeck, W.K. Klemperer, W.W. Warnock, The Astrophysical Journal,196:13-39 (1975 February 15)

[15] Shapiro I.I., J.J. Wittels, C.C. Conselman III, D.S. Robertson, A.R. Whitney, H.F. Hinteregger, C.A. Knight, A.E.E. Rogers, T.A. Clark, L.K. Hutton, A.E. Niell, The Astronomical Journal, Volume 84, Number 10 (October 1979)

Appendix 1

Mathematical expressions, notations and indices

Ψ_{ij}	fringe phase on baseline i-j
Φ_{ij}	phase of the complex visibility function on baseline i-j
θ_i	phase at station i
γ_{ij}	fringe visibility
ρ_{ij}	correlation coefficient
C_{ijk}	phase closure variable for the three stations i,j,k
R_{ijkl}	amplitude closure variable for the four stations i,j,k,l
$\hat{\underline{X}}$	estimate of vector $\underline{X}$
A^t	matrix transpose of A
P^{-1}	matrix inverse of P
$\underline{Y}^o$	vector containing observed data
$\underline{Y}^m$	vector containing variables derived from a model
SNR	signal-to-noise ratio
$\propto$	proportional to
mas	milliarcsecond
§	paragraph
FWHM	Full width at half maximum
#	number

UT	Universal Time
GST	Greenwich Sidereal Time
*	convolution product

Appendix 2

Model for the phases of the fringe visibility used in PCLOS [1]

A model for the phase of the complex visibility on baseline i-j can be written by

$$\Phi_{ij} = \Psi_{ij} + \theta_j - \theta_i \qquad \text{(A1)}$$

where θ_j and θ_i are the phases at each station. The purpose of the phase closure method, as discussed in §1.2, is to find the least squares correction $\delta\hat{\theta}_i$ to the station phases. Let the vector $\underline{Y}$ be composed of the Φ_{ij}. To each Φ_{ij} corresponds a y_k whose index k is defined by

$$k = \text{index}(i,j) = \min(i,j) + (\max(i,j)-1)\ (\max(i,j)-2)/2 \qquad \text{(A2)}$$

This function establishes an unequivocal correspondance between every pair of baseline indices i-j and the index k. Let the elements of the vector $\underline{X}$ be the station phases (θ_i). If we define the matrix $A = \partial\underline{Y}/\partial\underline{X}$ then it follows from Equation (A1) that A has the configuration given below in the case of three stations:

$$A = \begin{pmatrix} -1 & 1 & 0 \\ -1 & 0 & 1 \\ 0 & -1 & 1 \end{pmatrix} \qquad \text{(A3)}$$

If Λ_x is the variance-covariance matrix of the stations phases based on a priori knowledge and if P^{-1} is a matrix which weights the observations, then the Bayes least-squares estimation technique yields for $\delta\underline{\hat{X}}$:

$$\delta\underline{\hat{X}} = (A^t P^{-1} A + \Lambda_x^{-1})^{-1} \quad (A^t P^{-1} \delta\underline{Y} + \Lambda_x^{-1} \underline{m}_{\delta x}) \qquad \text{(A4)}$$

where $\delta\underline{Y}$ is composed of the $\delta y_k = (y_k^o - y_k^m)$, where y_k^o is the "observed" phase on baseline i-j, y_k^m is the model phase on the same baseline. $\underline{m}_{\delta x}$ is the expectation value of $\delta\underline{X}$. In our case, it is zero because we assume that the adjustments on the station phases are of zero mean.

In Equation (A4) there is the implicit assumption that the matrix $(A^t P^{-1} A + \Lambda_x^{-1})$ is non-singular. This situation can be insured by properly choosing Λ_x. In practice what is done is to assume that the errors in the phases are uncorrelated, thus making Λ_x diagonal. This kind of matrix insures that $(A^t P^{-1} A + \Lambda_x^{-1})$ is non-singular. Moreover, the same a priori uncertainty is taken for every station phase. An a priori uncertainty on the fringe-phase of 4^o corresponds to a mean value of the fringe-phase uncertainty which lies between 9^o and 1^o .

Similarly, the weighting matrix P^{-1} is also taken to be

diagonal. The values chosen to weight the observations are just the squares of the SNR's:

$$P^{-1} = \begin{pmatrix} SNR_1^2 & 0 & 0 \\ 0 & SNR_2^2 & 0 \\ 0 & 0 & SNR_3^2 \end{pmatrix} \qquad \text{(A5)}$$

Appendix 3

Model for the amplitudes used in ACLOS [1]

a) Linearization by differentiation

The model adopted for the correlation coefficient is

$$y_k = y_k^n \, x_i \, x_j \qquad \text{(A6)}$$

where $x_i = 1/\sqrt{h_i}$ as defined in Equation (19) and y_k^n is the theoretical correlation coefficient if gains and system temperatures are at their nominal values. The index k is the integer number corresponding to the baseline i-j (Equation A2). The purpose of the amplitude closure method is to find the least squares estimates of the x_i. Recalling Equation (20) of §1.3

$$y_k^o - y_k^m = (y_k^n \, x_{io}) \, \Delta x_j + (y_k^n \, x_{jo}) \, \Delta x_i \qquad \text{(A7)}$$

Taking the a priori estimates of the x_i to be unity, we obtain:

$$y_k^o - y_k^m = y_k^n \, \Delta x_j + y_k^n \, \Delta x_i \qquad \text{(A8)}$$

Let the elements of $\underline{X}$ be $(\underline{X})_i = x_i$ and the elements of $\underline{Y}$ be $(\underline{Y})_k = y_k$. The matrix formulation of Equation (A8) is

$$\underline{Y}^{o} - \underline{Y}^{m} = A\ \delta\underline{X} \tag{A9}$$

where the matrix A is defined similarly to the coefficient matrix A of Appendix 2 and $(\delta\underline{X})_j = \Delta x_j$. In the case of 4 stations we obtain:

$$A = \begin{pmatrix} y_1^n & y_1^n & 0 & 0 \\ y_2^n & 0 & y_2^n & 0 \\ y_3^n & 0 & 0 & y_3^n \\ 0 & y_4^n & y_4^n & 0 \\ 0 & y_5^n & 0 & y_5^n \\ 0 & 0 & y_6^n & y_6^n \end{pmatrix} \tag{A10}$$

The Bayes least squares estimation technique yields for $\delta\hat{\underline{X}}$

$$\delta\hat{\underline{X}} = (A^t\ P^{-1}\ A + \Lambda_x^{-1})^{-1}\ (A^t\ P^{-1}\ \underline{Y} + \Lambda_x^{-1}\ \underline{m}_x) \tag{A11}$$

where P^{-1} is a weighting matrix. It is taken to be diagonal.

b) Logarithmic linearization

Taking the logarithm of Equation (A6) gives

$$\log y_k = \log y_k^n + \log x_i + \log x_j \tag{A12}$$

This time we want to find the least squares estimate of the $\log x_i$ given the model in Equation (A12) and the $\log y_k^o$. To the first order we have:

$$\log y_k^o - \log y_k^m = \Delta \log x_i + \Delta \log x_j \qquad \text{(A13)}$$

Let $(\underline{X})_i = \log x_i$ and $(\underline{Y})_k = \log y_k$. Again we can define a coefficient matrix as before and express Equation (A13) as

$$\underline{Y}^o - \underline{Y}^m = A \quad \delta \underline{X} \qquad \text{(A14)}$$

where A is the following matrix in the case of 4 stations

$$A = \begin{pmatrix} 1 & 1 & 0 & 0 \\ 1 & 0 & 1 & 0 \\ 1 & 0 & 0 & 1 \\ 0 & 1 & 1 & 0 \\ 0 & 1 & 0 & 1 \\ 0 & 0 & 1 & 1 \end{pmatrix} \qquad \text{(A15)}$$

Appendix 4

The two-dimensional approximation of the three-dimensional Fourier transform [8]

When calculating the Fourier transform, it is critical to remember that the problem is initially three-dimensional. The complex visibility V is a function of the baseline vector $\vec{b}$ and the brightness distribution B is the Fourier transform of the complex visibility function. Thus,

$$B(\vec{s}) \backsim \iiint g(\vec{b})\ V(\vec{b})\ \exp(2\pi i\ \vec{b}.\vec{s})\ d\vec{b} \qquad (A16)$$

where $g(\vec{b})$ is a weighting function. The frame of reference is defined by the unit vector source which is in the direction of the radio source and the east-west and the north-south directions perpendicular to it. In this coordinate system the components of $\vec{b}$ are u along the east-west direction, v along the north-south direction, and w. The notation $d\vec{b}$ means du dv dw. $\vec{s}$ is taken as a unit vector and its three directional cosines are (x,y,z) with respect to the u, v and w axes, respectively. For the approximation of a point source $\vec{s}$ =(0,0,1). In reality, because we are mapping around a point the x and y components of $\vec{s}$ are no longer zero but always satisfy

$$x^2+y^2 \ll 1$$

but since $z \simeq 1-1/2(x^2+y^2)$ we can rewrite the exponential term of Equation (A16)

$$\exp(2\pi i\ \vec{b}.\vec{s}) \simeq \exp(2\pi iw)\ \exp(2\pi i[(ux+vy)-\frac{w}{2}\ (x^2+y^2)]) \qquad (A17)$$

The two-dimensional approximation consists of neglecting the $\frac{w}{2}\ (x^2+y^2)$ term which must always always be small compared to unity. For example, using $wx^2=0.01$ and taking w around 6000 km/3.75 cm gives $x \simeq 1.\ 10^{-5}$ rd $\simeq$ 2 seconds of arc That means that the procedure CLEAN is inadequate for mapping region bigger than 2 seconds of arc around the center of the source. For our purpose, the two-dimensional approach is a good approximation. The term $\exp(2\pi iw)$ can be taken into account in $g(\vec{b})$.

Appendix 5

a) Influence of the source structure on the group delay correction [15]

In the general case the visibility V can be written

$$V(u,v) = Re[V(u,v)] + i\ Im[V(u,v)] \qquad (A18)$$

Let ϕ be the phase of V(u,v), we have the relationship

$$F = \tan\phi = \frac{Im[V(u,v)]}{Re[V(u,v)]} \qquad (A19)$$

where u is the east-west component and v the north-south component of the baseline vector as viewed from the source. The contribution of the source structure to the group delay at (u_o,v_o) is

$$\tau = \frac{1}{2\pi}\frac{\partial\phi}{\partial f}\Big|_{(u_o,v_o)} = \frac{1}{2\pi}\frac{\partial\phi}{\partial F}\frac{dF}{df}\Big|_{(u_o,v_o)} \qquad (A20)$$

where f is the frequency. Differentiating ϕ with respect to F, and F with respect to f, we obtain respectively

$$\frac{\partial\phi}{\partial F} = \frac{1}{1+F^2} \qquad (A21)$$

and

$$\frac{dF}{df} = \frac{Re[V(u,v)] \frac{d(Im[V(u,v)])}{df} - Im[V(u,v)] \frac{d(Re[V(u,v)])}{df}}{Re[V(u,v)]^2}$$

From this last equation it can be seen that at the points where Re[V(u,v)] is near zero (i.e. where the correlated flux density goes to zero), the group delay correction will be significant [15]. This situation will happen for a radio source like 4C39.25 which is made of two components of almost equal brightness.

b) Influence of a small component of flux density on the group delay correction

Given a brightness distribution, we can derive the complex visibility function. Assuming a two-dimensional problem we have the following relationship

$$V(u,v) = \Sigma\, B(x,y)\, \exp 2\pi i(xu+yv) \qquad (A22)$$

Let us now consider the problem of a source having a main component and a small component. The brightnesses are in the ratio of R:1 as indicated in the figure below.

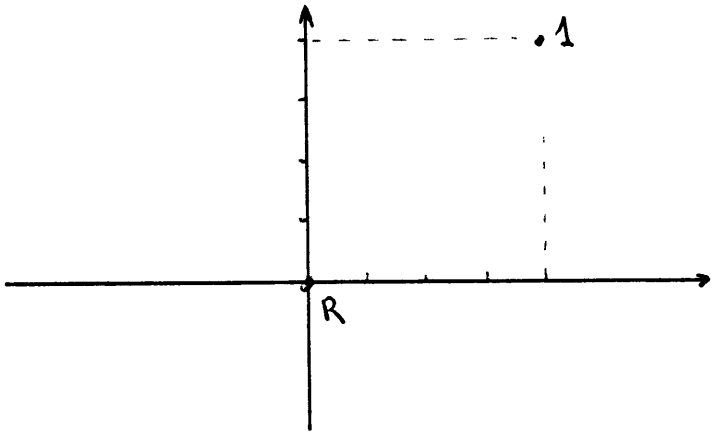

In this example, since $B(0,0) = R$ and $B(x_o,y_o) = 1$,the visibility function has the following expression

$$V(u,v)= R+\cos 2\pi(x_o u+y_o v)+ i \sin 2\pi(x_o u+y_o v) \quad (A23)$$

where u and v are given by [3]

$$u= (bf/c) \cos\delta_b \sin(\alpha_b-\alpha_s) = h f$$

$$v= (-bf/c) [\sin\delta_s \cos\delta_b \cos(\alpha_b-\alpha_s)-\sin\delta_b \cos\delta_s] = k f \quad (A24)$$

and x_o and y_o are the coordinates of the small component. δ_s and α_s are declination and right ascension of the source, δ_b is the baseline declination , α_b is the baseline right ascension and b is the length of the baseline.
For 3C345, $\delta_s \simeq 39^{\circ}.90$ and the baseline declination δ_b is constant during the time of an experiment but $\alpha_b=\alpha_{bo}+\Omega t$ where Ω is the rotation rate of the Earth and t the GST. For simplicity, let

$$F= \tan \phi = \sin A/(R+\cos A) \quad (A25)$$

with

$$A= 2\pi(x_o u+y_o v) \quad (A26)$$

Differentiating ϕ with respect to the frequency gives

$$\frac{\partial \phi}{\partial f} = \frac{\partial(\tan F)^{-1}}{\partial F} \frac{\partial F}{\partial f} = \frac{1}{1+F^2} \left[\frac{\partial F}{\partial u} \frac{du}{df} + \frac{\partial F}{\partial v} \frac{dv}{df} \right] \quad (A27)$$

then, we determine $\partial F/\partial u$ from Equations (A25) and (A26)

$$\frac{\partial F}{\partial u} = \frac{2\pi x_o}{(R+\cos A)^2}[\cos A\ (R+\cos A) + \sin A\ \sin A] \qquad (A28)$$

In the same way, we can determine $\partial F/\partial v$ and substituting for $\partial F/\partial f$ in Equation (A27)

$$\frac{\partial \phi}{\partial f} = \frac{1}{1+\tan^2\phi}\ 2\pi\ \frac{(R\cos A+1)}{(R+\cos A)^2}\ (x_o h+y_o k) \qquad (A29)$$

For a brightness ratio R=100, a baseline length b=5000 km, a frequency f=8 GHz and a component whose coordinates are x_o=4 mas and y_o=4 mas, we can approximate the formula as

$$\tau = \frac{1}{2\pi}\ \frac{\partial \phi}{\partial f} \simeq \frac{1}{R}\ (x_o h+y_o k) \simeq 3\ 10^{-12}\ s \qquad (A30)$$

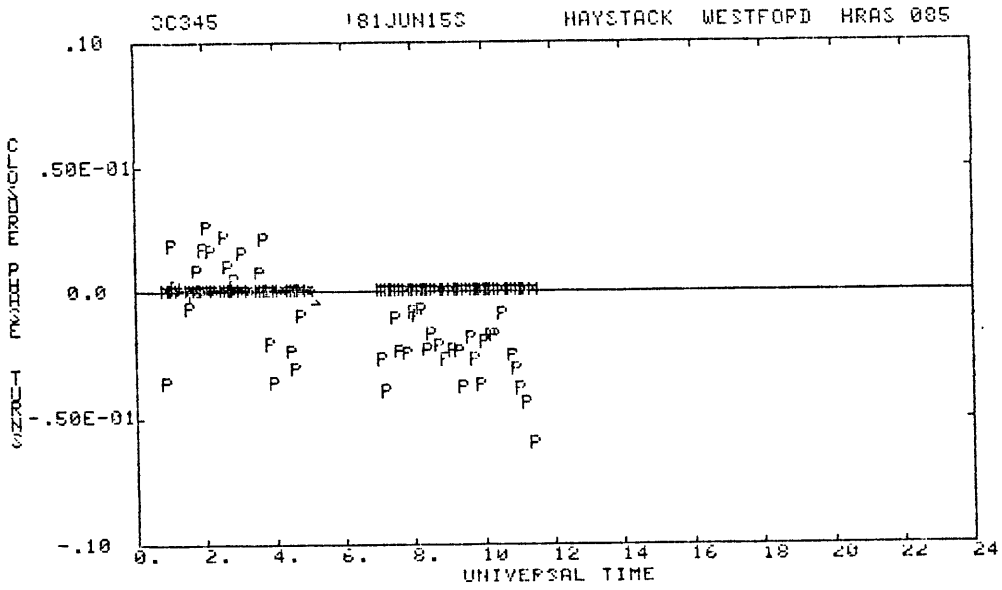

Figure 2.1:

Phase closure on HA-WE-HR at S-band (ν 2.3 GHz) obtained during the 3-day experiment of June 1981. The P's represent the observed phase closure and the M's represent the phase closure given by the point source model.

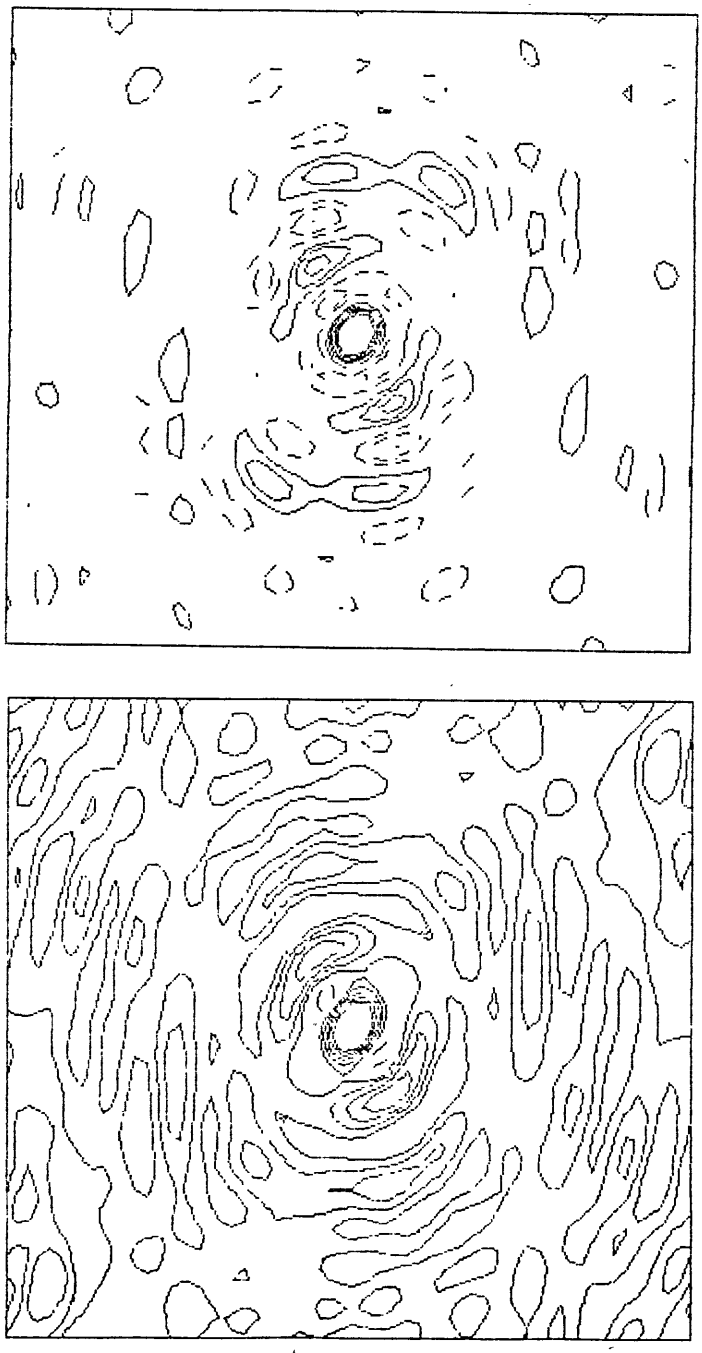

Figure 2.2:

Dirty beams of the 3C345 X-band experiment for June 1981 obtained with uniform (above)and non-uniform (below) weighting. The horizontal and the vertical scales are the same. The width of the boxes are 11.2 mas. The contours are drawn at 5, 10, 20, 30, 40 and 50% of the peak value. The negative contours are symbolized by dashed lines: they are drawn at -30, -20, -10, -5 % of the peak value. The inner contour of the main lobe is at 50% of the peak value.

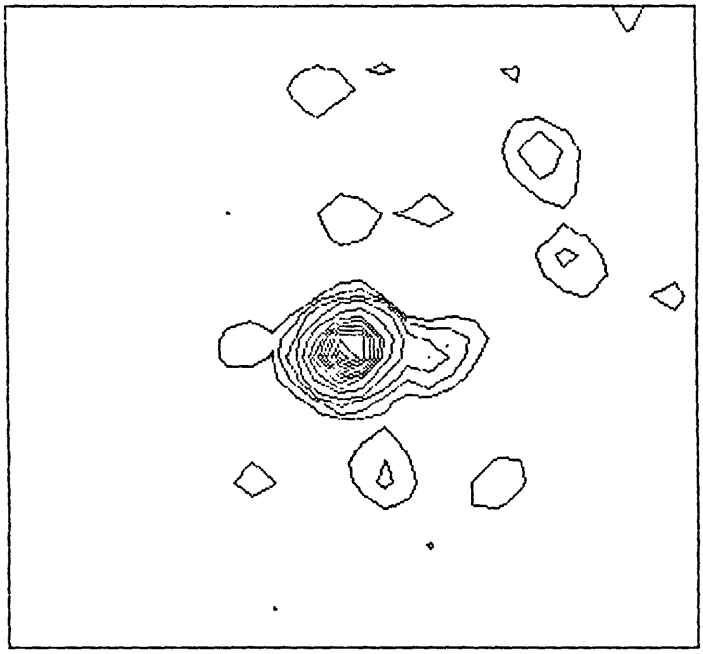

Figure 2.3: 3C345 X-band 15,16,17 June 1981

Map after 10 iterations when the point source initial model is offset from the center by 0.50 mas at a position angle of 135^{o}. The width of the box is 8 mas. The restoring beam is circular with a FWHM of 0.55 mas.

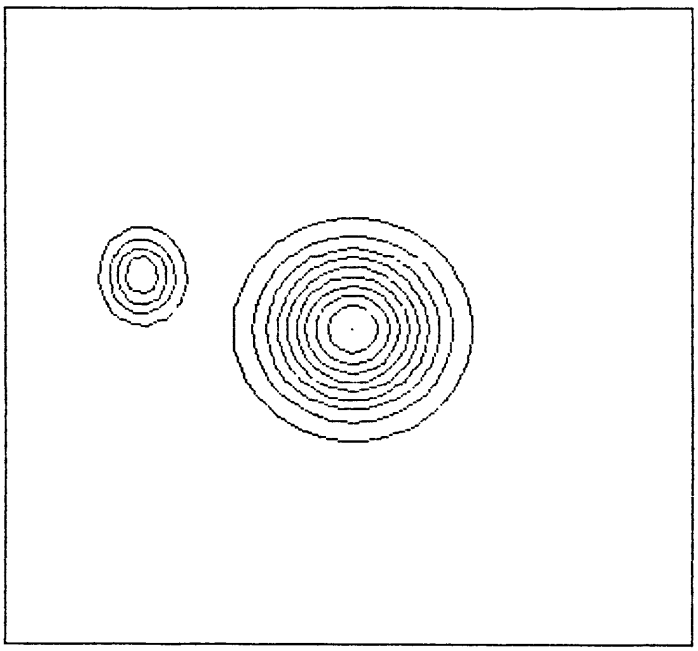

Figure 2.4a:

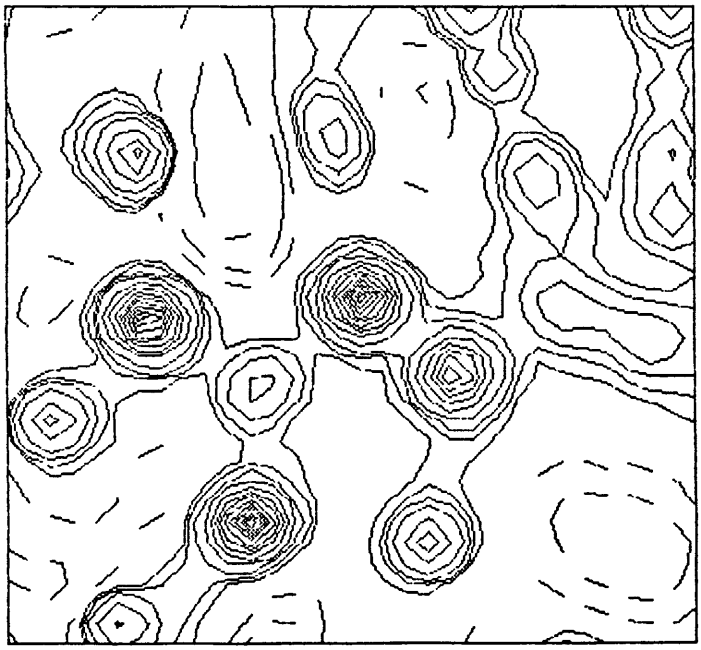

Figure 2.4b:

Figure 2.4a:

Initial model composed of 2 components. The smaller one is 2.5 mas from the main one at a position angle of 75°. Its relative brightness is 0.5. The contour are drawn every 10% of the peak brightness.

Figure 2.4b:

Map after 30 iterations. The scale is the same as for the model. The width of the box is 8 mas. The circular restoring beam has a FWHM of 0.55 mas. The negative contours are in dashed lines. The positive contours are shown at 1, 2.5, 5, 10, 20, 30, 40, 50, 60, 70, 80, 90% of the peak brightness.

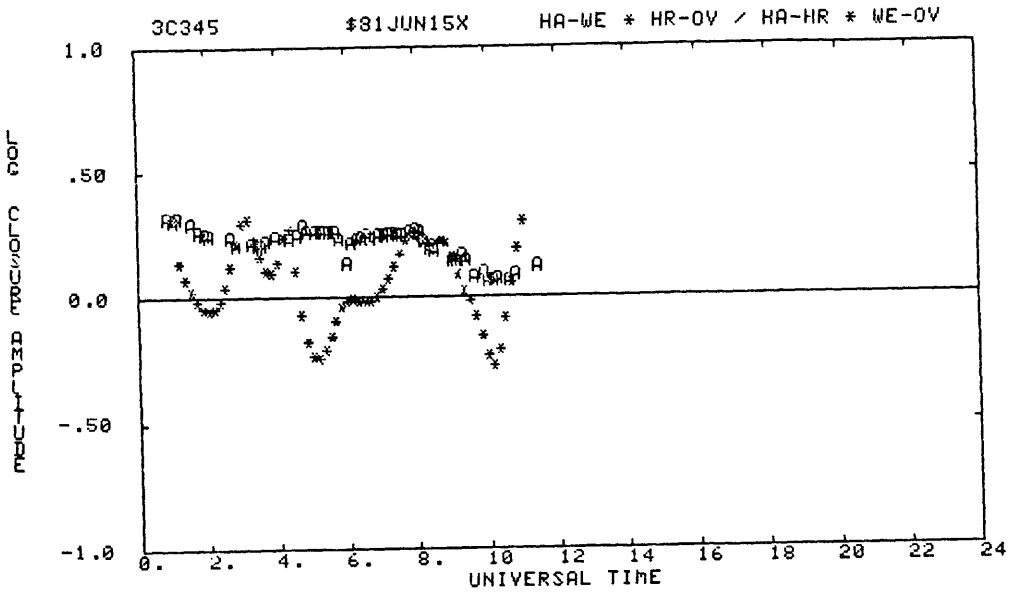

Figure 2.4c:

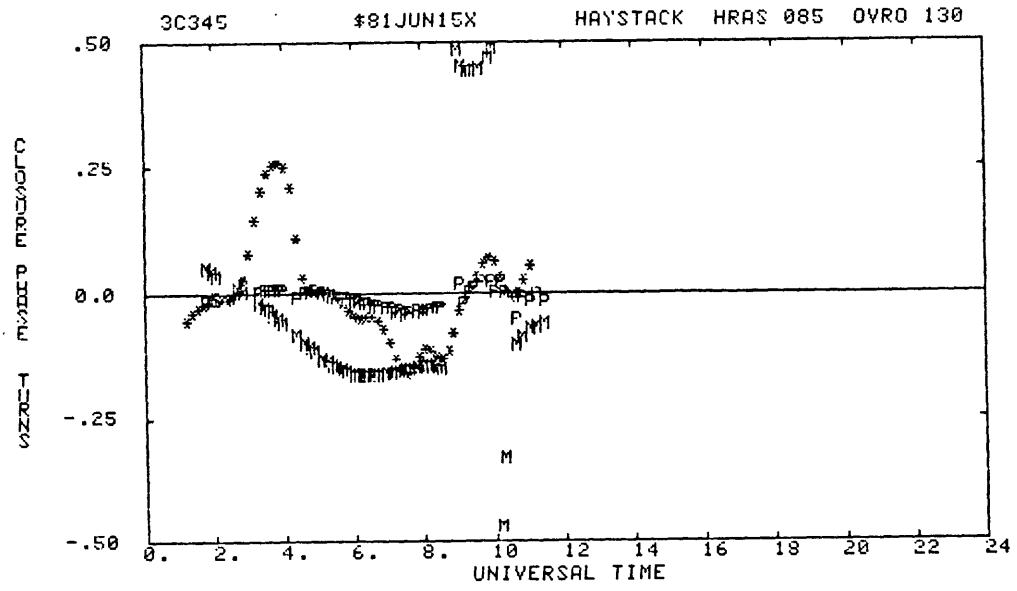

Figure 2.4d:

Figure 2.4c: 3C345 X-band 15,16,17 June 1981 experiment

Amplitude closure for HA-WE, HR-OV, HA-HR and WE-OV on a logarithm scale. The *'s show the amplitude closure given by the model after the 30^{th} iteration. The A's show the observed amplitude closure

Figure 2.4d:

Phase closure is expressed in fraction of 360°. The *'s represent the phase closure given by the model, the P's are the observed phase closure and the M's show the phase closure obtained from the initial model.

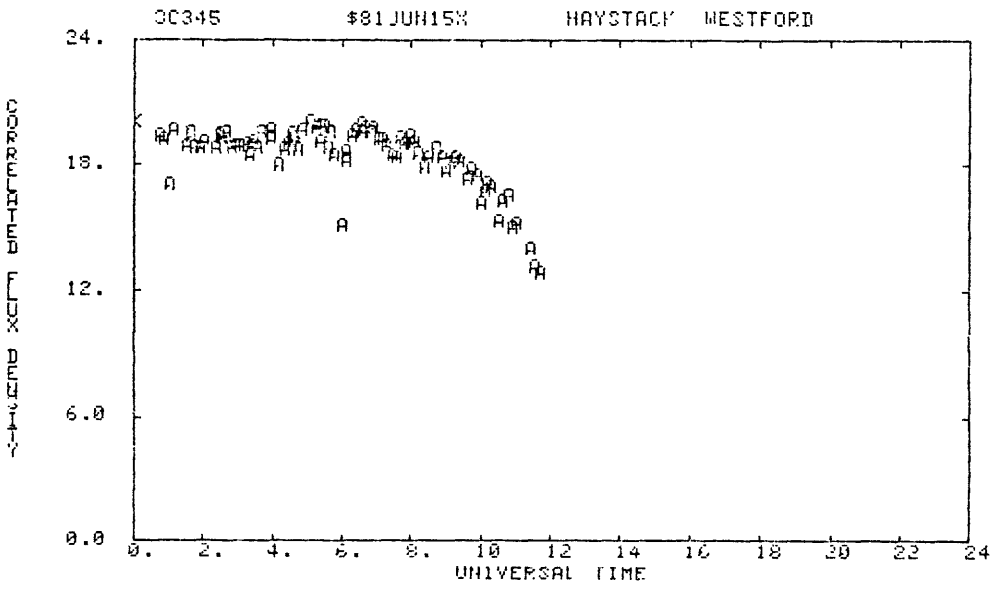

Figure 2.5:

Correlated flux density on HA-WE at X-band during the special and the geodetic experiment. Whereas one would expect a constant flux density on such a short baseline, notice the decreasing trend with time. The data show two amplitudes referred as "bad" points in §2.3

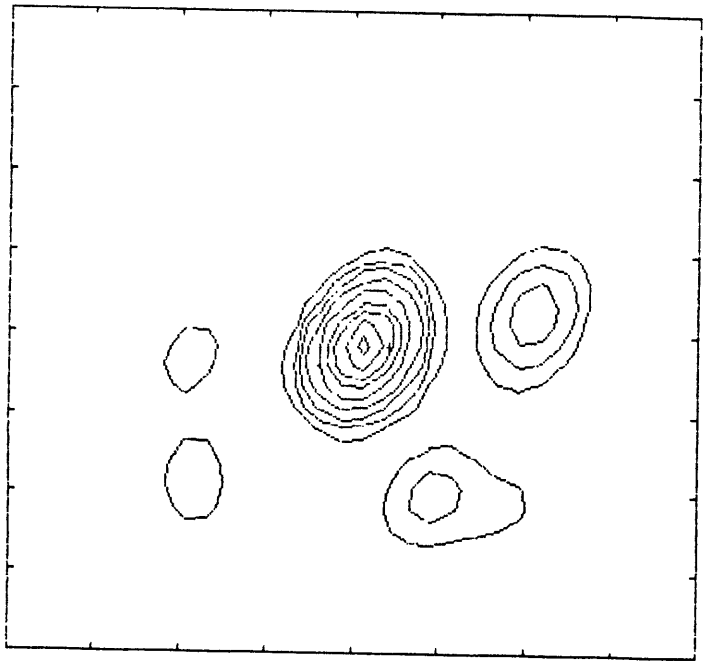

Figure 2.6b

RESTORING BEAM

HALF POWER LEVEL

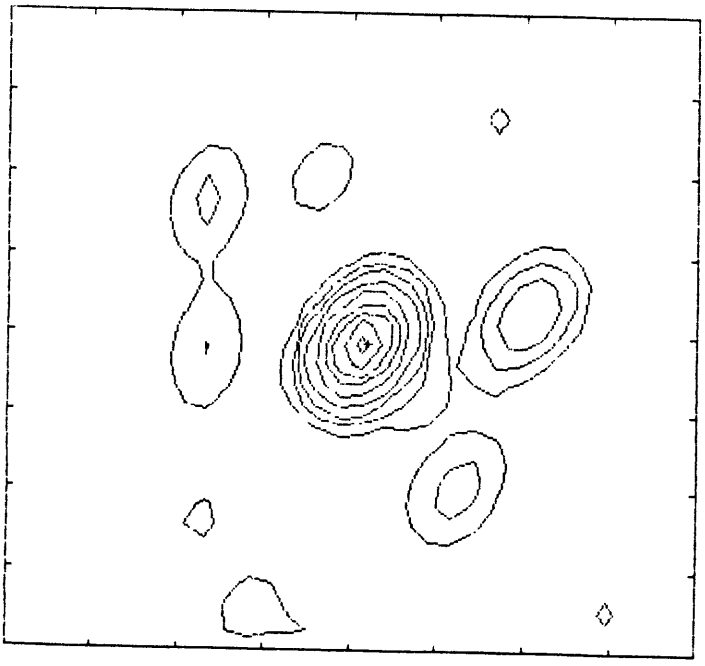

Figure 2.6a

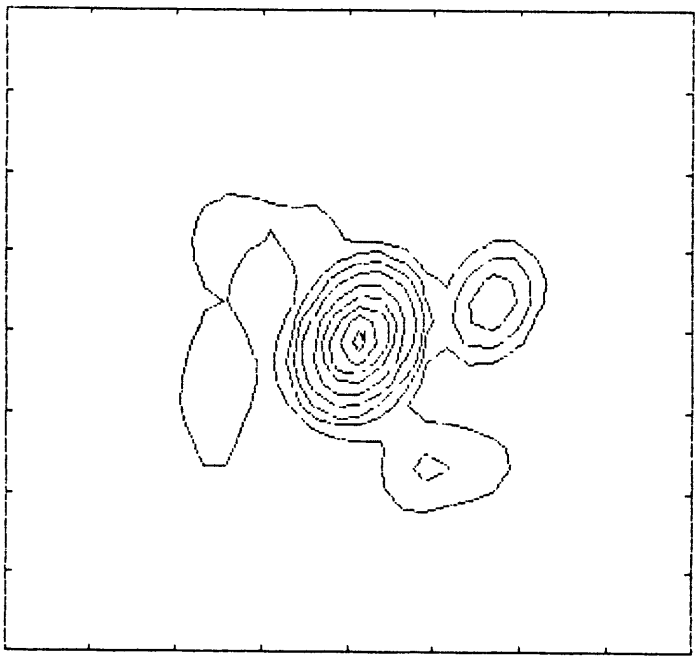

Figure 2.6c

RESTORING BEAM

HALF POWER LEVEL

Figures 2.6:

X-band maps of 3C345 obtained when the linear dimensions of the field of mapping are successively reduced 8 mas(a), 4 mas(b), 3.2 mas(c), 2.24 mas(d), 1.6 mas(e). The restoring beam (overresolved by 1.8) is 0.90 mas by 0.60 mas at a position angle of -25°. The + represents the center of brightness.

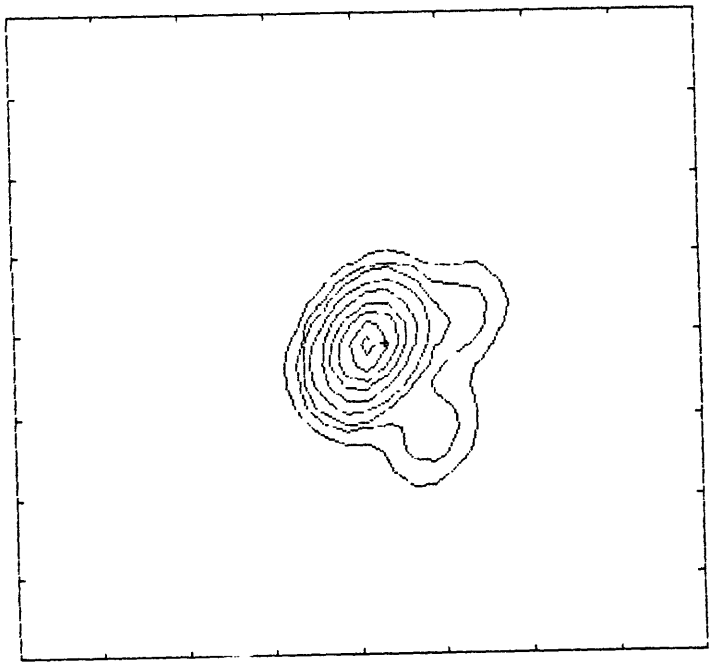

Figure 2.6d

RESTORING BEAM

HALF POWER LEVEL

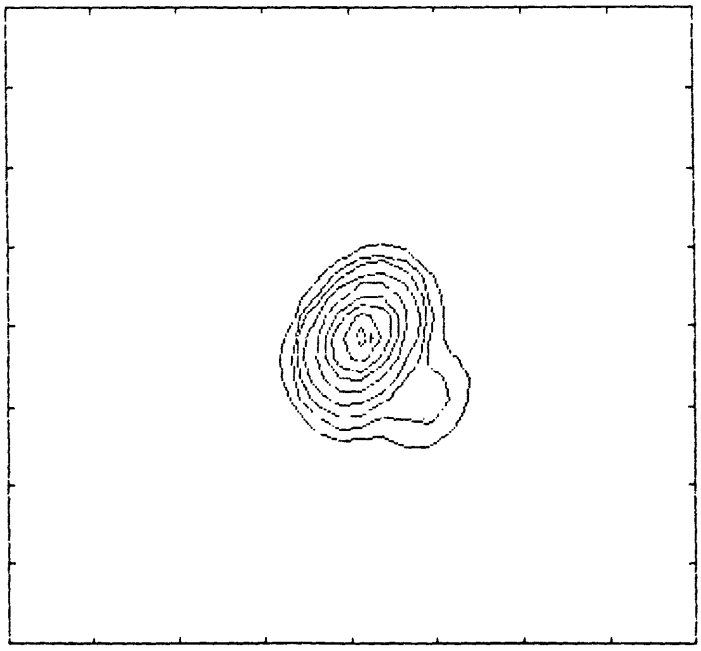

Figure 2.6e

Figure 2.7a

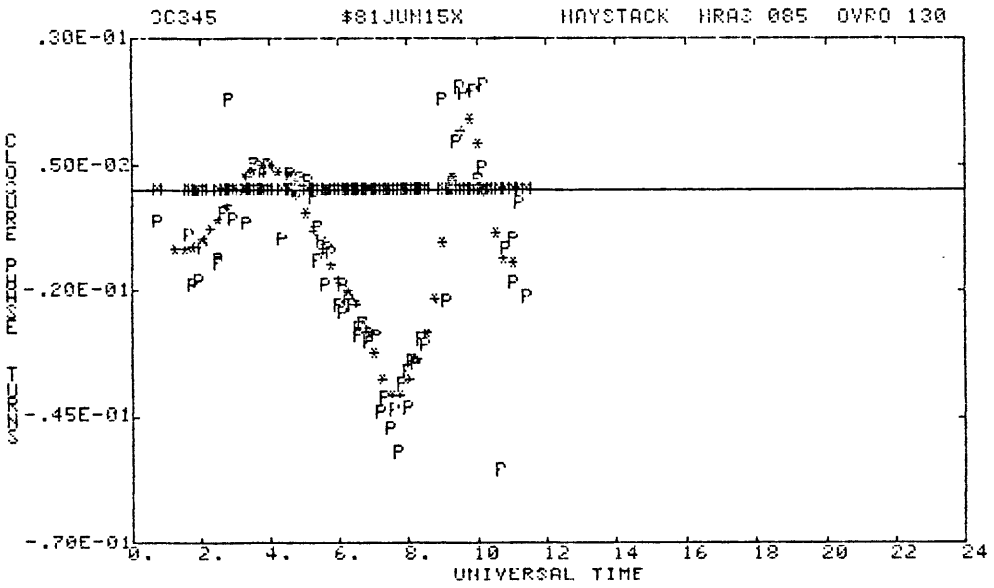

Figure 2.7b

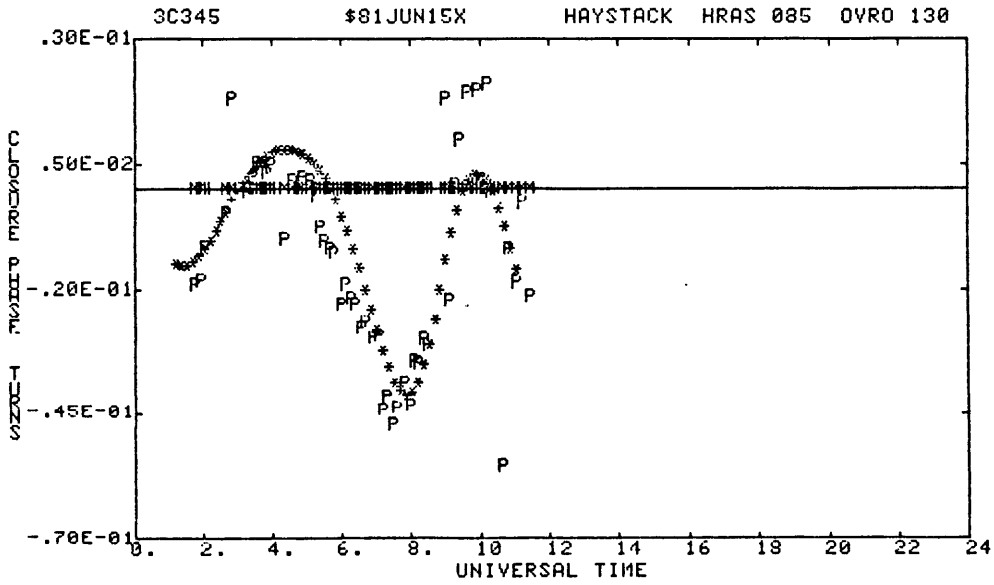

Figure 2.7c

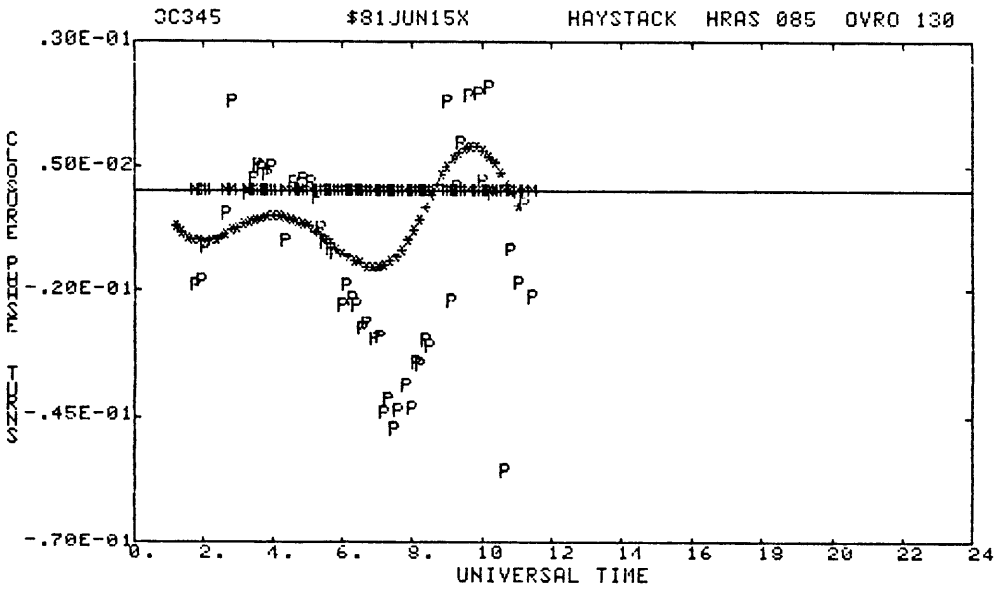

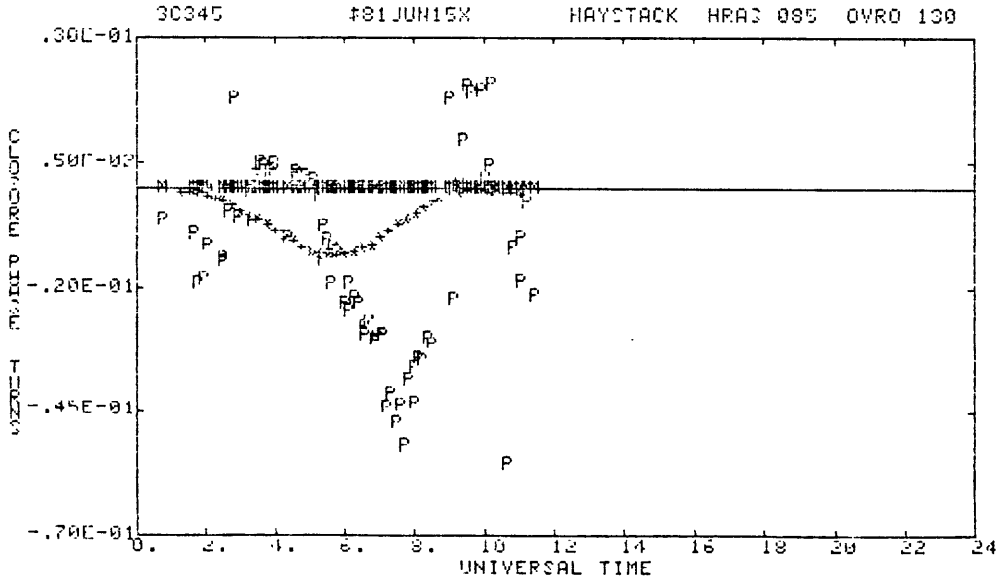

Figure 2.7d

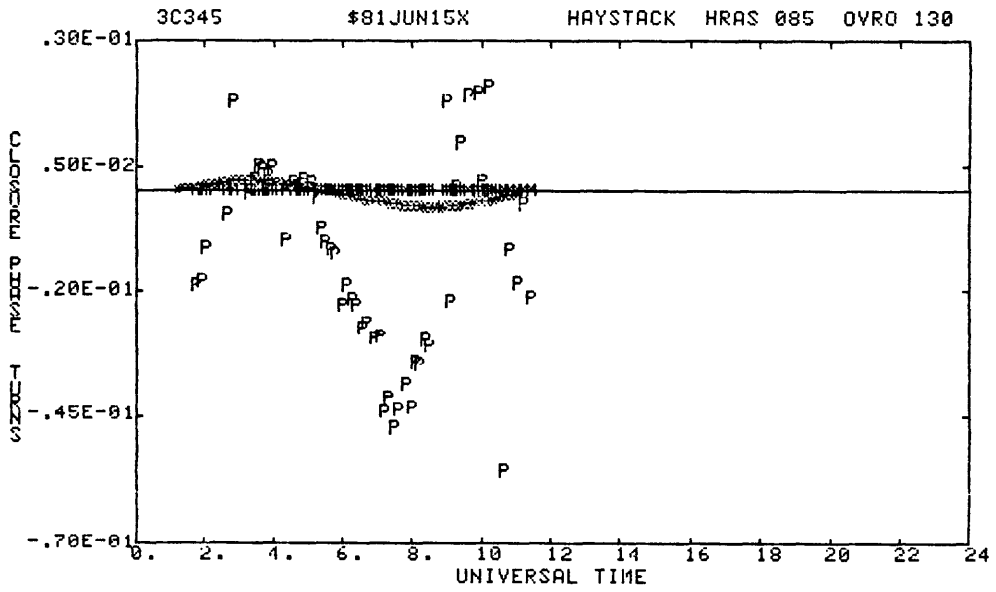

Figure 2.7e

Figures 2.7:

Deterioration of the phase closure when reducing successively the linear dimensions of field of mapping 8 mas(a), 4 mas (b), 3.2 mas(c), 2.24 mas (d) and 1.6 mas (e). The P's are the observed phase closure and the *'s are the closures given by the model.

Figure 2.8a: 3C345 X-band 15,16,17 June 1981

Amplitude closure obtained by the final map and plotted on a linear scale. The A's represent the observed amplitude closure and the *'s represent the amplitude closure given by the model.

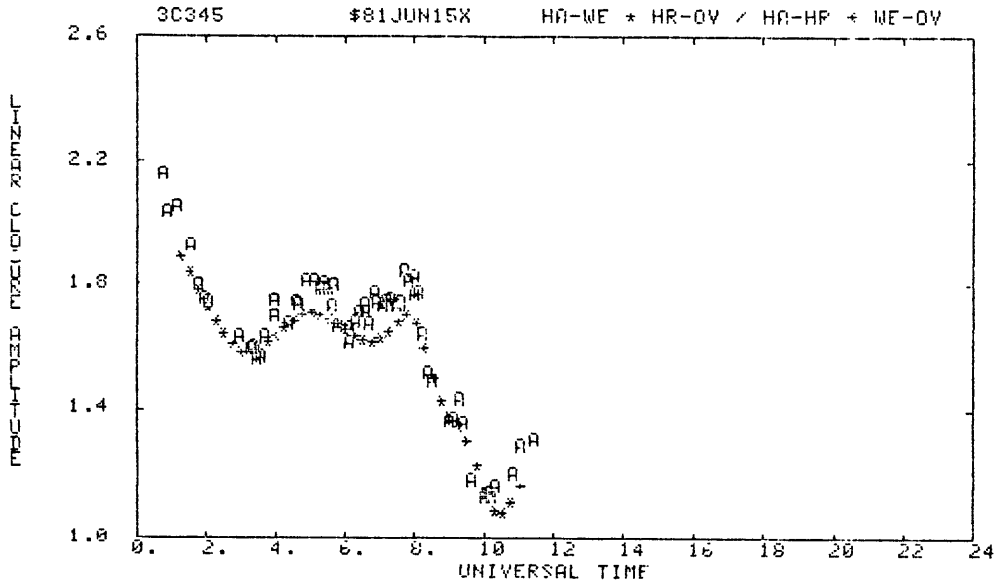
3C345
$81JUN15X
HA-WE * HR-OV / HA-HR * WE-OV
2.6
2.2
1.8
1.4
1.0
0.
2.
4.
6.
8.
10
12
14
16
18
20
22
24
UNIVERSAL TIME

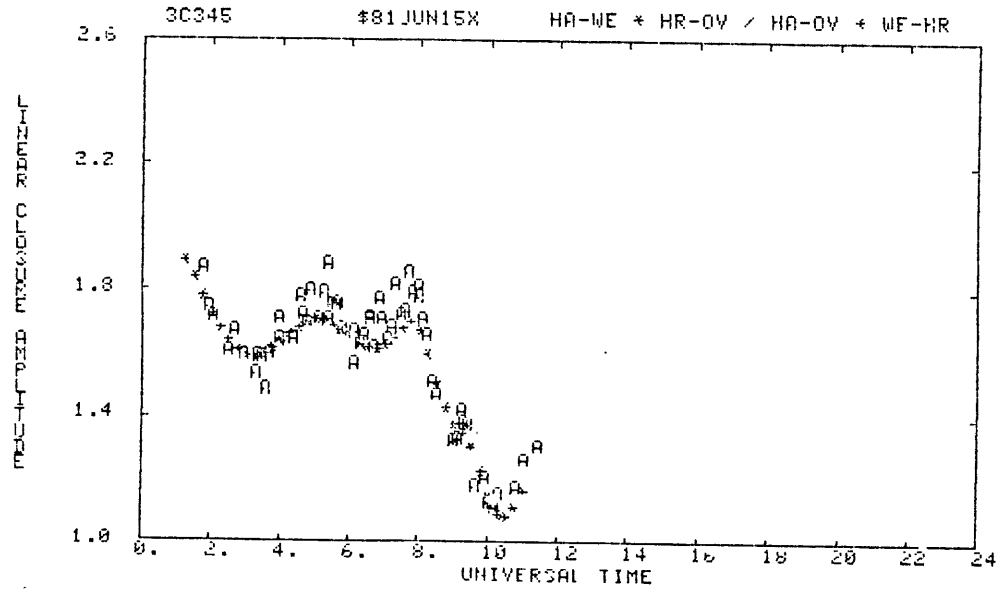
3C345
$81JUN15X
HA-WE * HR-OV / HA-OV * WE-HR
2.6
2.2
1.8
1.4
1.0
0.
2.
4.
6.
8.
10
12
14
16
18
20
22
24
UNIVERSAL TIME

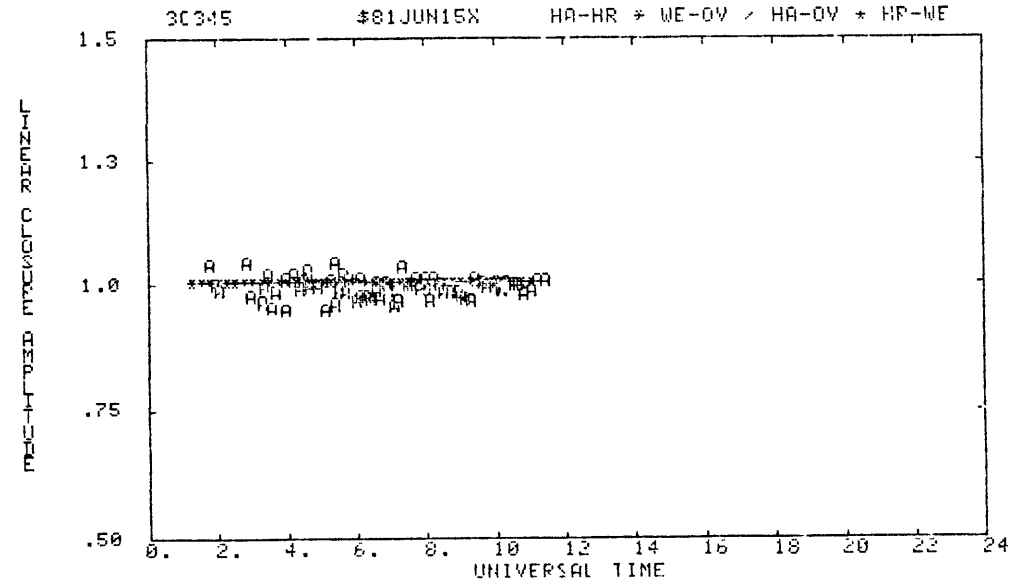
3C345
$81JUN15X
HA-HR * WE-OV / HA-OV * HR-WE
1.5
1.3
1.0
.75
.50
0.
2.
4.
6.
8.
10
12
14
16
18
20
22
24
UNIVERSAL TIME

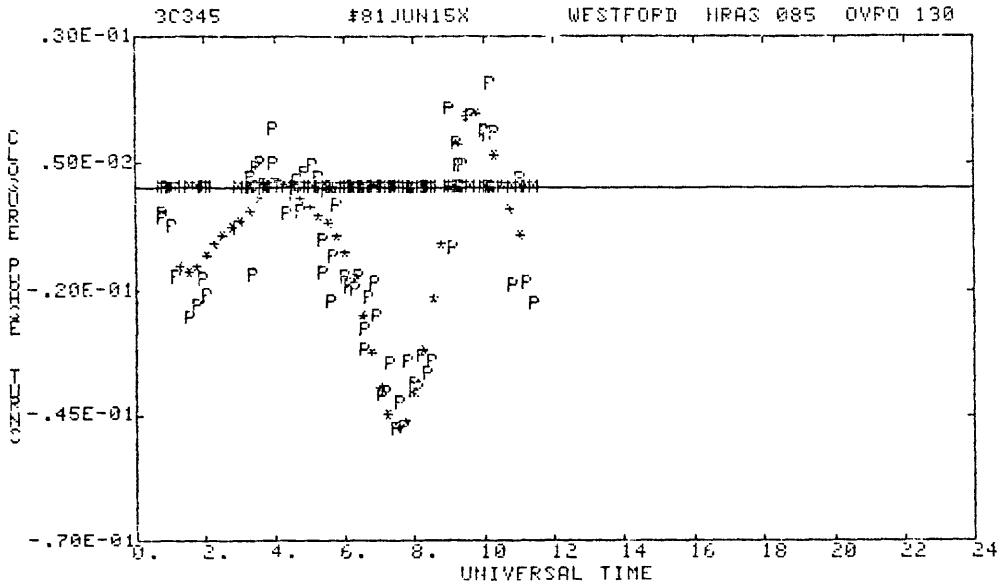

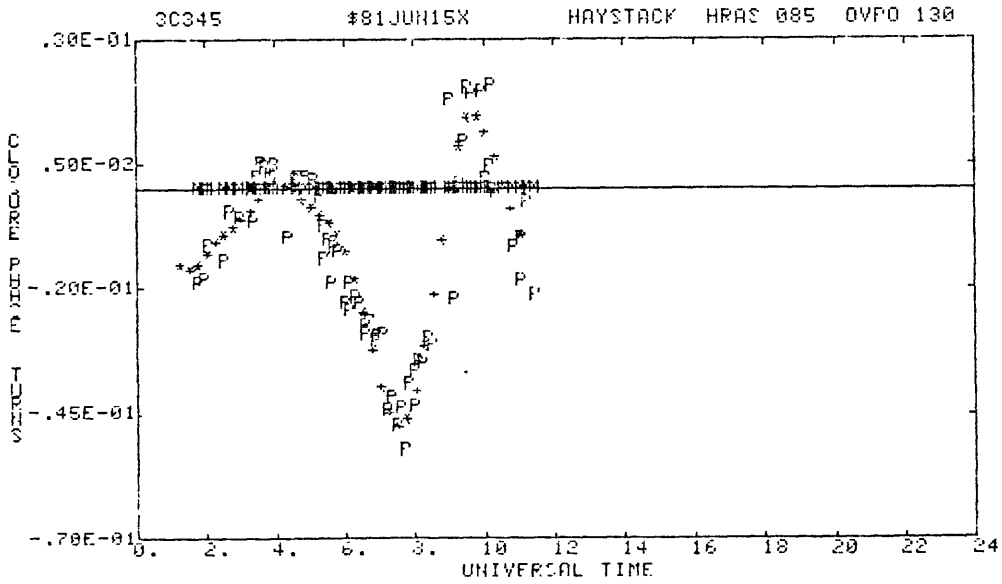

Figure 2.8b: 3C345 X-band 15,16,17 June 1981

Phase closures expressed in fractions of 360°. The P's represent the observed phase closure, the *'s are the phase closure given by the final model and the M's are the phase closure given by the initial model (point source). Note that the model gives the same phase closure on HA-HR-OV and WE-HR-OV. The *'s have the same locations on both plots.

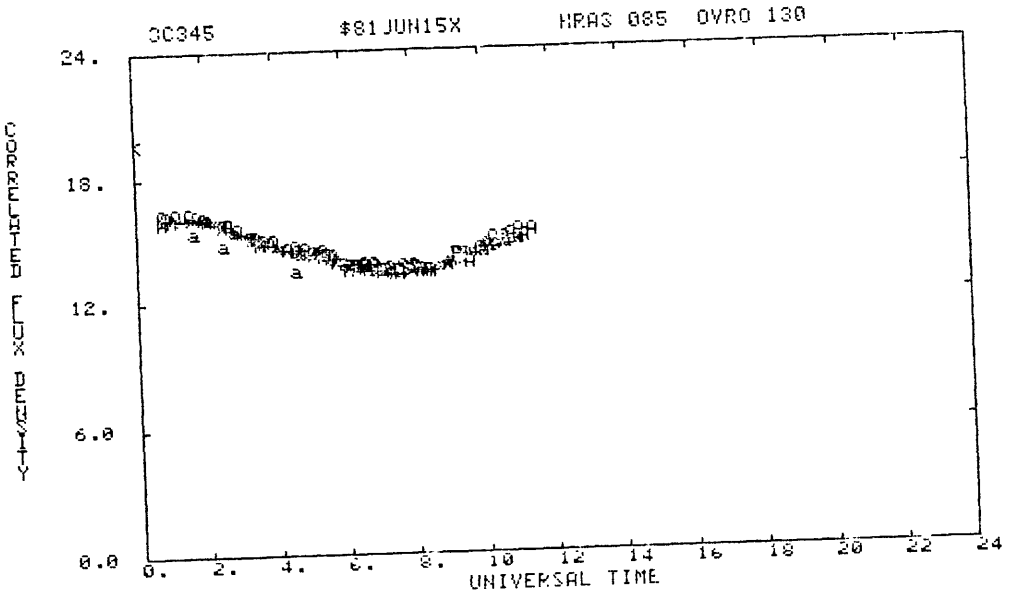

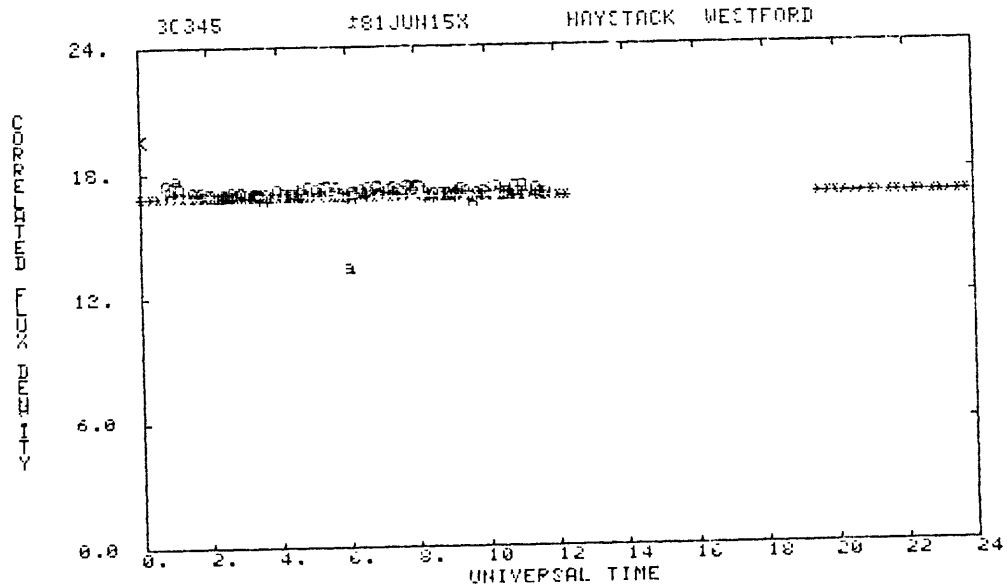

Figures 2.8c: 3C345 X-band 15,16,17 June 1981

show the correlated flux density on the six different baselines with gain correction applied for the final map. The lower case letter, a, means downweighted point. The A's are the observed amplitudes and the *'s are the amplitudes predicted by the model.

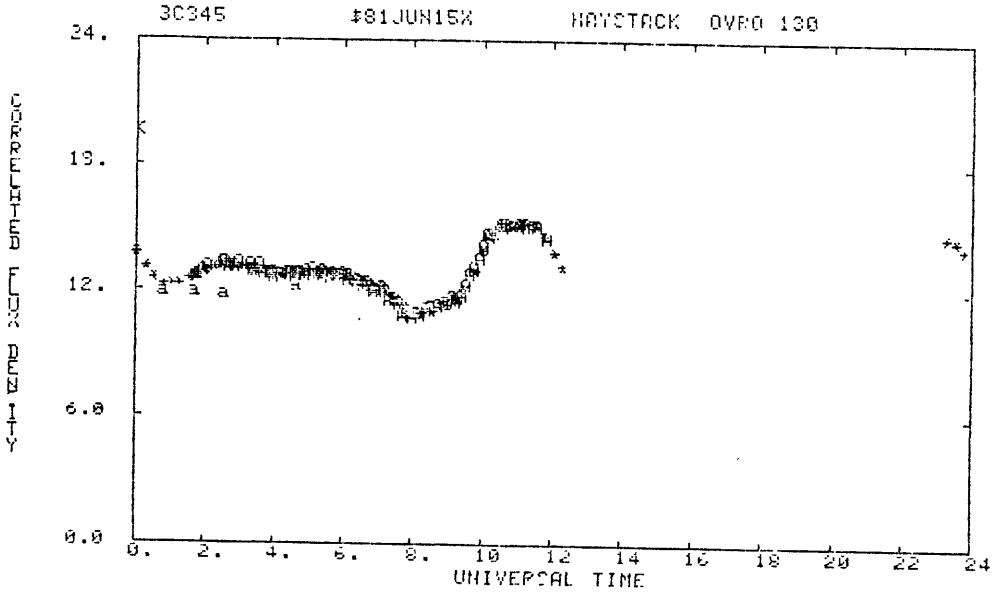
3C345
#81JUN15X
HAYSTACK OVRO 130
CORRECTED FLUX DENSITY
24.
18.
12.
6.0
0.0
0.
2.
4.
6.
8.
10
12
14
16
18
20
22
24
UNIVERSAL TIME

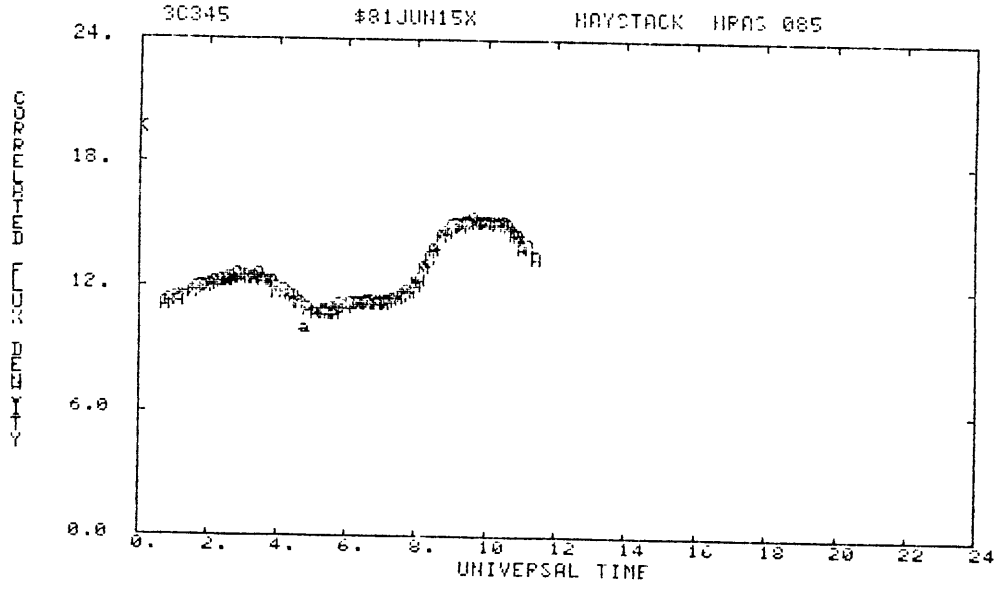
3C345
#81JUN15X
HAYSTACK HRAO 085
CORRECTED FLUX DENSITY
24.
18.
12.
6.0
0.0
0.
2.
4.
6.
8.
10
12
14
16
18
20
22
24
UNIVERSAL TIME

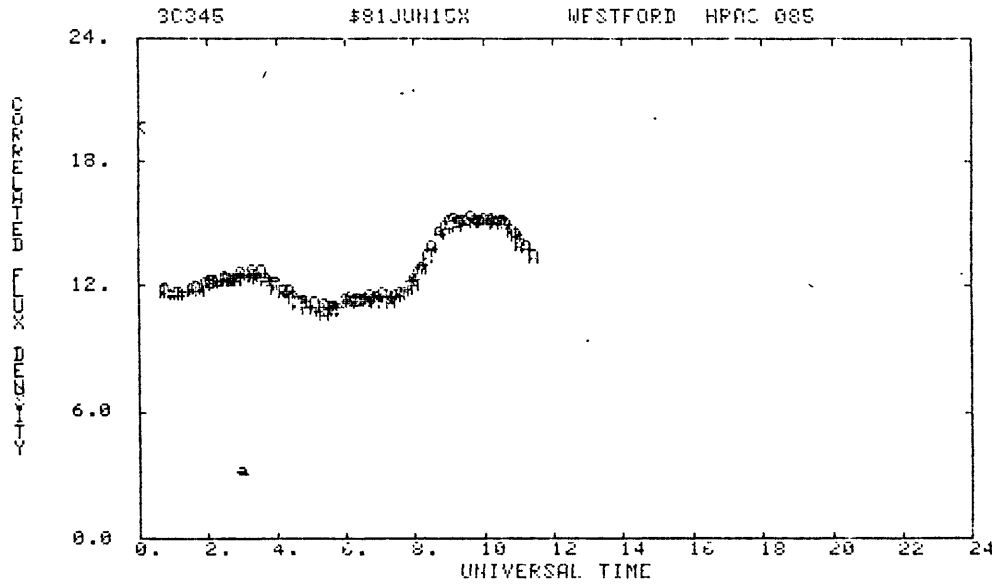
3C345 $81JUN15X WESTFORD HRAO 085
24.
18.
12.
6.0
0.0
0. 2. 4. 6. 8. 10 12 14 16 18 20 22 24
UNIVERSAL TIME

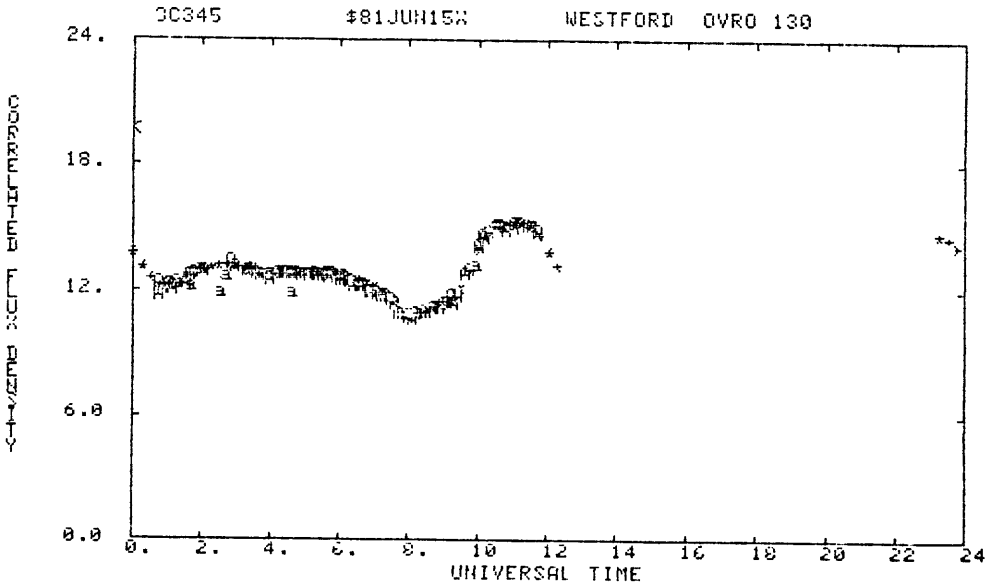
3C345 $81JUN15X WESTFORD OVRO 130
24.
18.
12.
6.0
0.0
0. 2. 4. 6. 8. 10 12 14 16 18 20 22 24
UNIVERSAL TIME

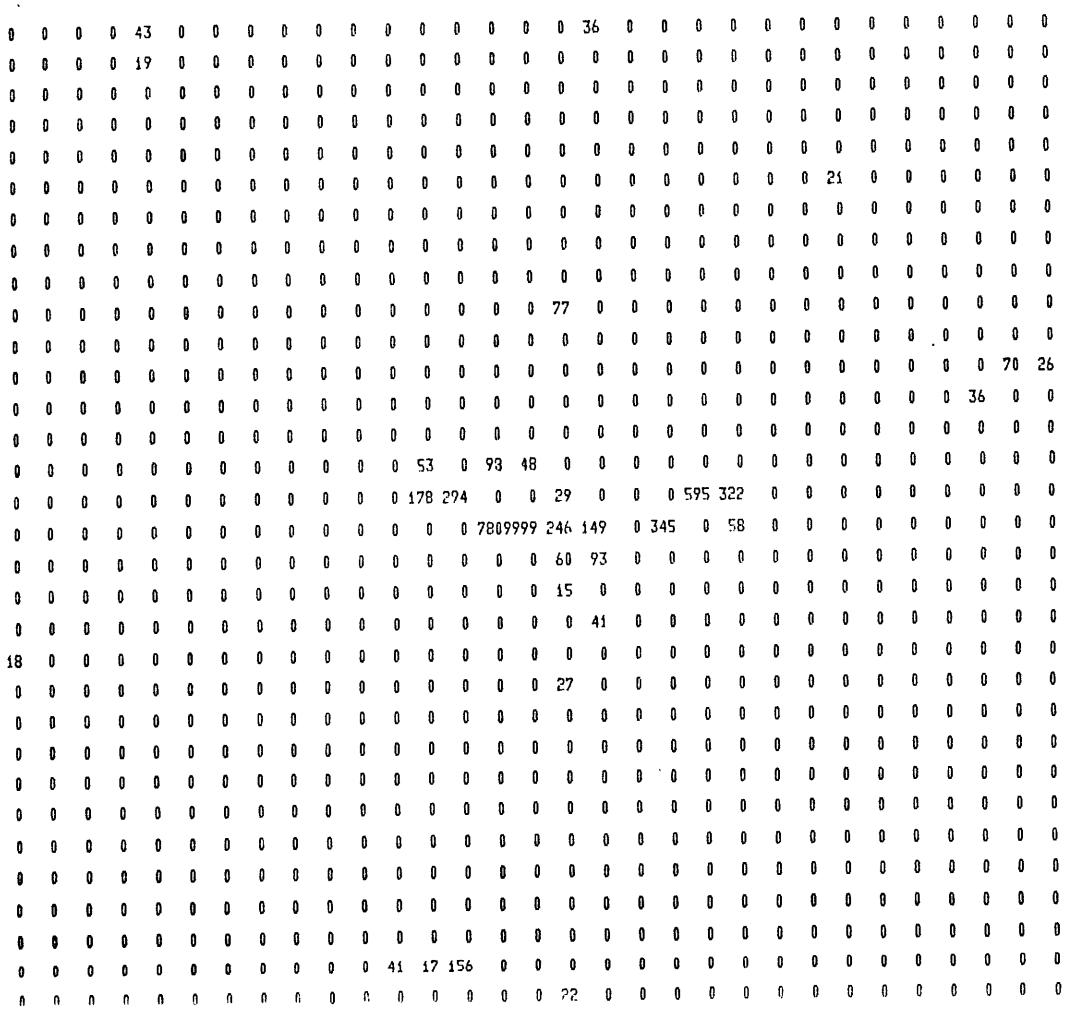

Figure 2.9a: CLEAN COMPONENTS 3C345 X-band

The clean components obtained from the "special" experiment and the geodetic experiment are calculated with a grid spacing of 0.35 mas. The flux densities are expressed as fractions of the peak value which is normalized to 10000.

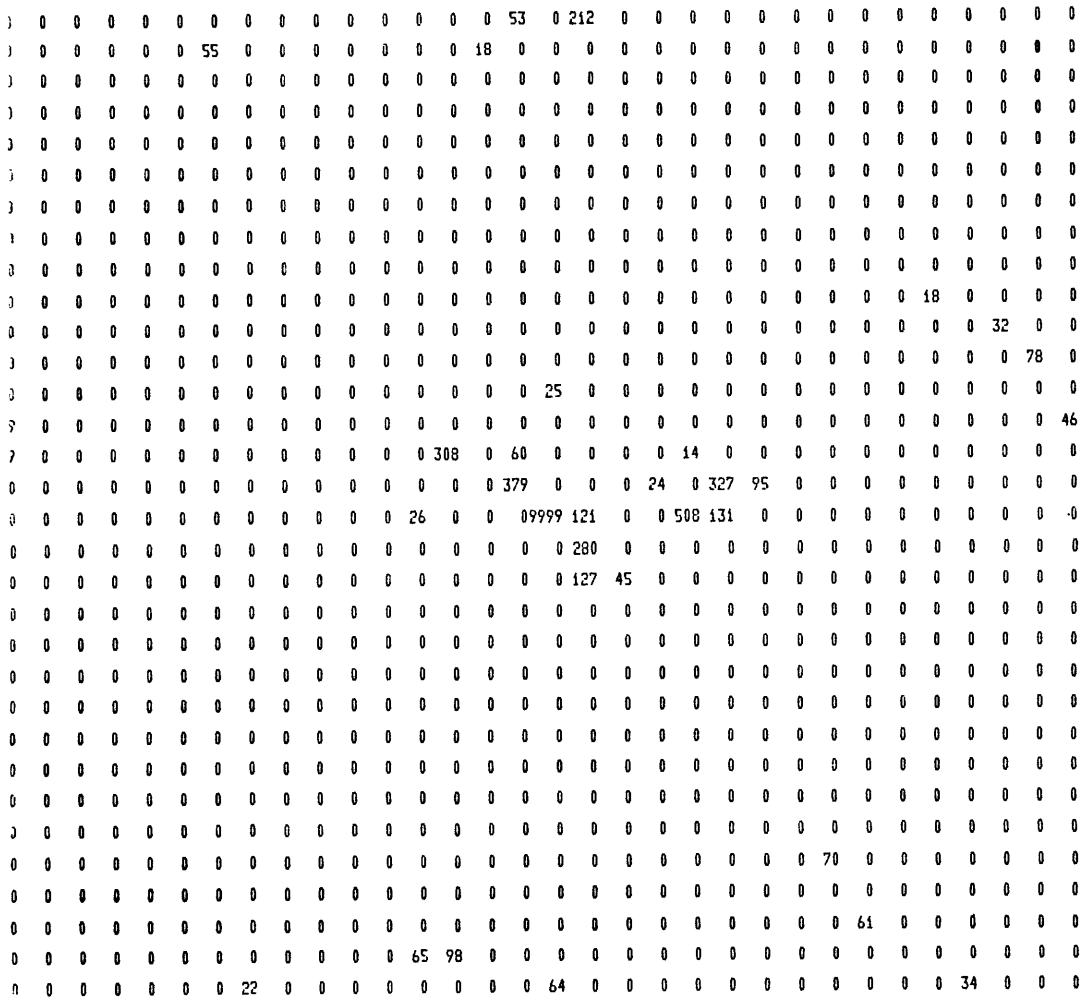

Figure 2.9b: CLEAN COMPONENTS 3C345 X-Band

The clean components obtained from the geodetic experiment only are calculated with a grid spacing of 0.35 mas. The flux densities are expressed as fractions of the peak values which is normalized to 10000.

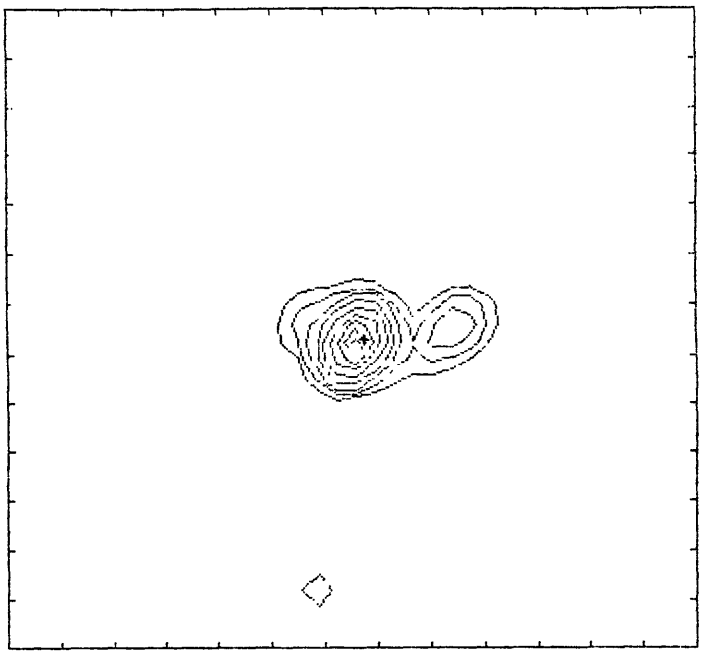

Figure 2.9 c:

RESTORING BEAM

HALF POWER LEVEL

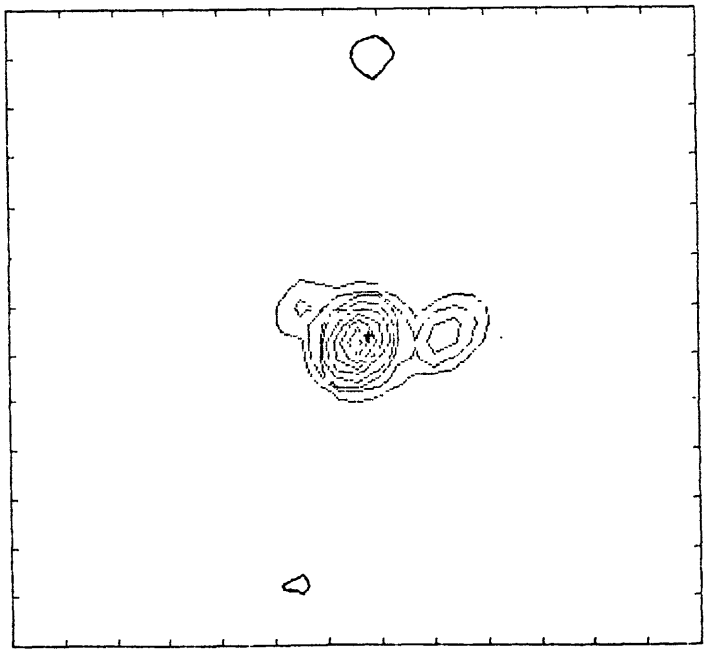

Figure 2.9 d:

Figure 2.9 c and Figure 2.9 d

3C345 X-band June 1981

Map obtained from data collected during the 3 days of experiment (Figure 2.9 c) and map obtained from data collected during the geodetic experiment only (Figure 2.9 d). Contours are shown at 1, 2.5, 5, 10, 20, 35, 50, 70 and 90% of the peak value. The restoring beam (FWHM) is 0.90 mas by 0.60 mas at a position angle of -25^{o} (overresolved by 1.8). The + shows the center of brightness. Tickmarks are every mas.

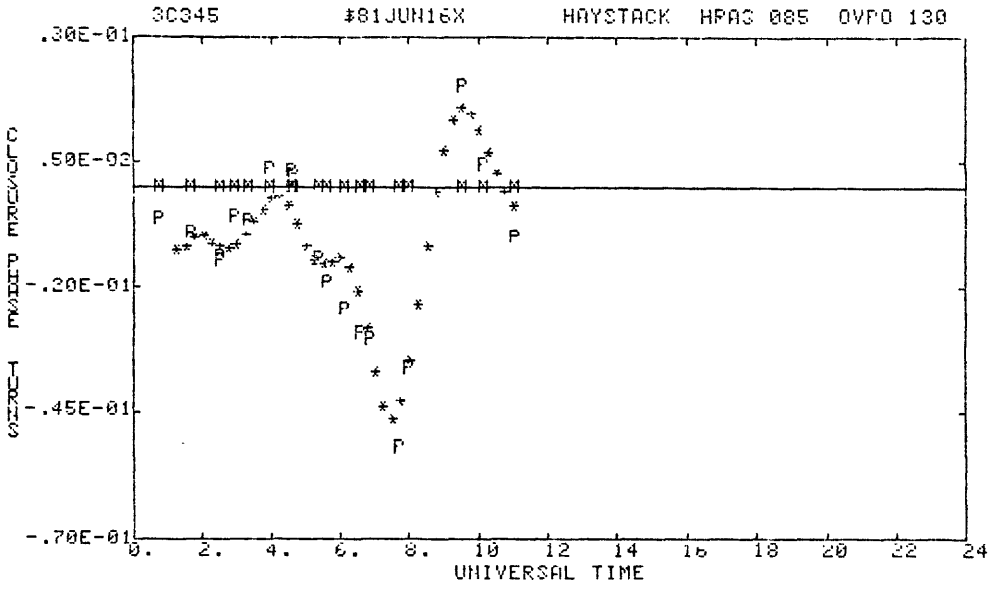

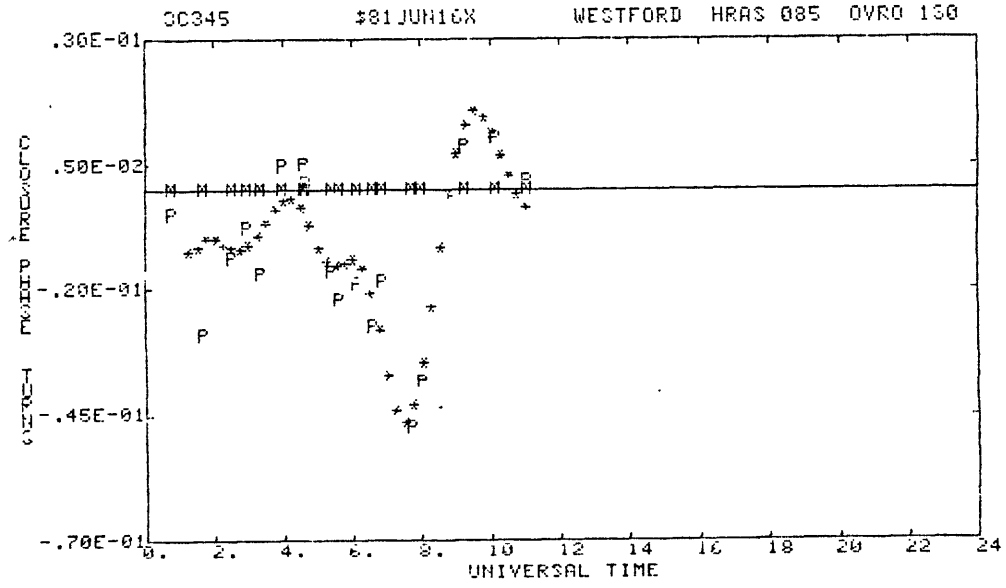

Figure 2.10a:

Phase closures HA-HR-OV and WE-HR-OV expressed as fractions of 360^{o}. The P's represent the observed phase closure, the *'s are the phase closure given by the map obtained from the geodetic experiment.

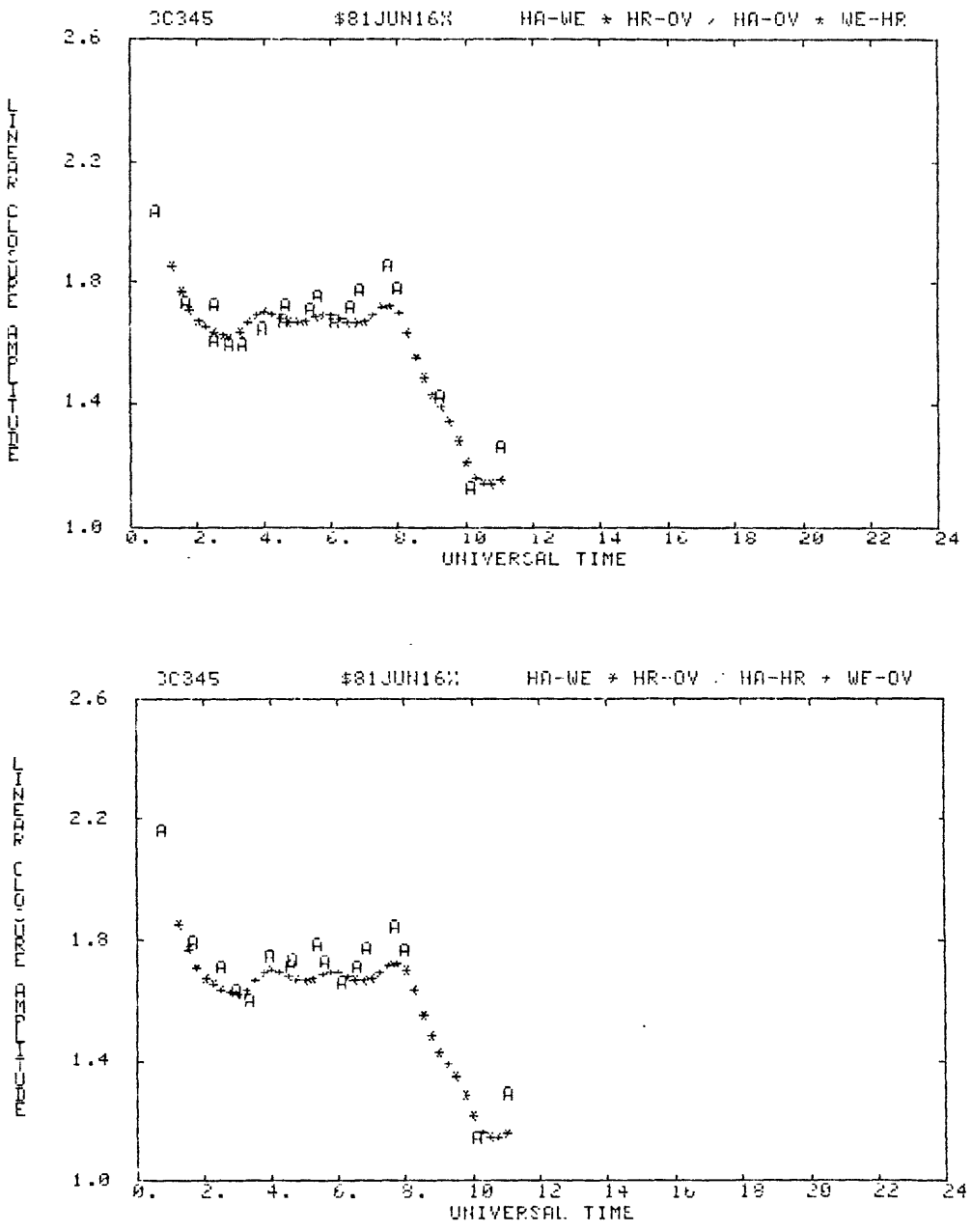

Figure 2.10b:

Linear amplitude closures. The A's are the observed amplitude closure and the *'s represent the amplitude closure predicted by the map obtained from the geodetic experiment.

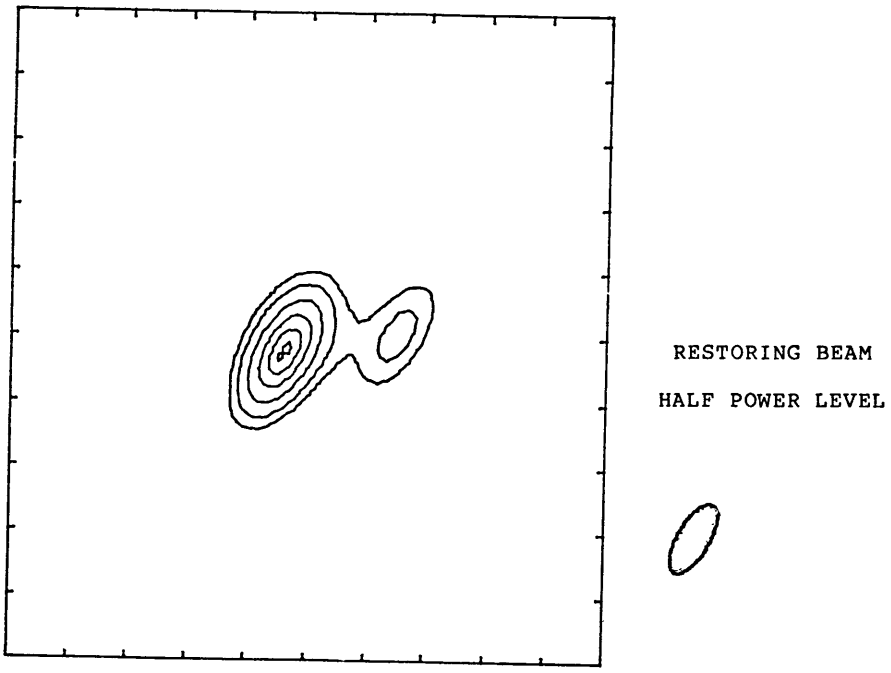

Figure 2.11:

3C345 at X-band (8341 MHz) in July 1980. The first reliable contour is at 4% of the peak brightness. The others are at 10, 25, 50, 75 and 95%. The total flux density is 6.37 Jy. The restoring beam is 1.10 mas by 0.48 mas at a position angle of -32°. The tickmarks are every 0.9 mas.

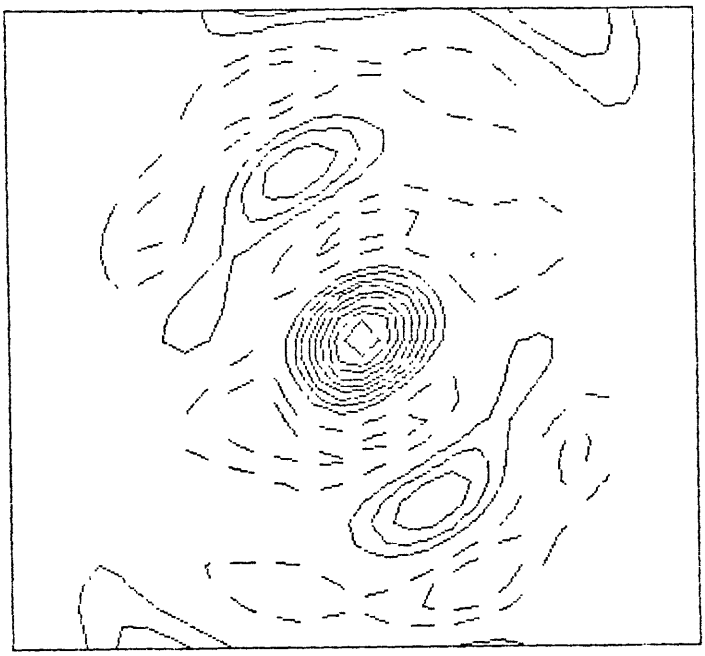

Figure 2.12a:

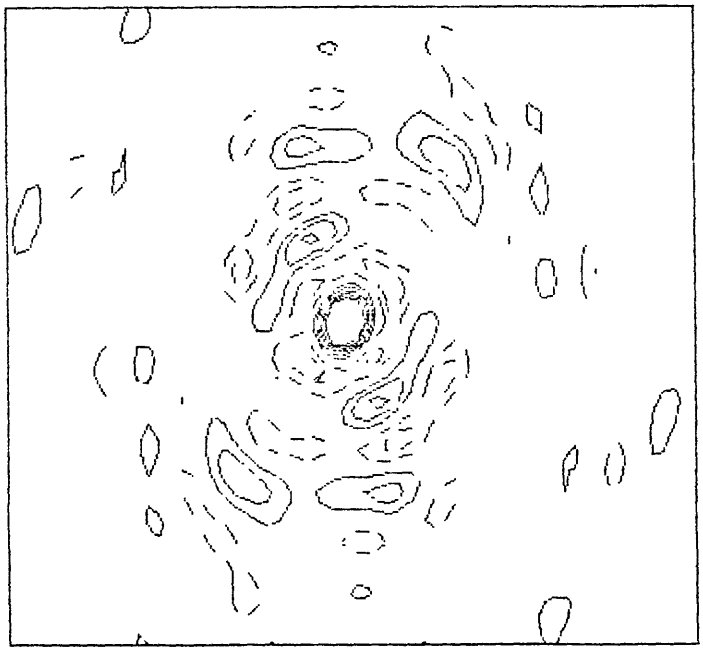

Figure 2.12b:

Figure 2.12a:

Dirty map of 3C345 at S-band obtained from the "special" experiment. The width of the box is 36.80 mas. Contours are drawn from -30% to 100% of the peak value (10% by 10%). Negative contours are in dashed lines.

Figure 2.12b:

Dirty beam of the "special" experiment at S-band. The width of the box 73.60 mas. Contours are drawn at 5, 10, 20, 30, 40 and 50% of the peak value. Negative contours are drawn at -30, -20, -10, -5% of the peak value.

Figure 2.13a:

Matrix of the clean components at S-band. The grid spacing is 1.15 mas. Each flux density is expressed as a fraction of the peak value which is normalized to 1000.

Figure 2.13b:

Map of 3C345 at S-band after 10 iterations. The contours are shown at 1, 2.5, 5, 10, 20, 35, 50, 70 and 90% of the peak value. The tickmarks are every 3 milliarcseconds. The restoring beam is 5.40 mas by 3.60 mas at a position angle of -25°. The + indicates the center of brightness.

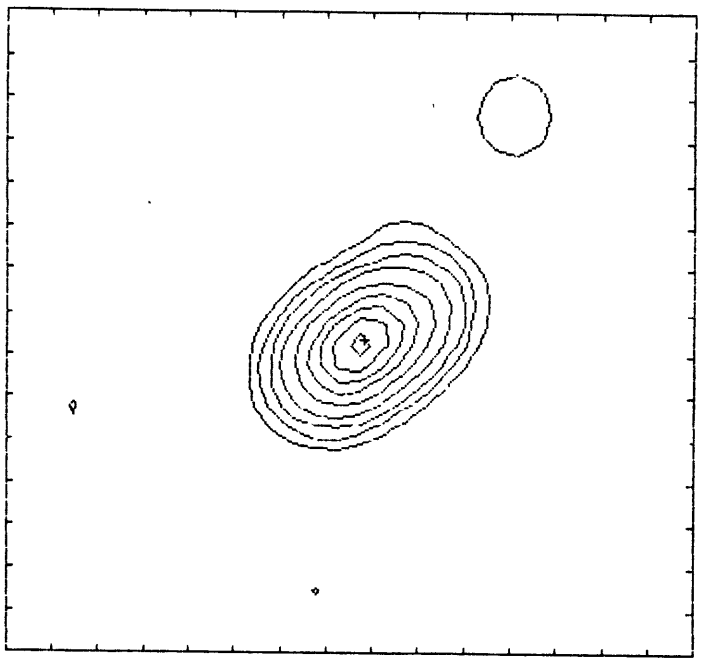

RESTORING BEAM

HALF POWER LEVEL

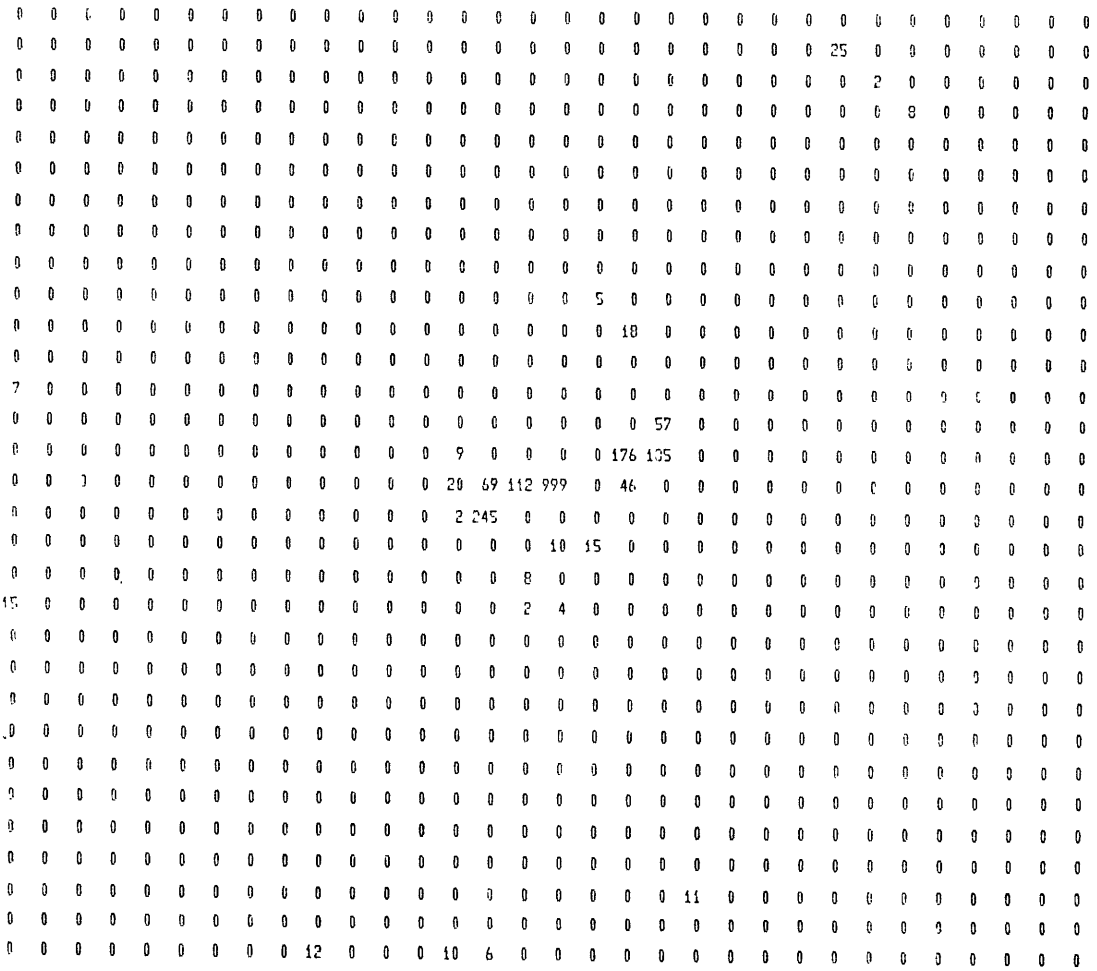

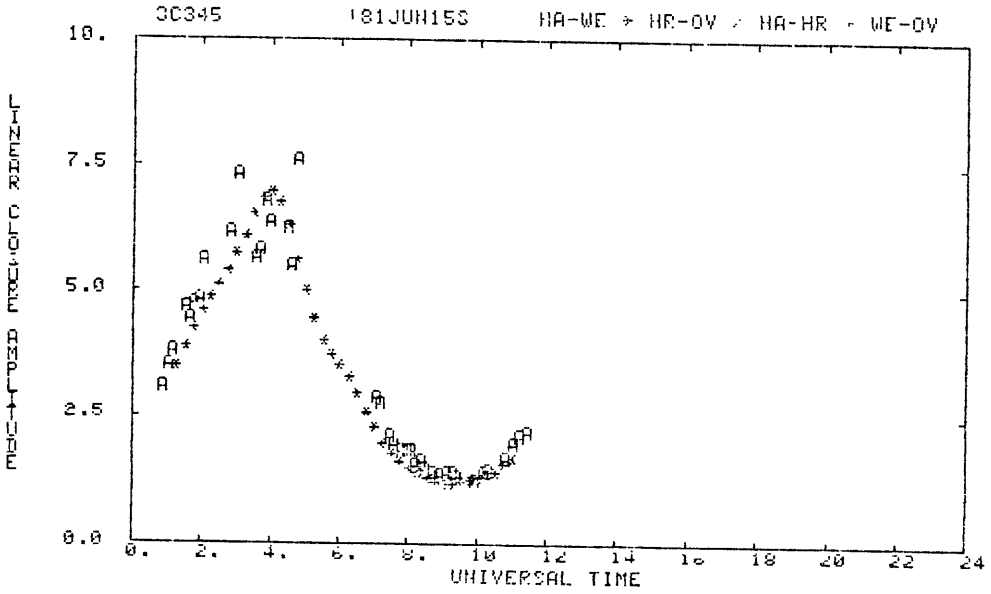

Figure 2.14a: 3C345 S-band June 1981

Amplitude closure HA-HR-OV plotted on a linear scale. The A's are the observed amplitude closure, the *'s are the amplitude closure predicted by the model.

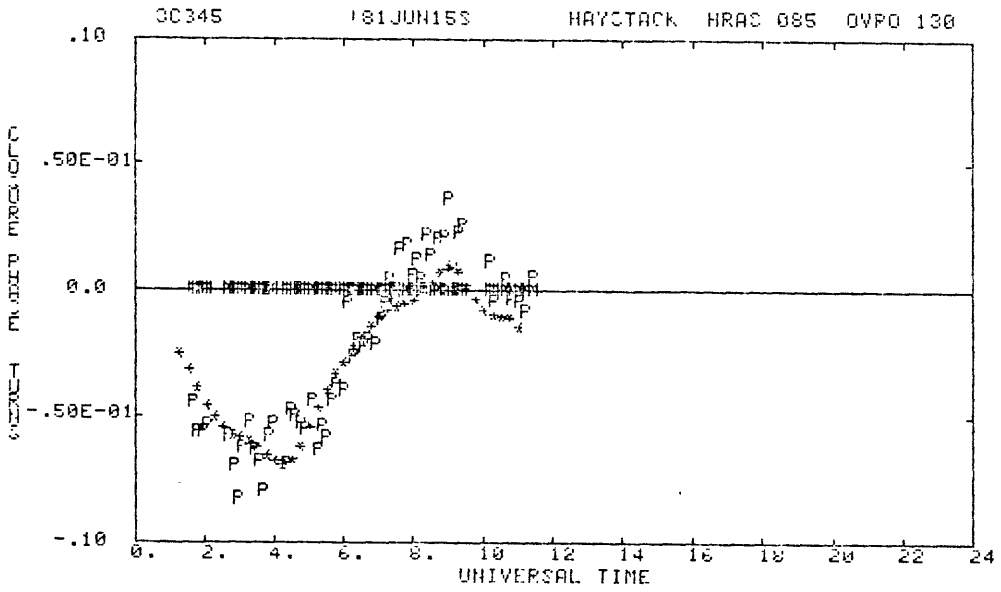

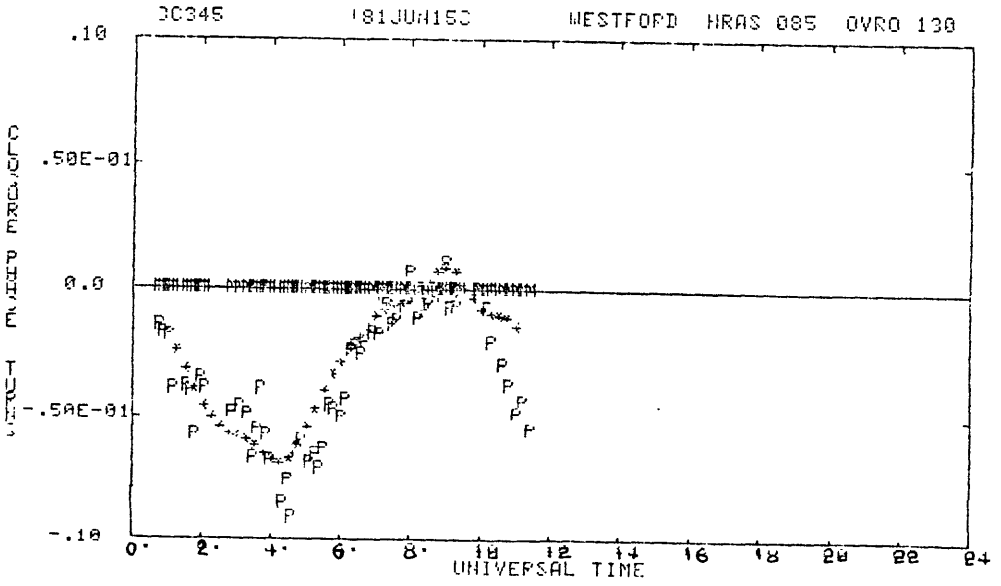

Figure 2.14b: 3C345 S-band June 1981

Phase closures HA-HR-OV and WE-HR-OV expressed as fractions of 360°. The P's are the observed phase closure, and the *'s are the phase closure given by the model. The *'s retain the same position on both plots although the phase closure are not exactly the same on both phase closures.

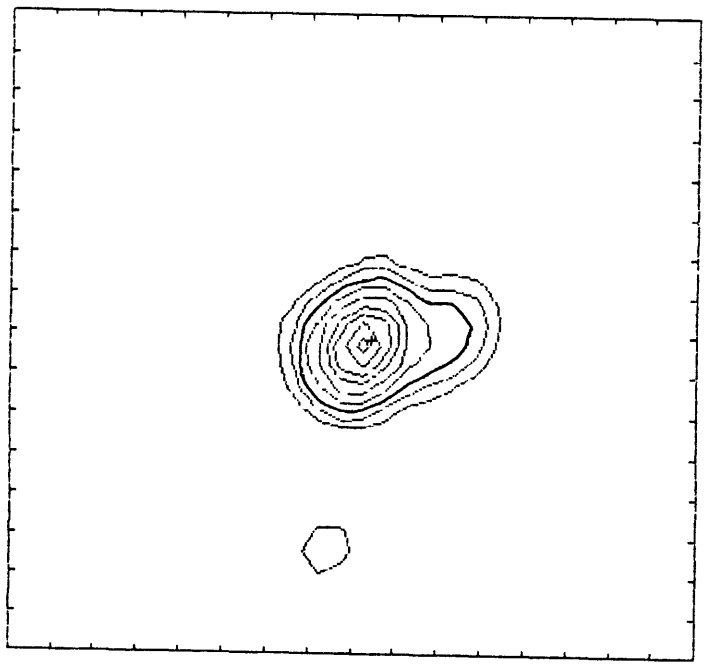

X-band map

RESTORING BEAM

HALF POWER LEVEL

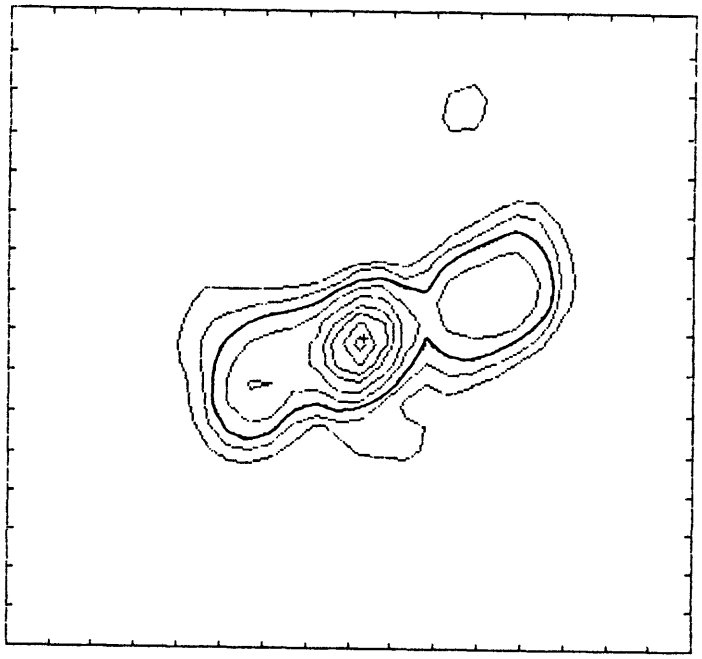

S-band map

Figure 2.15:

X-band map (ν 8.3 GHz) and S-band map (ν 2.3 GHz) of 3C345 obtained from data collected during the 3-day experiment in June 1981. Contours are shown at 1, 2.5, 5, 10, 20, 35, 50, 70 and 90% of the peak brigthness. Contours below 5% are likely unreliable. Tickmarks are every mas. The restoring beam is 1.60 mas by 1.10 mas at a position angle of -25°. The + indicates the center of brightness.

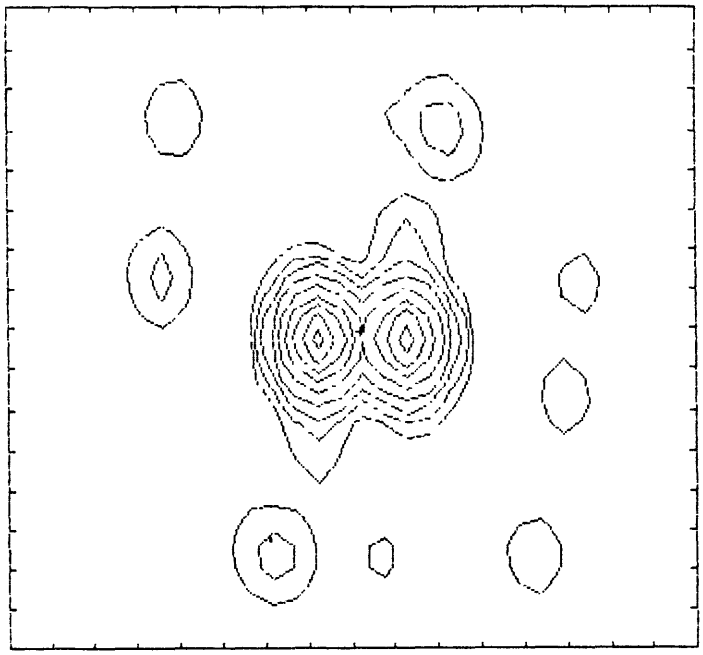

FAKE MAP

RESTORING BEAM

HALF POWER LEVEL

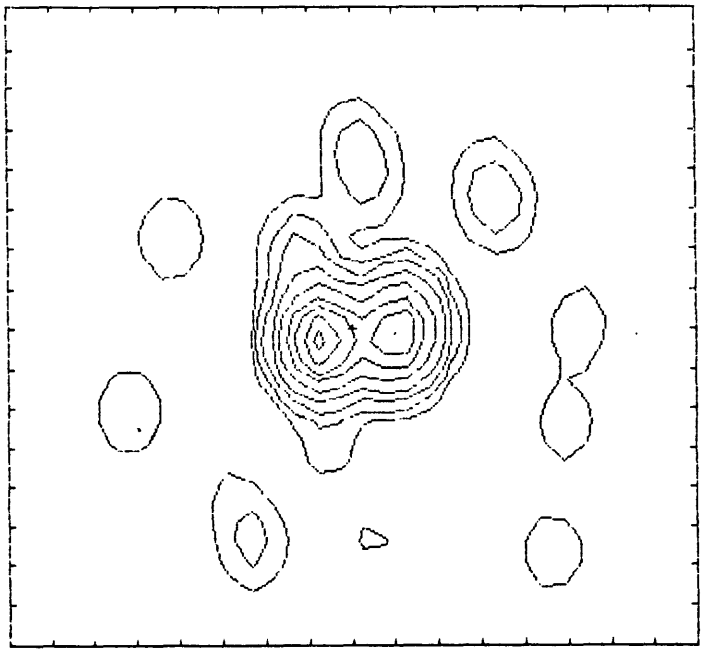

Figure 3.1.1: 4C39.25 X-band June 1981

Maps obtained from fake data and real data. Contours are shown at 1, 2.5, 5, 10, 20, 35, 50, 70 and 90% of the peak value. The reconstructing beam (FWHM) is 1.64 mas by 1.00 mas at zero position angle. the + shows the center of brightness.

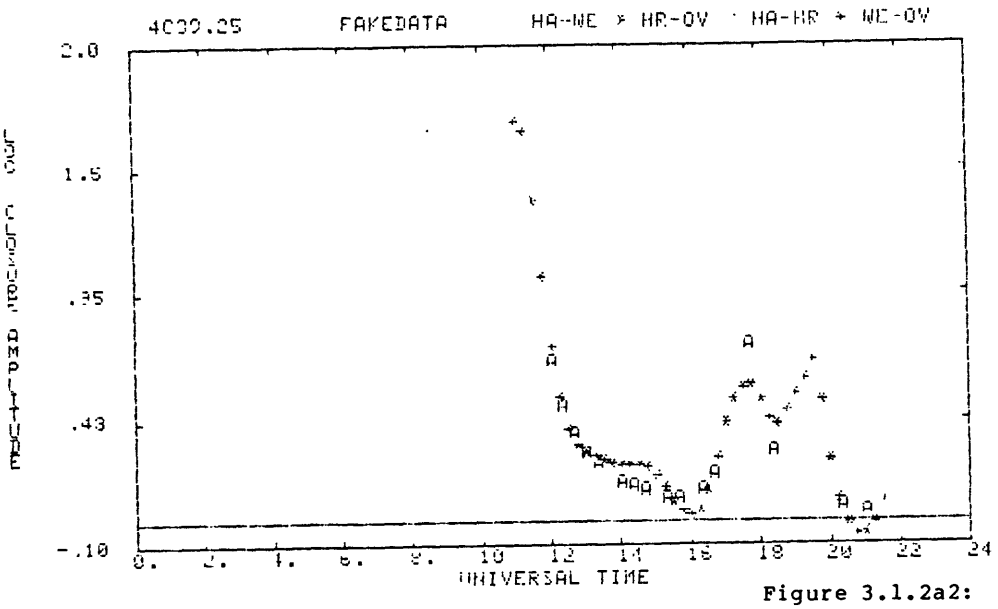

Figure 3.1.2a2:

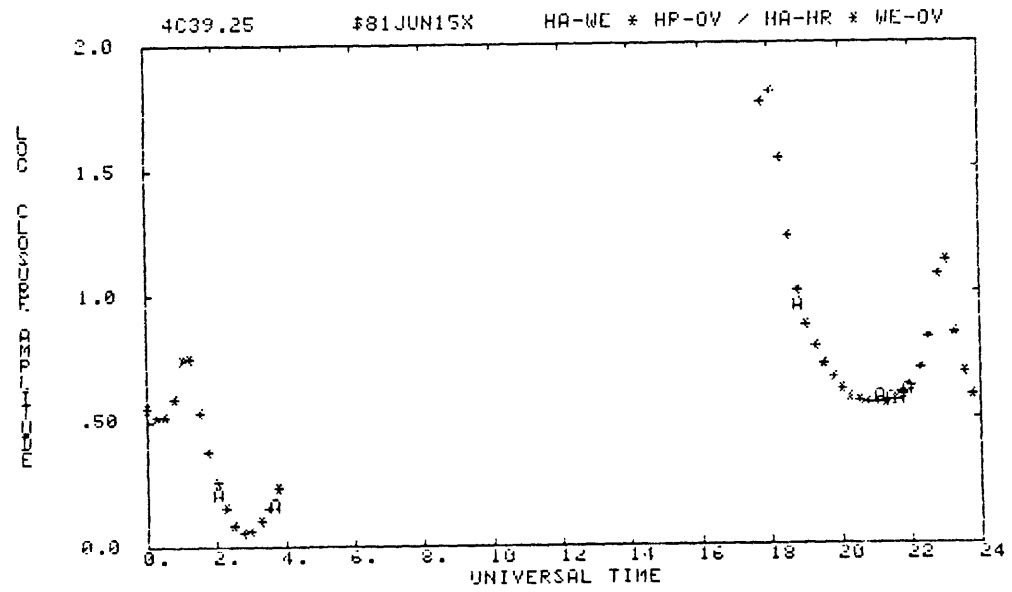

Figure 3.1.2a1:

Figure 3.1.2a: 4C39.25 X-band June 1981

Comparison on a logarithmic scale of the amplitude closure obtained from the real data (a1) and the fake data (a2). The A's are the observed amplitude closures and the *'s are the amplitude closures predicted by the model.

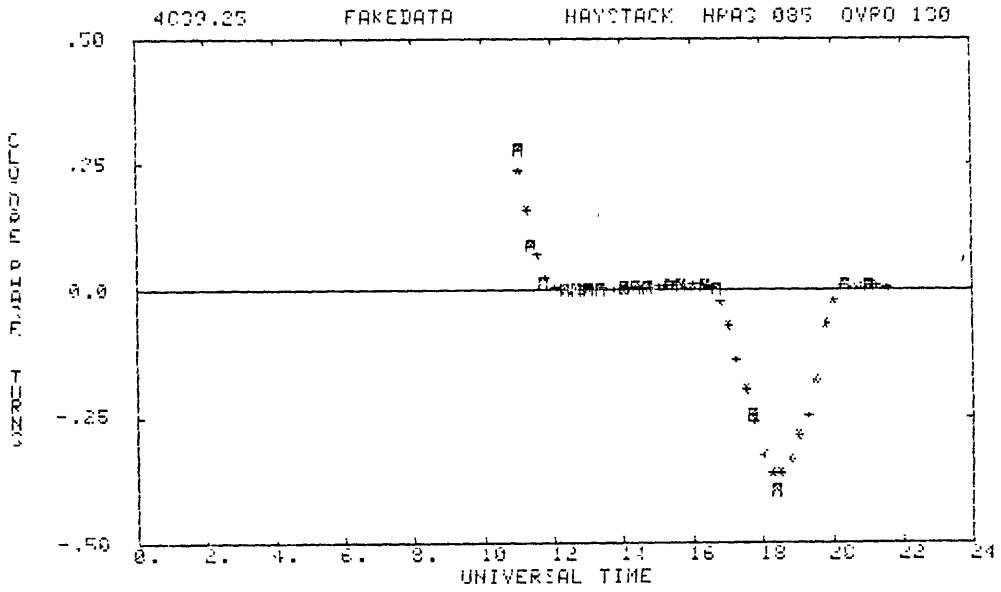

Figure 3.1.2b2:

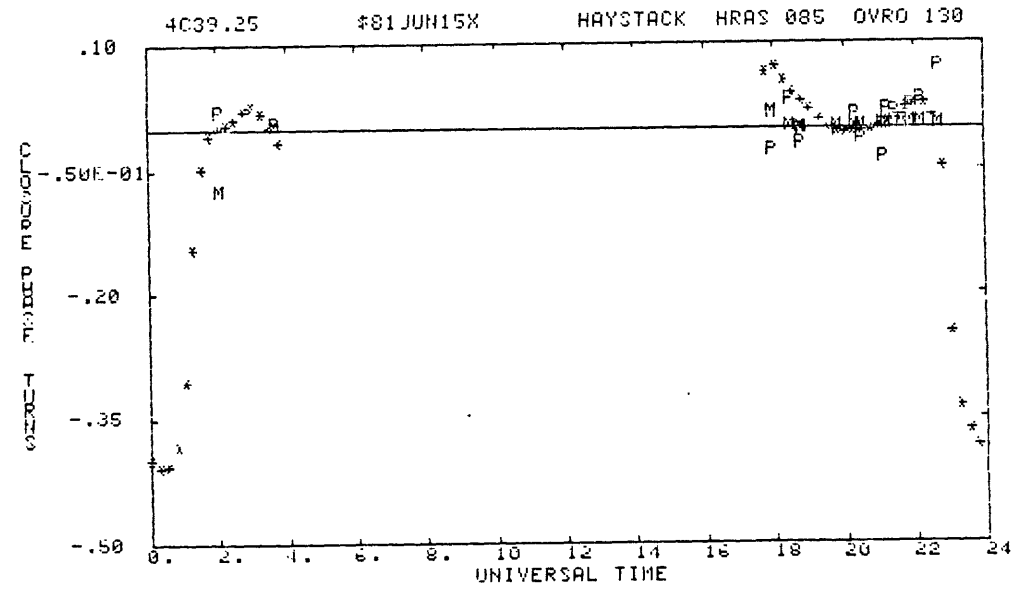

Figure 3.1.2b1:

Figure 3.1.2b: 4C39.25 X-band June 1981

Phase closure HA-HR-OV for the real data (b1) and fake data (b2). The phase closures are expressed as fractions of 360°. The P's are the closures given by the observations or fake observations and the *'s are the closures predicted by the model.

Figure 3.1.2c1:

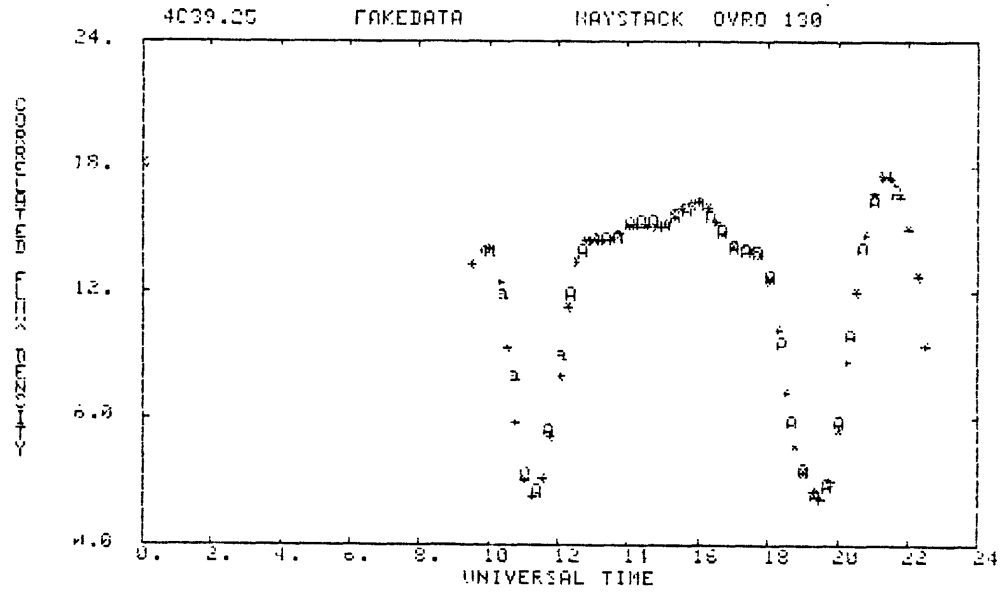

Figure 3.1.2c2:

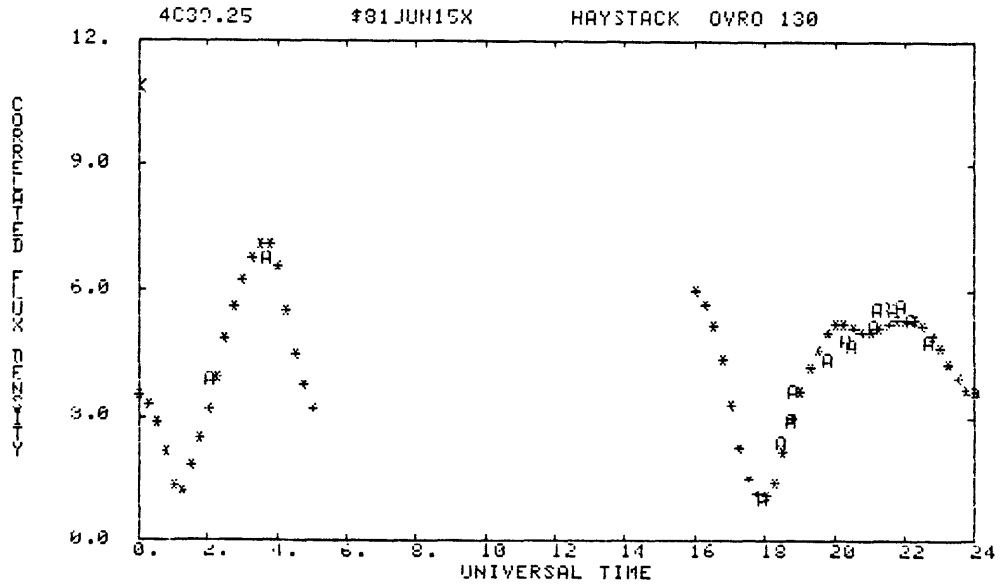

Figure 3.1.2c:

Correlated flux density on HA-OV at for the June 1981 experiment. Figure c1 corresponds to the fake data and Figure c2 to the real data. The A's are the observed amplitudes, *'s the amplitudes predicted by the model.

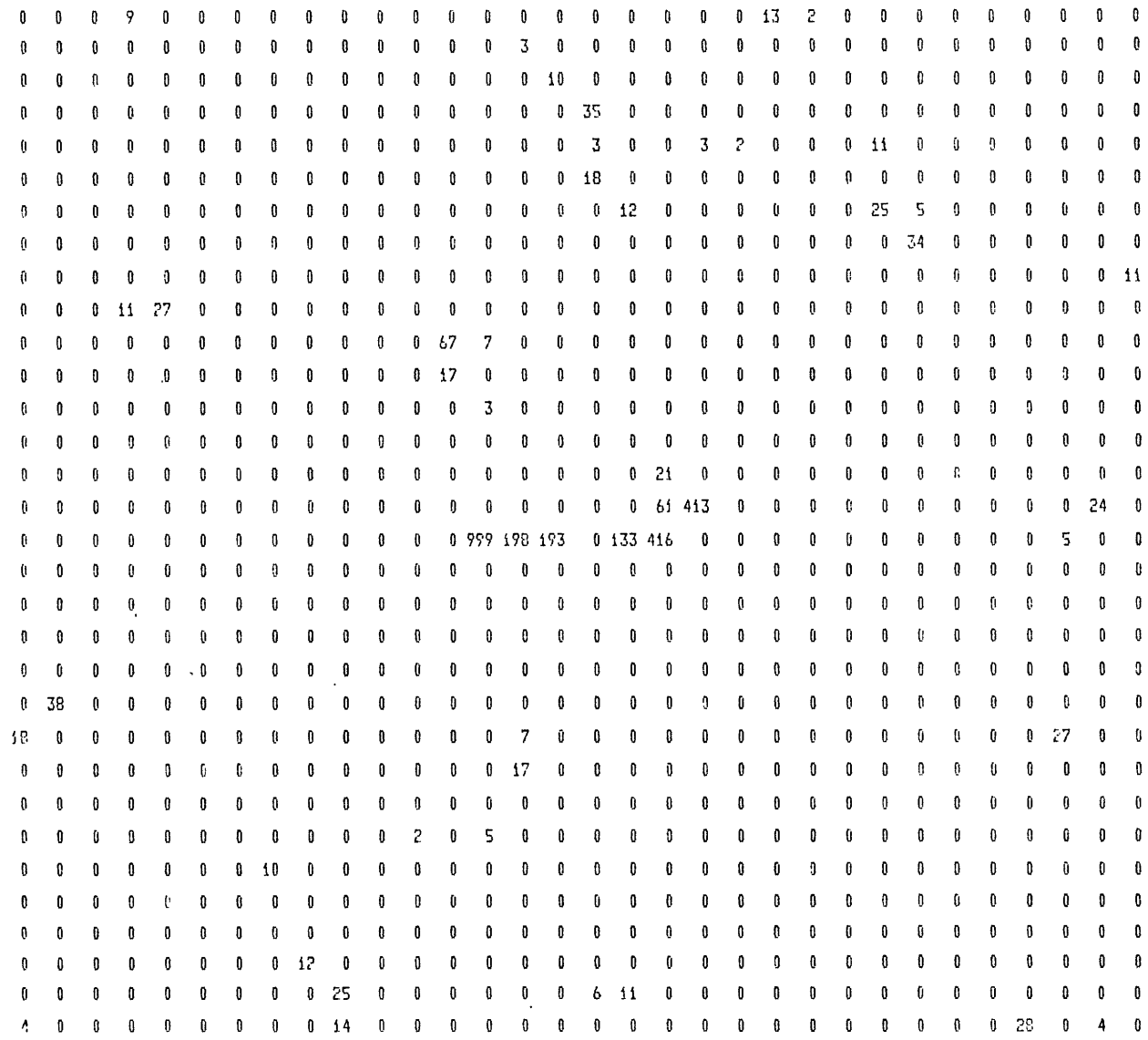

Figure 3.1.3: 4C39.25 X-band June 1981

The clean components are calculated with a grid spacing of 0.35 mas. The flux densities are expressed as fractions of the peak value which is normalized to 1000.

X-band June 1981

Figure 3.2.1: OJ287 CLEAN COMPONENTS- CLEAN MAP

The clean components are calculated using a grid spacing of 0.40 mas. Flux densities are expressed as fractions of the peak value which is normalized to 1000. The restoring beam (FWHM) is 2.20 mas by 1.10 mas at a position angle of -15^{o}. The contours are shown at 1, 2.5, 5, 10, 20, 35, 50, 70 and 90% of the peak value. Tickmarks are every milliarcsecond. the + represents the center of brightness.

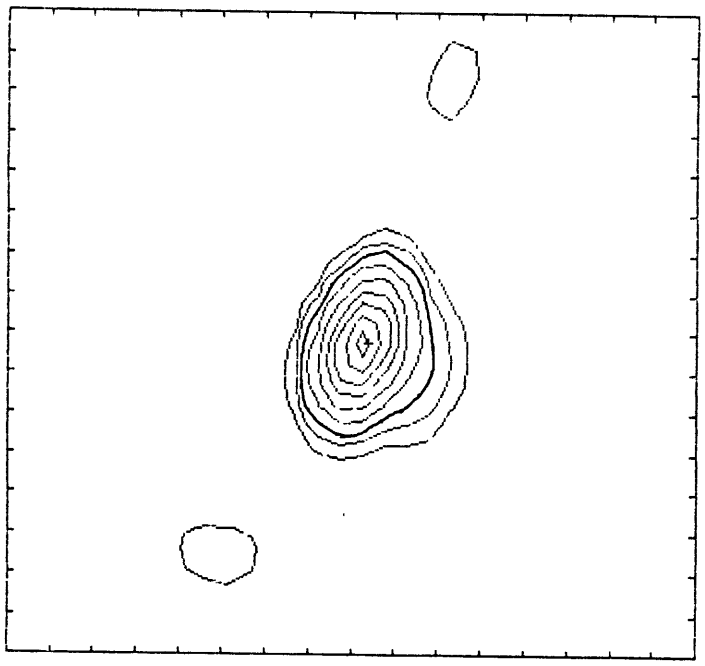

RESTORING BEAM

HALF POWER LEVEL

```
0 0 0 0 0 0 0 0 0 0 0 0 0 0 0 0 0 0 0 0 19 0 0 0 0 0 0 0 0 0 0
0 0 0 0 0 0 0 0 0 0 0 0 0 0 0 0 0 0 0 0 0 0 0 0 0 0 0 0 0 0 0
0 0 0 0 0 0 0 0 0 0 0 0 0 0 0 0 0 0 0 0 0 0 0 0 0 0 0 0 0 0 0
0 0 0 0 0 0 0 0 0 0 0 0 0 0 0 0 0 0 0 0 0 0 0 0 0 0 0 0 0 0 0
0 0 0 0 0 0 0 0 0 0 0 0 0 0 0 0 0 0 0 0 0 0 0 0 0 0 0 0 0 0 0
0 0 0 0 0 0 0 0 0 0 0 0 0 0 0 0 0 0 0 0 0 0 0 0 0 0 0 0 0 0 0
0 0 0 0 0 0 0 0 0 0 0 0 0 0 0 0 0 0 0 0 0 0 0 0 0 0 0 0 0 0 0
0 0 0 0 0 0 0 0 0 0 0 0 0 0 0 0 0 0 0 0 0 0 0 0 0 0 0 0 0 0 0
0 0 0 0 0 0 0 0 0 0 0 0 0 0 0 0 0 0 0 0 0 0 0 0 0 0 0 0 0 6 0
0 0 0 0 0 0 0 0 0 0 0 0 0 0 0 0 0 0 0 0 0 0 0 0 0 0 0 0 0 0 0
0 0 0 0 0 0 0 0 0 0 0 0 0 0 0 0 0 0 0 0 0 0 0 0 0 0 0 0 1 0 0
0 0 0 0 0 0 0 0 0 0 2 0 0 0 0 0 0 0 0 0 0 0 0 0 0 0 0 0 0 0 0
0 0 0 0 0 0 0 0 0 0 0 0 0 0 0 0 0 0 0 0 0 0 0 0 0 0 0 0 0 0 0
0 0 0 0 0 0 0 0 0 0 0 0 0 0 0 0 0 0 0 0 0 0 0 0 0 0 0 0 0 0 0
0 0 0 0 0 0 0 0 0 0 0 0 0 0 0 0 0 0 0 0 0 0 0 0 0 0 0 0 0 0 0
0 0 0 0 0 0 0 0 0 0 0 0 0 0 0 0 0 1 0 0 0 0 0 0 0 0 0 0 0 0 0
0 0 0 0 0 0 0 0 0 0 0 0 0 3 0 0 0 0 0 0 0 0 0 0 0 0 0 0 0 0 0
0 0 0 0 0 0 0 0 0 0 0 0 0 0 0 63 999 12 0 0 0 0 0 0 0 0 0 0 0 0 0
0 0 0 0 0 0 0 0 0 0 0 0 0 0 0 0 0 0 25 39 0 0 0 0 0 0 0 0 0 0 0
0 0 0 0 0 0 0 0 0 0 0 0 0 0 0 0 0 0 2 14 0 0 0 0 0 0 0 0 0 0 0
0 0 0 0 0 0 0 0 0 0 0 0 0 0 0 0 0 0 0 5 8 0 0 0 0 0 0 0 0 0 0
0 0 0 0 0 0 0 0 0 0 0 0 0 0 0 0 0 0 0 1 0 0 0 0 0 0 0 0 0 0 0
0 0 0 0 0 0 0 0 0 0 0 0 0 0 0 0 0 0 0 0 0 0 0 0 0 0 0 0 0 0 0
0 0 0 0 0 0 0 0 0 0 0 0 0 0 0 0 0 0 0 0 0 0 0 0 0 0 0 0 0 0 0
0 0 0 0 0 0 0 0 0 0 0 0 0 0 0 0 0 0 0 0 0 0 0 0 0 0 0 0 0 0 0
0 0 0 0 0 0 0 0 0 0 0 0 0 0 0 0 0 0 0 0 0 0 0 0 0 0 0 0 0 0 0
0 0 0 0 0 0 0 0 0 0 0 0 0 0 0 0 0 0 0 0 0 0 0 0 0 0 0 0 0 0 0
0 0 0 0 0 0 0 0 0 0 0 0 0 0 0 0 0 0 0 0 0 0 0 0 0 0 3 0 0 0 0
0 0 0 0 0 0 0 0 0 0 0 0 0 0 0 0 0 0 0 0 0 0 0 0 0 0 0 0 0 0 0
0 0 0 0 0 0 0 0 0 0 0 0 0 0 0 0 0 0 0 0 0 0 0 0 0 0 0 0 0 0 0
0 0 0 0 0 0 0 0 0 0 0 0 0 0 0 0 0 0 0 0 0 0 0 0 0 0 0 0 0 0 0
0 0 0 0 0 9 0 0 0 0 0 0 0 0 0 0 0 0 0 0 0 0 0 0 0 0 0 0 0 0 0
0 0 0 0 0 0 0 11 0 8 0 0 0 0 0 0 0 0 0 0 0 0 0 0 0 0 0 0 0 0 0
0 0 0 0 0 0 0 0 0 0 0 0 0 0 0 0 0 0 0 0 0 0 0 0 0 0 0 0 0 0 0
0 0 0 0 0 0 0 0 0 0 0 0 0 0 0 0 0 0 0 0 0 0 0 0 0 0 0 0 0 0 0
```

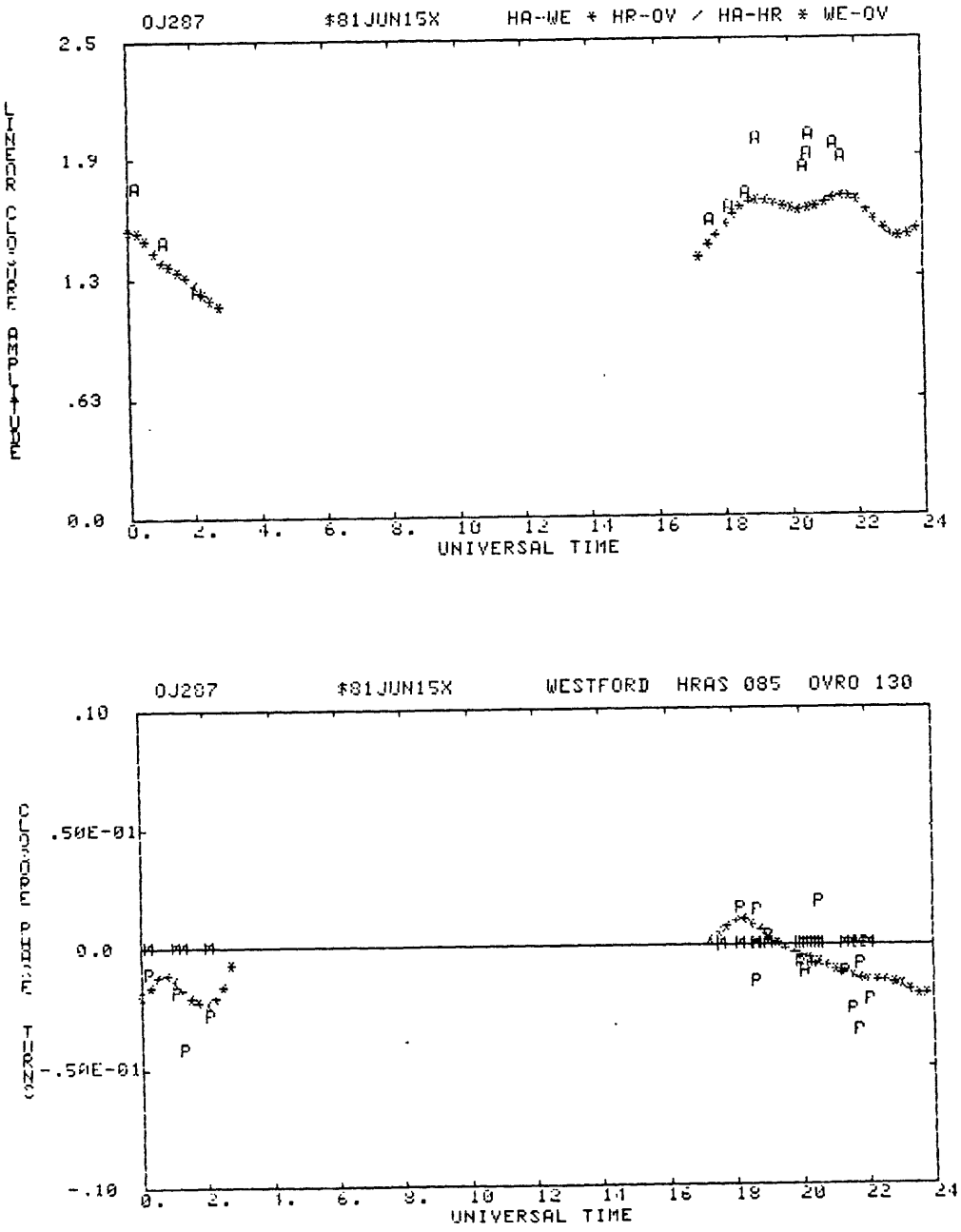

Figure 3.2.2: 0J287 X-band June 1981

Linear amplitude closure HA-HR, HR-OV, OV-WE, WE-HA and phase closure WE-HR-OV. The *'s give the closure predicted by the model, the A's are the observed amplitude closure and the P's are the observed phase closure. The phase closures are expressed as fractions of 360°.

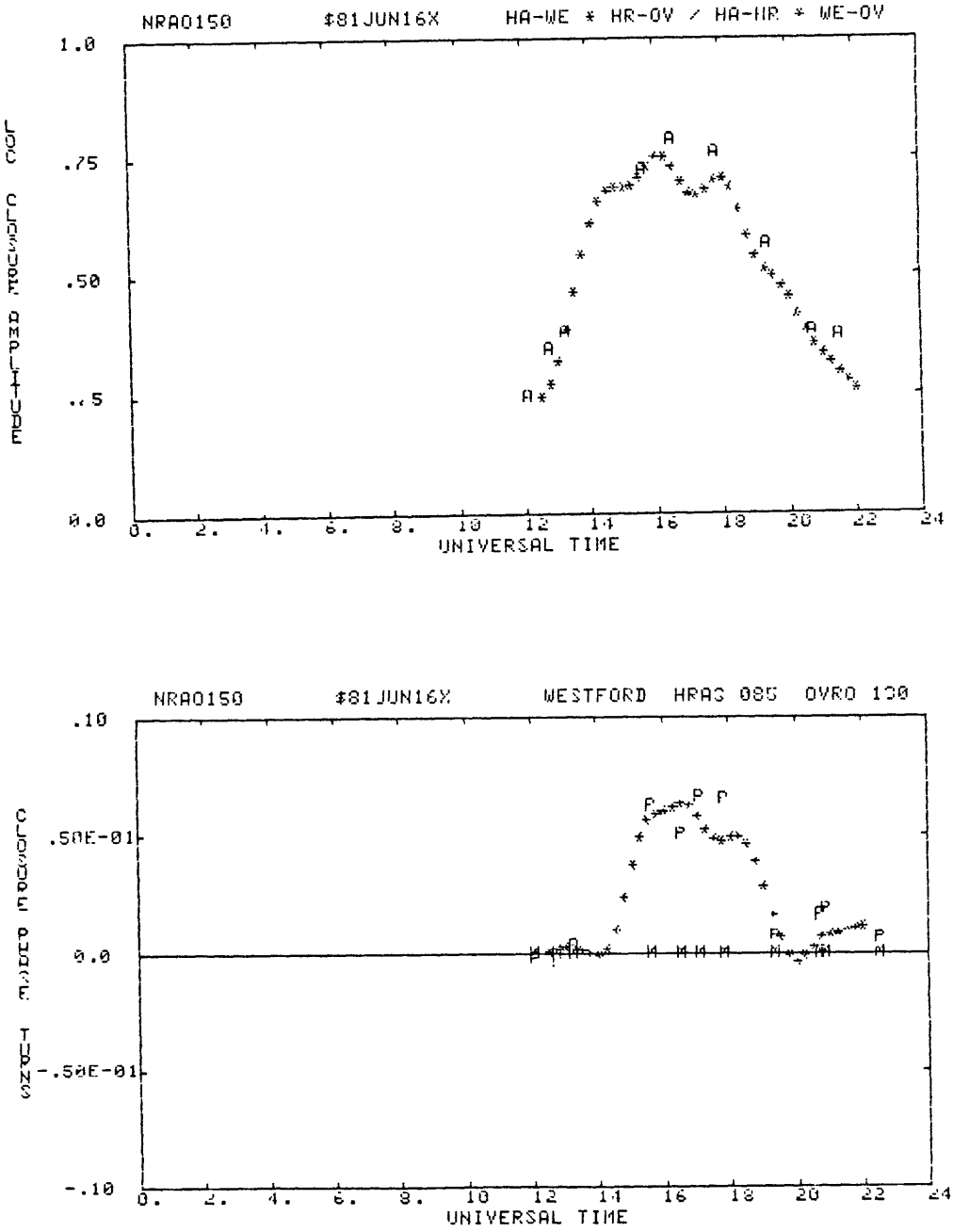

Figure 3.3.1: NRAO 150 X-band June 1981

Closure amplitude HA-HR, HR-OV, OV-WE, WE-HA on a logarithmic scale and phase closure WE-HR-OV. The A's are the observed amplitude closure, the P's are the observed phase closure and the *'s are the closures (amplitude or phase) predicted by the model. The phase closures are expressed as fractions of 360°.

X-band June 1981

Figure 3.3.2: NRAO 150 CLEAN COMPONENTS- CLEAN MAP

The clean components are calculated using a grid spacing of 0.30 mas. Flux densities are expressed as fractions of the peak value which is normalized to 1000. The restoring beam (FWHM) is 2.25 mas by 1.00 mas at a position angle of -35^{o}. The contours are shown at 1, 2.5, 5, 10, 20, 35, 50, 70 and 90% of the peak value. Tickmarks are every milliarcsecond. The + shows the center of brightness.

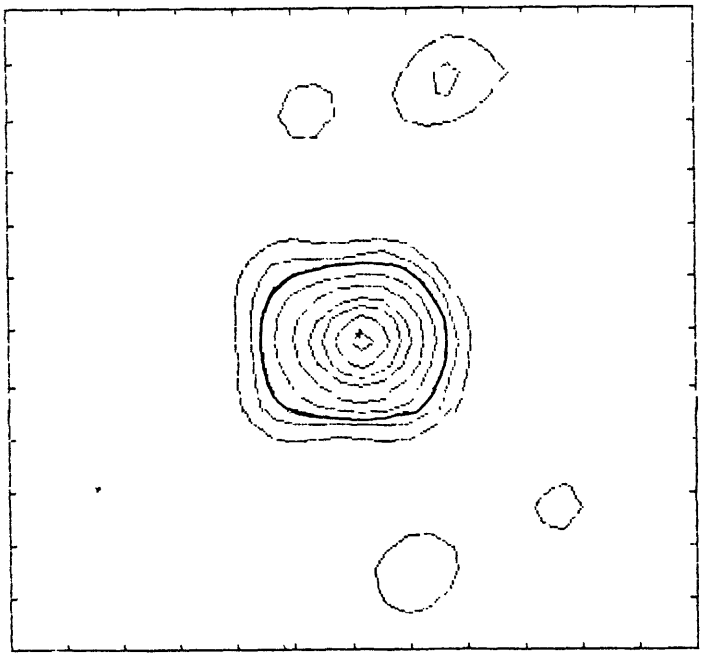

RESTORING BEAM

HALF POWER LEVEL

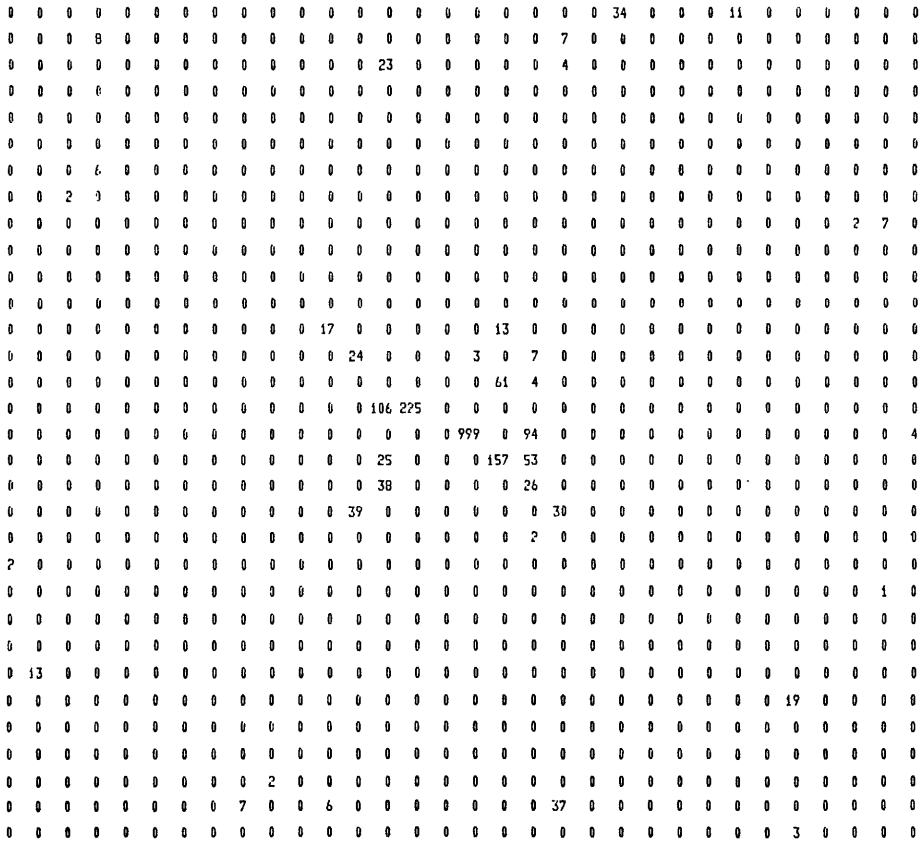

X-band June 1981

Figure 3.4.1: 3C273B CLEAN COMPONENTS- CLEAN MAP

The clean components are calculated using a grid spacing of 0.50 mas. Flux densities are expressed as fractions of the peak value which is normalized to 1000. The restoring beam (FWHM) is 4.00 mas by 1.00 mas at a position angle of -15^{o}. The contours are shown at 1, 2.5, 5, 10, 20, 35, 50, 70 and 90% of the peak value. Tickmarks are every milliarcsecond. The + shows the center of brightness.

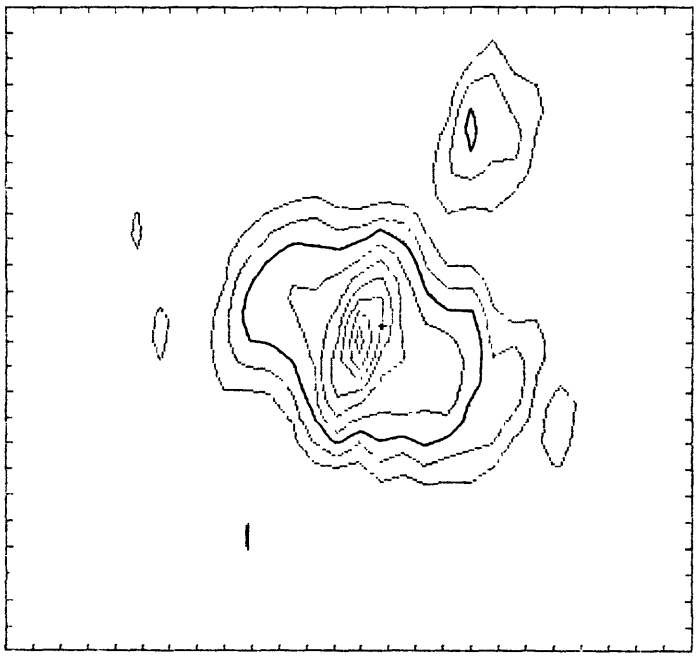

RESTORING BEAM

HALF POWER LEVEL

0 0 0 0 0 0 0 0 0 0 0 0 0 0 0 0 0 0 0 0 0 32 0 0 45 0 0 0 0 7 0
0 0 0 0 0 0 0 0 0 0 0 0 0 0 0 0 0 0 0 0 0 0 0 0 0 0 0 0 0 0 0
0 0 0 0 0 0 0 0 0 0 0 0 0 0 0 0 0 0 0 0 0 0 0 0 0 0 0 0 0 0 0
0 0 0 0 0 0 0 0 0 0 0 0 0 0 0 0 0 0 0 0 0 0 0 0 0 9 0 51 0 0 0
0 0 0 0 0 0 0 0 0 0 0 0 0 0 0 0 0 0 0 0 0 0 0 0 0 0 0 0 0 0 0
0 0 5 0 0 0 0 0 0 0 0 0 0 0 0 0 0 0 0 0 0 0 0 0 0 0 0 0 0 0 0
0 0 0 0 0 0 0 0 0 0 0 0 0 0 0 0 0 0 0 0 0 0 0 0 0 0 0 0 0 0 0
0 0 0 0 0 0 0 2 0 0 0 0 0 0 0 0 0 0 0 0 0 0 0 0 0 0 0 0 0 0 0
0 0 0 0 0 0 0 0 0 0 0 0 0 0 0 0 0 0 0 0 0 0 0 0 0 0 0 0 0 0 0
7 0 0 0 0 0 0 0 0 0 0 0 0 0 0 0 0 0 0 0 0 0 0 0 0 0 0 0 0 0 0
0 0 0 0 0 0 0 0 0 0 0 0 0 0 0 0 0 0 0 0 0 0 0 0 0 0 0 0 0 0 0
0 0 0 0 0 0 0 0 0 0 0 0 0 0 0 0 0 0 0 0 0 0 0 0 2 0 0 0 0 0 0
0 0 0 0 0 0 0 4 25 64 0 07 0 0 0 0 0 0 0 0 0 0 0 0 0 0 0 0 0 0 0
0 0 0 0 0 0 0 0 0 0 0 0 0 92 0 0 0 0 0 0 0 0 0 0 0 0 0 0 0 0 0
0 0 0 2 0 0 0 0 4 0 0 0 0 43 0 0 0 0 0 0 0 0 0 0 0 0 0 0 0 0 0
0 0 0 0 0 0 0 0 0 0 0 0 0 19 0 22 106 170 0 0 0 0 0 0 0 0 0 0 0 0 0
0 0 4 0 0 0 0 0 0 0 0 0 0 17 0 0 999 0 174 0 0 0 6 0 0 0 0 0 0 0 0 0
0 0 11 0 0 0 0 1 0 0 0 0 0 0 3 0 0 0 0 0 0 0 33 0 0 0 0 0 0 0 0 0
0 0 0 0 0 0 0 0 0 0 0 0 0 0 0 0 0 17 129 123 0 0 41 0 0 0 0 9 0 0 0 0
0 0 0 0 0 0 0 0 0 0 0 0 0 0 0 0 0 0 0 0 11 134 80 0 0 0 0 19 0 0 0 0
0 0 0 0 0 0 0 0 0 0 0 0 0 0 0 0 0 0 0 0 0 0 0 0 0 0 0 0 0 0 0 0
0 0 0 0 0 0 0 0 0 0 0 0 0 0 0 0 0 0 0 0 0 0 0 0 55 0 0 0 0 0 0 3
0 0 0 0 0 0 0 0 0 0 0 0 0 0 0 0 0 0 0 0 0 0 19 0 0 0 0 0 0 0 0 0
0 0 0 0 0 0 0 0 0 0 0 0 0 0 0 0 0 0 0 0 0 0 6 0 0 0 0 0 0 0 0 0
0 0 0 0 0 0 0 0 0 0 0 0 0 0 0 0 0 0 0 0 0 0 0 0 0 0 0 0 2 0 0 0
0 0 0 0 0 0 0 0 0 0 0 0 0 0 0 0 0 0 0 0 0 0 0 0 0 0 0 0 0 0 0 0
0 0 0 0 0 0 0 0 0 0 0 0 0 0 0 0 0 0 0 0 0 0 0 0 0 0 0 0 0 0 0 0
0 0 0 0 0 0 0 0 0 0 0 0 0 0 0 0 0 0 0 0 0 0 0 0 0 0 0 3 0 0 0 0
0 0 0 0 8 0 0 0 0 0 0 0 0 0 0 0 0 0 0 0 0 0 0 0 0 0 0 0 0 0 0 0
0 0 0 0 0 0 0 0 0 0 0 0 0 0 0 0 0 0 0 0 0 0 0 0 0 0 0 0 0 0 0 0
0 0 0 0 0 0 0 0 0 0 0 0 0 0 0 0 0 0 0 0 0 0 0 0 0 0 0 0 0 0 0 0
0 16 0 0 0 0 0 0 27 0 0 0 0 0 0 0 0 0 0 0 0 0 0 0 0 0 0 0 0 0 0

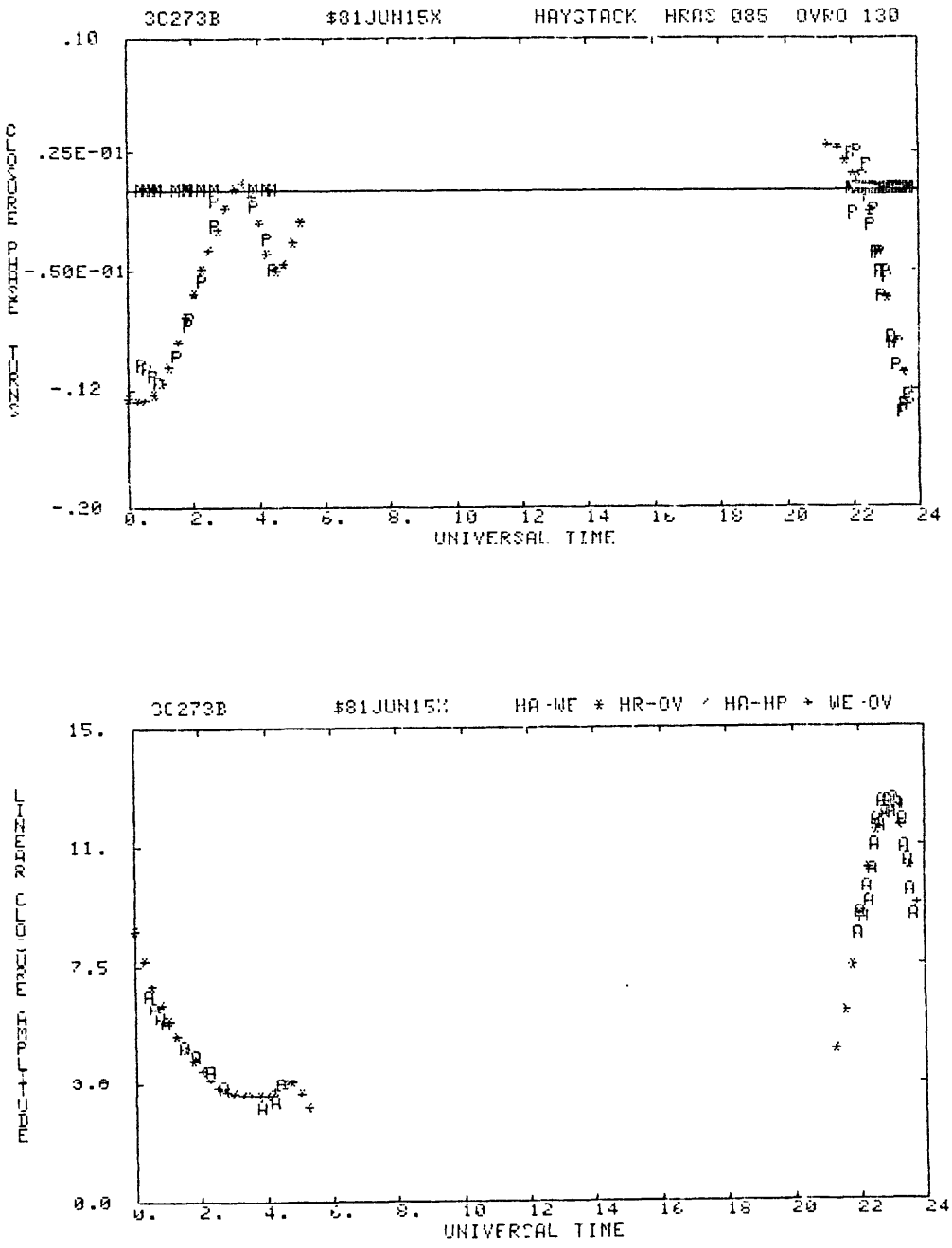

Figure 3.4.2: 3C273B X-band June 1981

Closure amplitude HA-HR, HR-OV, OV-WE, WE-HA on a linear scale and phase closure HA-HR-OV. The A's are the observed amplitude closure, the P's are the observed phase closure and the *'s are the closures (amplitude or phase) predicted by the model. The phase closures are expressed as fractions of 360^{o}.

X-band June 1981

Figure 3.5.1: 0552+398 CLEAN COMPONENTS- CLEAN MAP

The clean components are calculated using a grid spacing of 0.30 mas. Flux densities are expressed as fractions of the peak value which is normalized to 1000. The restoring beam (FWHM) is 1.15 mas by 1.00 mas at a position angle of -10^{o}. The contours are shown at 1, 2.5, 5, 10, 20, 35, 50, 70 and 90% of the peak value. Tickmarks are every milliarcsecond. The + shows the center of brightness.

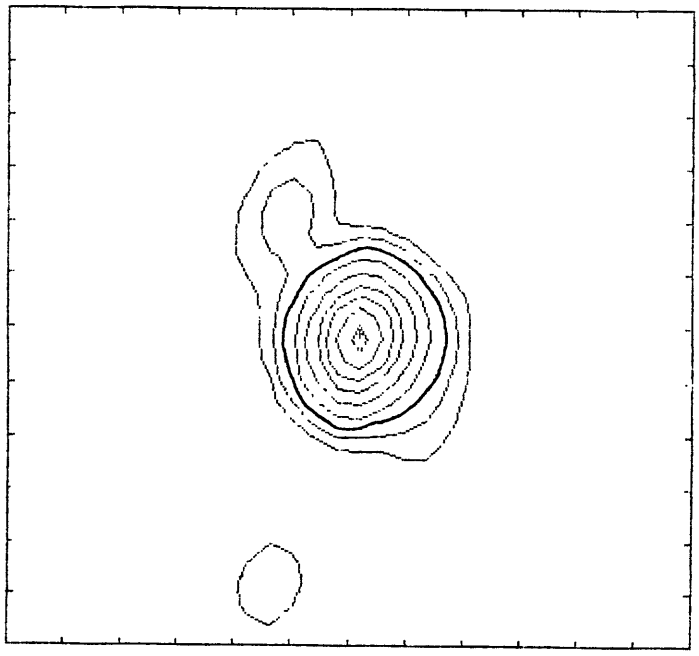

RESTORING BEAM

HALF POWER LEVEL

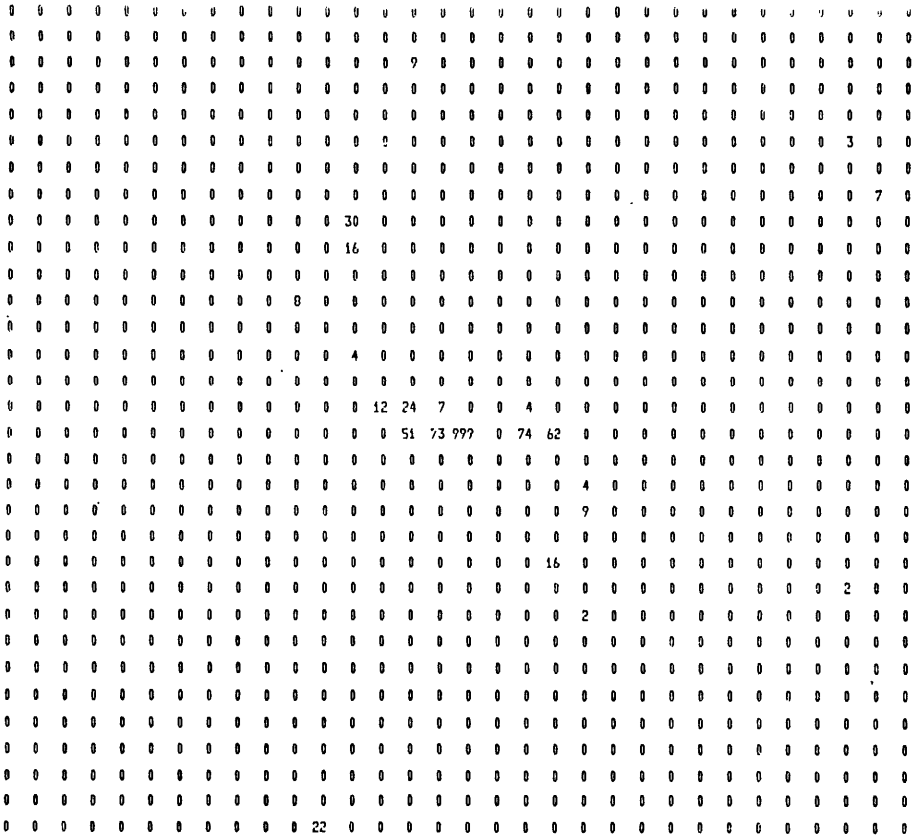

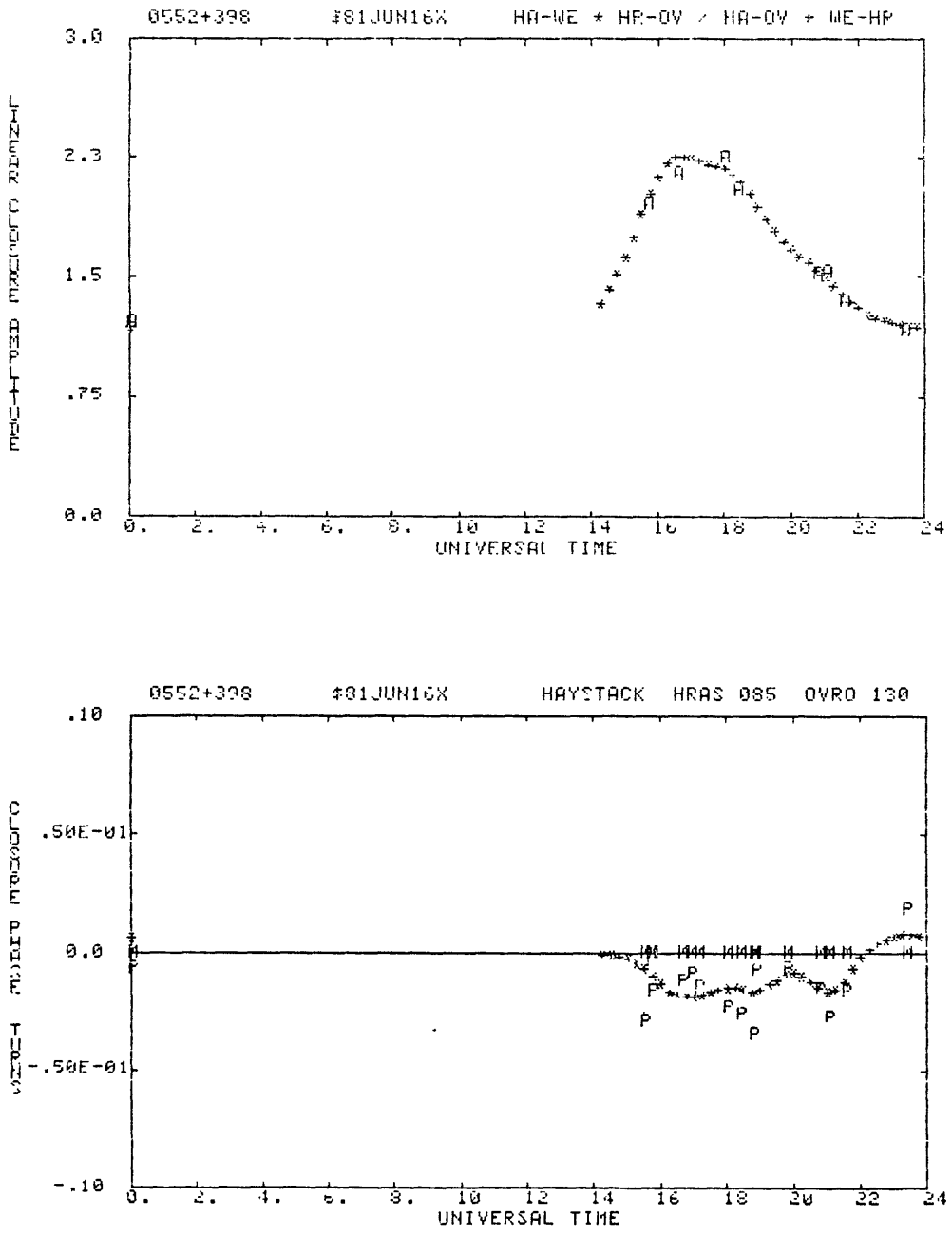

Figure 3.5.2: 0552+398 X-band June 1981

Closure amplitude HA-HR, HR-OV, OV-WE, WE-HA on a linear scale and phase closure HA-HR-OV. The A's are the observed amplitude closure, the P's are the observed phase closure and the *'s are the closures (amplitude or phase) predicted by the model. The phase closures are expressed as fractions of 360^{o}.

X-band June 1981

Figure 3.6.1: VRO 42.22.01 CLEAN COMPONENTS- CLEAN MAP

The clean components are calculated using a grid spacing of 0.35 mas. Flux densities are expressed as fractions of the peak value which is normalized to 1000. The restoring beam (FWHM) is 1.15 mas by 1.05 mas at a position angle of 0^{o}. The contours are shown at 1, 2.5, 5, 10, 20, 35, 50, 70 and 90% of the peak value. Tickmarks are every milliarcsecond. The + shows the center of brightness.

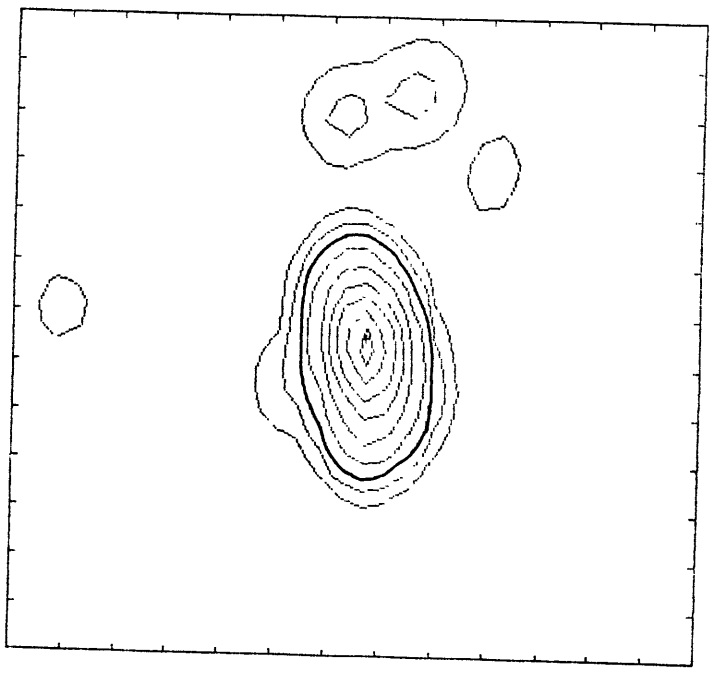

RESTORING BEAM

HALF POWER LEVEL

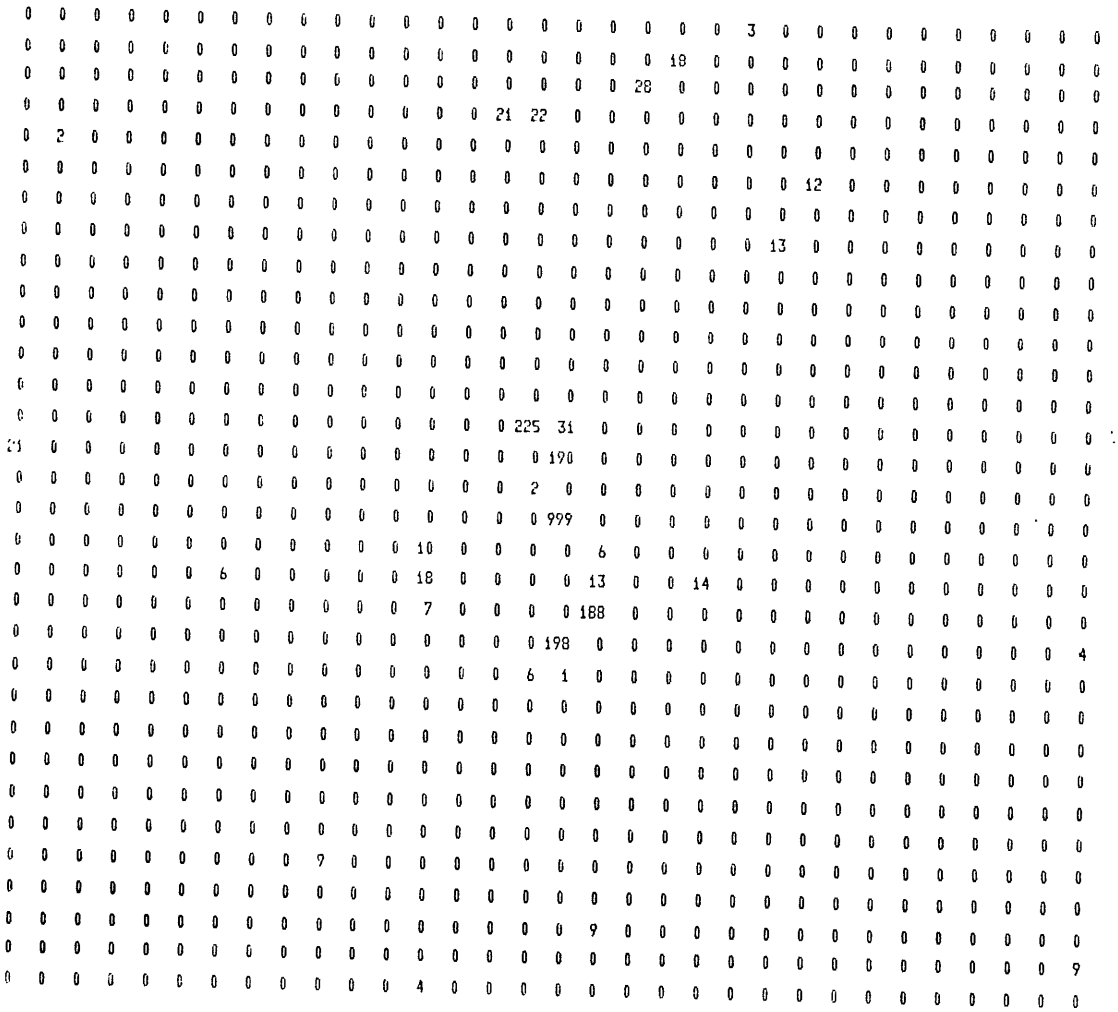

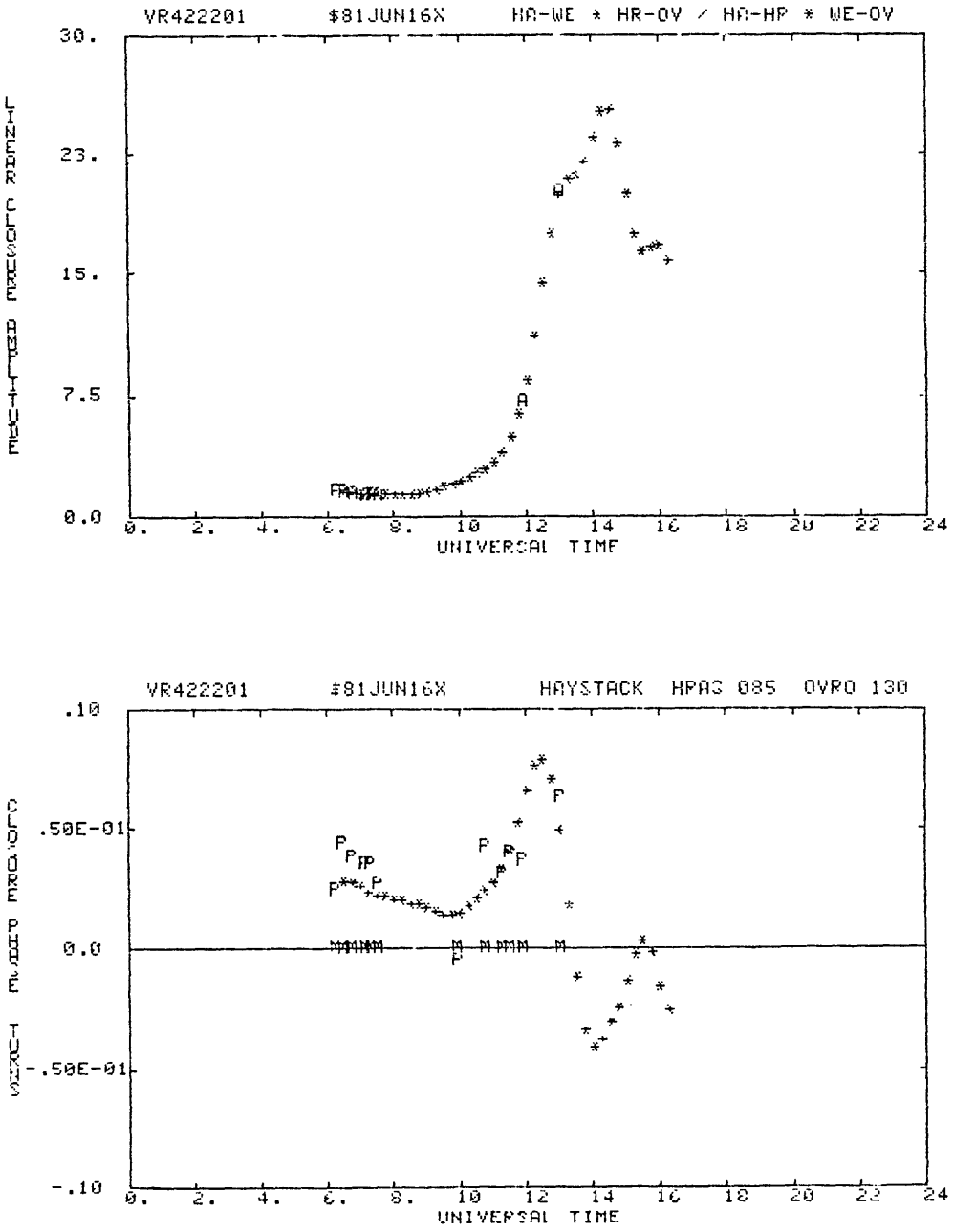

Figure 3.6.2: VRO 42.22.01 X-band June 1981

Closure amplitude HA-HR, HR-OV, OV-WE, WE-HA on a linear scale and phase closure HA-HR-OV. The A's are the observed amplitude closure, the P's are the observed phase closure and the *'s are the closures (amplitude or phase) predicted by the model. The phase closures are expressed as fractions of 360°.